

Use of an Atg16l1 mouse model to study the role played by autophagy in neuroprotection

Bertalan Bicsák M.D.

University of East Anglia, Faculty of Medicine and Health Sciences

**A thesis submitted for the degree of Doctor of Philosophy.
December, 2015**

This copy of the thesis has been supplied on condition that anyone who consults it is understood to recognise that its copyright rests with the author and that use of any information derived there-from must be in accordance with current UK Copyright Law. In addition, any quotation or extract must include full attribution.

Abstract

Atg16l1 is an autophagy protein, most known for its association with Crohn's disease. While knockout models of autophagy pathway components recapitulated neurodegeneration in laboratory mouse, the effect of Atg16l1 KO on neuronal protein homeostasis has been unknown. This study found Atg16l1 KO lethal on the first postnatal day, in the absence of gross deformity; as neonates fail to commence suckling. Histopathological analysis revealed the accumulation of detergent-insoluble aggregates of polyubiquitinated proteins in their central nervous system and in various other tissues. While polyubiquitinated aggregates are commonly associated with human neurodegenerative diseases, cell damage or accumulation of pathogenic proteins was not observed.

To investigate autophagy in the context of virus-host interaction, Semliki Forest Virus infection was tested in Atg16l1 KO tissues. Atg16l1 KO had no effect on virus proliferation in organotypic brain slice cultures while viral nsP1 and capsid expression was reduced in Atg16l1 KO embryonic fibroblast cultures. Semliki Forest Virus markers did not colocalize with autophagosomes in autophagy competent cells. While Semliki Forest Virus causes widespread encephalitis *in vivo*, virus replication is limited *ex vivo* in organotypic brain slice cultures.

Autophagy induction by diet is of great medical interest as epidemiological data suggest a protective effect against neurodegenerative diseases of the elderly. An important aim of this study was to determine the autophagy induction threshold of polyphenols concentrated in red wine. Resveratrol and quercetin induced autophagy in a non-canonical manner at or above 10 μ M in tissue cultures. These results underpin the feasibility of pharmacological but not the dietary administration of polyphenols for therapeutic purposes.

Table of contents

Abstract.....	2
Table of contents	3
List of figures and tables	5
Acknowledgement	7
1. INTRODUCTION	8
1.1. An overview of autophagosomal degradation pathways and the role of the autophagy protein Atg16	8
1.1.1. Autophagy process and function	11
1.1.2. Regulation of autophagy induction.....	14
1.1.3. Substrate selection for autophagic degradation	19
1.1.4. Atg16(l1): at the crossroads of autophagy and inflammation.....	23
1.2. Semliki Forest Virus infection in Atg16 KO mouse tissues.....	29
1.2.1. Semliki Forest Virus (SFV): overview, epidemiology.....	29
1.2.2. Semliki Forest Virus structure and life cycle	32
1.2.3. Autophagy in Semliki Forest Virus infection	33
1.3. Autophagy induction <i>in vitro</i> by red wine polyphenols.....	37
1.3.1. Dietary polyphenols: promises and pitfalls in disease prevention	37
1.3.2. Polyphenol bioactivity and autophagy induction	41
2. MATERIALS AND METHODS	42
2.1. Materials	42
2.2. Methods.....	48
3. RESULTS.....	65
3.1. Ubiquitinated protein aggregates in Atg16 KO mice	65
3.1.1. Study objectives:.....	65
3.1.2. Phenotype description of the Atg16 KO mice.....	65
3.1.3. Neuronal pathology of Atg16 KO mice	68

3.1.4. Polyubiquitinated aggregates are not associated with human neurodegenerative disease markers	74
3.1.5. Cell death in Atg16 KO tissues	77
3.1.6. Summary	80
3.2. Semliki Forest Virus infection in Atg16 KO mouse tissues	81
3.2.1. Study objectives:	81
3.2.2. Semliki Forest Virus infection in monolayer cultures	84
3.2.3. Semliki Forest Virus infection in organotypic brain cultures	88
3.2.4. Summary	92
3.3 Autophagy induction <i>in vitro</i> by red wine polyphenols	93
3.3.1. Study objectives:	93
3.3.2. Polyphenol studies in monolayer cultures	94
3.3.3. Summary	102
4. DISCUSSION	103
4.1. Ubiquitinated protein aggregates in Atg16 KO mice	103
4.1.1. Why do Atg16 KO mice die?	103
4.1.2. Neuronal pathology of autophagy KO mice – correlation and differences between human neurodegenerative disease	105
4.1.3. Cell death in Atg16 KO tissues	108
4.2. Semliki Forest Virus infection in Atg16 KO mouse tissues	110
4.2.1. Atg16 KO does not impair SFV infection	110
4.2.2. SFV infection impairs autophagy by protein synthesis dysregulation	112
4.3. Autophagy induction <i>in vitro</i> by red wine polyphenols	114
4.3.1. Dose-dependent induction of autophagy <i>in vitro</i> and <i>in vivo</i> – lessons from nutritional studies	114
4.3.2. Polyphenol effects in neural tissue <i>in vivo</i> and <i>ex vivo</i>	116
4.3.3. Pharmacological targeting of the autophagy pathway	117
4.3.4. Polyphenol signalling pathways in autophagy induction	119
List of abbreviations	120
List of references	123

List of figures and tables

Fig. 1.1. a) Membrane transport pathways to the lysosome b) The origin of the autophagosomal membrane. c) Protein interactions in autophagosome biogenesis. p. 9-11.

Fig. 1.2. a) Regulation of autophagy by environmental factors. b) mTORC1 and mTORC2 complexes. p. 17-18.

Fig. 1.3. a) Ubiquitination and protein degradation pathways. b) Protein destination is determined by the Ub topology on the route to its degradation. c) Comparison of Atg16 orthologs in *S. cerevisiae*, *M. musculus* and *H. sapiens*. p. 22.

Fig. 1.4. a) Phylogenetic tree of (+)-strand RNA viruses. b) Schematic model of SFV structure c) SFV life-cycle d) Molecular structure of the four polyphenol classes: stilbenes, flavonoids lignans and phenolic acids. p. 34-36.

Fig. 2.1. a) Restriction endonuclease digestion patterns of the 5' end of mouse Atg16. b) Comparing Atg16 WT and KO Atg16 genomic DNA, mRNA transcript and translated peptide sequences. p. 55.

Fig. 2.2. a) Steps involved in generating the Atg16 KO mice. b) PCR strategy for genotyping Atg16 WT and KO mice. p. 56-57.

Fig. 3.1. a) Detection of Atg16 KO by PCR b) Detection of Atg16 KO by western blot. c) Genotype distribution of prepartum fetuses e) Autopsy findings of a representative Atg16 KO carcass f) Atg16 KO neonates showed reduced body weight and reduced blood glucose levels as compared to WT littermates. g) Haematoxylin-eosin staining of lung and heart sections of neonate mice. p. 67-68.

Fig. 3.2. a) Normal histological structure found in Atg16 KO brains. b) Lack of autophagy results in accumulation of autophagy substrates in Atg16 KO mice. p. 69-70.

Fig. 3.3. a) p62 and polyubiquitin-positive protein aggregates appear in Atg16 KO brains. b) Protein aggregates shown in various Atg16 KO brain regions. p. 71-72.

Fig. 3.4. a) Protein aggregates appear in Atg16 KO tissues, outside of the central nervous system. b) Polyubiquitinated aggregates are detergent-insoluble. p. 72-73.

Fig. 3.5. a) α -Synuclein does not co-localise with the intraneuronal inclusions in Atg16 KO brains. b) GSK-3 β does not co-localise with the intraneuronal inclusions in Atg16 KO brains. c) - d) Neurodegenerative disease markers are not elevated in Atg16 KO mice. p. 75-77.

Fig. 3.6. a) Atg16 KO does not impair viability of primary MEFs and OBCs. b) Abnormal cell death morphology in Atg16 KO MEFs. c) Apoptosis in Atg16 KO brains is not accelerated as compared to brains of WT littermates. d) Protein aggregation does not lead to apoptosis in Atg16 KO mice. p. 78-79.

Fig. 3.7. a) Cytopathic effect of SFV infection is indistinguishable in Atg16KO and WT cultures b) Flowchart of virus infection experiments c) WT and Atg16 KO MEFs are equally susceptible to SFV infection and apoptosis. d), e) & f) Infected MEFs commit apoptosis approx. 12hrs after SFV infection. p. 82-84.

Fig. 3.8. a) No difference found between Atg16 KO and WT MEF SFV production. b) Loss of Atg16 reduces viral protein expression in infected MEFs. c) Effects of SFV infection on autophagy protein levels. d), e) Replicating SFV does not associate with autophagy proteins. p. 85-86.

Fig. 3.9. a) Atg16 KO has no effect on SFV production. b) lysates of infected OBCs immunoblotted for SFV-nsP1 and SFV-capsid. c) Effects of SFV-infection on autophagy protein levels in OBCs. d) WST-1 assay in SFV-infected organotypic coronal brain cultures. e) Apoptotic cells in brain cultures are SFV-negative. f) Apoptosis is not significantly increased in SFV-infected OBCs. p. 89-91.

Fig. 3.10. a) No polyphenols in this study were cytotoxic at the highest concentration tested. b)-c) High concentrations of RSV or QRC induce formation of autophagosomes. d) representative images. p. 96.

Fig. 3.11. a)-b) LC3-western blots from RSV or QRC-treated HEK293 cultures show dose-dependent autophagy induction. c)-d) Western blots show a non-linear relationship between RSV or QRC concentration and p62 expression in SH-SY5Y cells. p. 97-98.

Fig. 3.12. a) p62-accumulation in RSV-treated cells below autophagy-inducing threshold concentration. b) Wortmannin abolished autophagy induction by amino acid starvation, but did not affect autophagy induction by RSV or QRC. p. 99-100.

Fig. 3.13. a) EC, Cy3G, Pe3G and Ma3G do not activate autophagy in HEK-293 GFP::LC3 cells. b) A proposed mechanism of autophagy activation by polyphenols. p. 100-101.

Table 1.1.	Autophagy mutant mice. p. 26-28.
Table 2.1.	Antibodies used in this doctoral research. p. 45-46.
Table 2.2.	Composition of stacking and separating gels. p. 51.

Acknowledgement

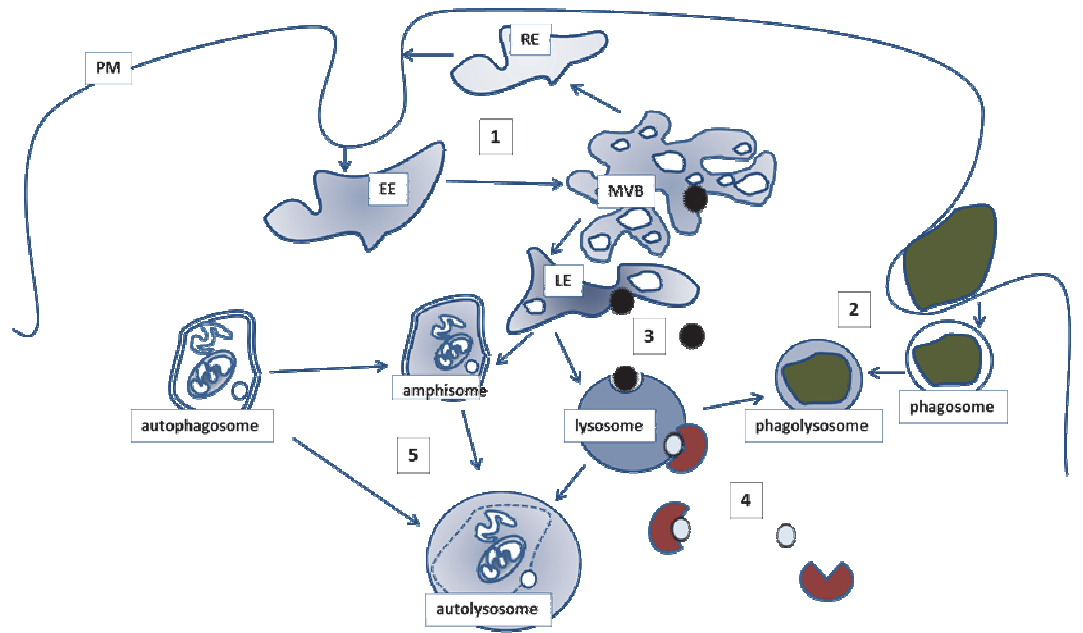
I am dedicating this thesis to I. Sz., a great teacher and a true friend, who opened my eyes to the little beauties of the nature and encouraged me to pursue the answers to my questions.

1. INTRODUCTION

1.1. An overview of autophagosomal degradation pathways and the role of the autophagy protein Atg16

The final destination for the degradation of intracellular or extracellular nutrients is the lysosome; a single-membraned cytosolic structure where low pH and lysosomal enzymes facilitate breakdown of complex molecules. Autophagy was originally described nearly half a century ago, as a transport route for cytoplasmic components into the lysosome (de Duve, 1963). Autophagy is a collective term for macroautophagy, microautophagy and chaperone-mediated autophagy (CMA). These membrane transport pathways are best understood in the context of other cellular transport pathways, which function in a coordinated way in the cell and finally terminate in the lysosome (Fig.1.1.a). Macroautophagy is the selective or bulk sequestration of cytosolic cargo into double membrane vesicles, which ultimately fuse with lysosomes. Unless specified otherwise, macroautophagy refers to autophagy in this thesis.

a



b

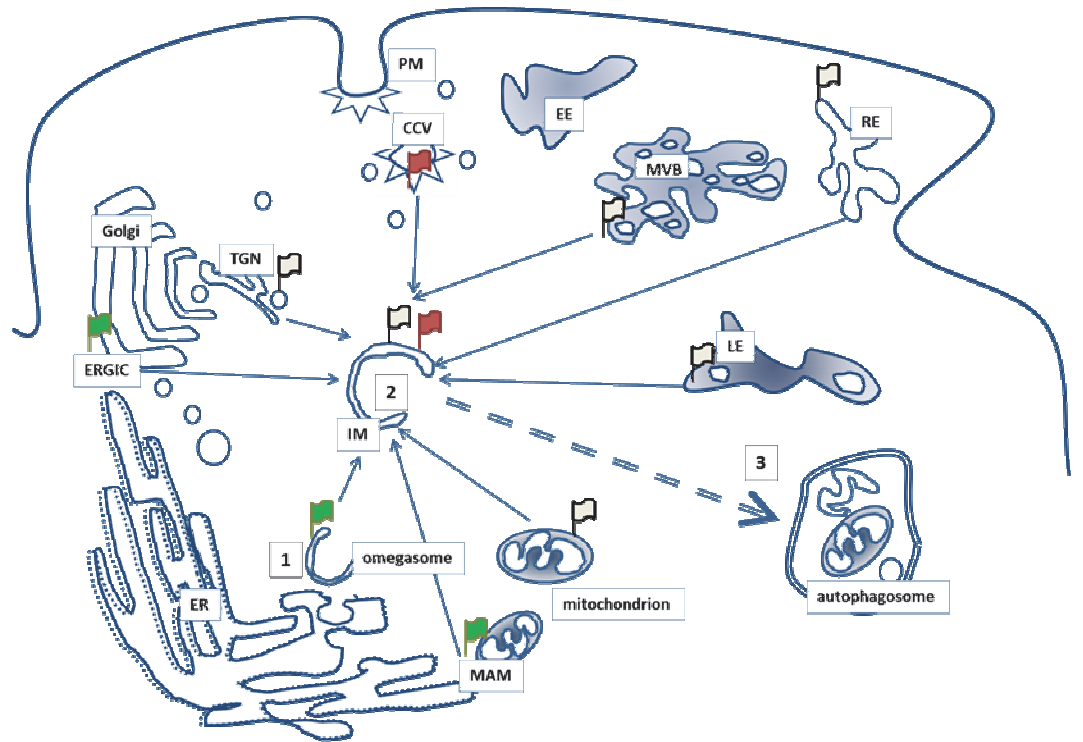
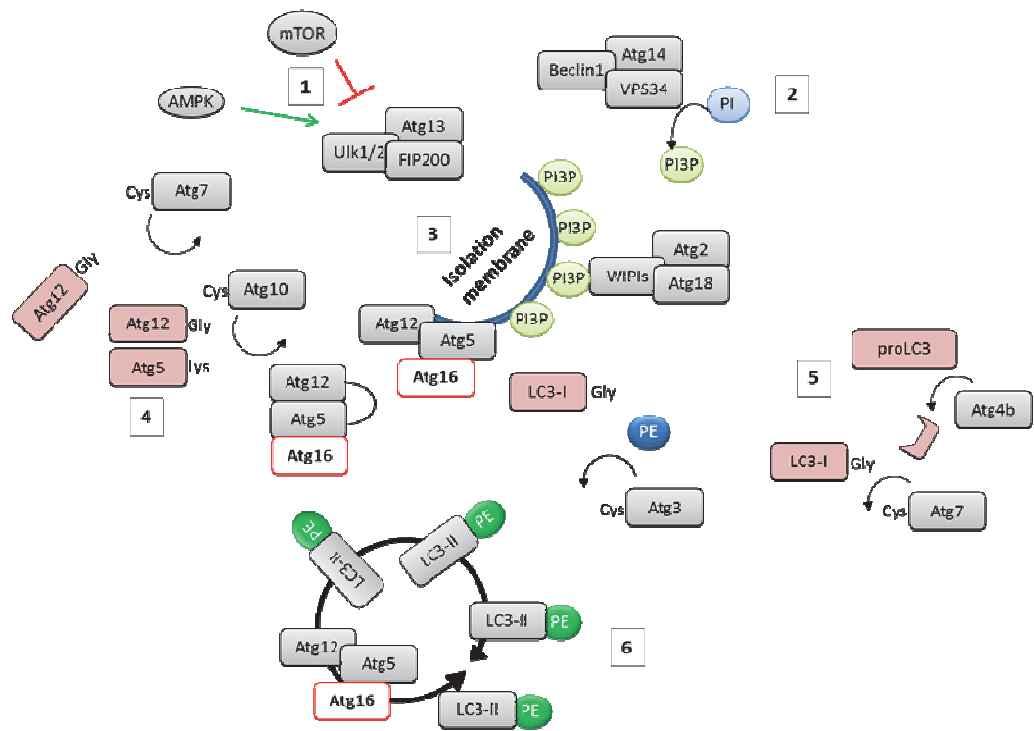


Fig. 1.1. a) Membrane transport pathways to the lysosome. 1) Endocytosis internalizes plasma membrane (PM) components for degradation or recycling. Intraluminal pH progressively decreases from early endosomes (EE) through multivesicular bodies (MVBs) to late endosomes (LE), while recycling endosomes (RE) are less acidic. Acidity is depicted by dark blue in the picture. Late endosomes fuse with lysosomes to ensure degradation of their cargo through low pH and lysosomal enzymes. 2) Cells may engulf exogenous material through heterophagy into phagosomes: this pathway bypasses the complex endocytotic network as phagosomes directly fuse with lysosomes. 3) Endogenous, cytosolic proteins can be taken up into late endosomes, multivesicular bodies and lysosomes through membrane invagination, in a process called microautophagy (Sahu et al. 2011; Li et al. 2012). 4) Chaperone-mediated autophagy operates at the lysosomal membrane to translocate specific proteins with a consensus KFERQ peptide sequence (Li et al. 2011). 5) Macroautophagy targets cytoplasmic components by de-novo formation of autophagosomes. Macroautophagy may interact with endosomal transport at the level of amphisomes, formed by fusion of autophagosomes and late endosomes. **b) The origin of the autophagosomal membrane.** 1) Omegasomes are sequestered from an endoplasmic reticulum (ER) „cradle”, currently viewed as the precursor of the 2) isolation membrane (IM), a crescent-shaped membranous structure, to which multiple cell components contribute. Marker proteins, such as DFCP (green flag), Atg9 (grey flag), Atg16 (red flag) can be traced down to the plasma membrane (PM), clathrin-coated vesicles (CCV), endosomal membranes (early endosome (EE), recycling endosome (RE), late endosome (LE)), trans-Golgi-network (TGN), ER–Golgi intermediate compartment (ERGIC), mitochondria-associated ER membrane (MAM). 3) These markers dissociate from completed autophagosomes. **c) Protein interactions in autophagosome biogenesis.** 1) The Ulk1/2-Atg13-FIP200 complex is a main sensor of upstream signals 2) Atg14-Vps34-Beclin generates phosphatidylinositol-3-phosphate (PI3P) from phosphatidylinositol (PI), to 3) recruit the Atg2-Atg18/WIPI as well as the Atg5-Atg12-Atg16 complexes to the isolation membrane. 4) Atg5-Atg12 and 5) LC3-phosphatidylethanolamine (PE) are formed by ubiquitination-like cleavage and conjugation steps. 6) Membrane-bound Atg5-Atg12-Atg16 and LC3-II are essential for the closure of the isolation membrane into an autophagosome.

c



1.1.1. Autophagy process and function

Autophagy has been first described as a cellular response to starvation. While preserving its original function during evolution, higher eukaryotes exploit this pathway for various additional functions: the mobilization of hepatic glycogen (Kotoulas et al., 2006), lipid droplets (Singh et al., 2009) and amino acid stores, which is especially important during neonatal starvation (Kuma et al., 2004). In addition to that, autophagy is implicated in regulation of tumor growth and carcinogenesis (Chen and Karantza-Wadsworth, 2009), host-pathogen interaction (Deretic and Levine, 2009), neuroprotection and neurodegeneration (Rubinsztein et al., 2005). Despite the surge of publications on autophagy, we are far from a clear understanding of its protective or damaging function.

The life cycle of an autophagosome can be divided into four stages: 1. Nucleation 2. Expansion 3. Maturation 4. Degradation (Simonsen and Tooze, 2009). The origin of autophagosomal membrane has long been an enigma for cell biology: earliest stage is possibly the omegasome, named after its characteristic omega-like shape in electromicroscopic sections, which is formed dynamically connected to the endoplasmic reticulum (ER) in a cradle-like membrane fold (Axe et al., 2008, Hayashi-Nishino et al., 2009, Ylä-Anttila et al., 2009). The omegasomal membrane, enriched in phosphatidylinositol 3-phosphate (PI(3)P), then expands to form a cup shaped isolation membrane (IM) as it sequesters cytoplasmic material and organelles; sealing them inside a double-membraned vesicle. As the composition of isolation membrane is different from that of the ER, various other sources, like the Golgi apparatus (Yamamoto et al., 2012), the ER– Golgi intermediate compartment (ERGIC), trans-Golgi-network (TGN), mitochondria (Hailey et al., 2010), mitochondria-associated ER membrane (MAM) and the plasma membrane (Ravikumar et al., 2010) have recently been postulated. A far from detailed overview of autophagosome biogenesis is depicted in Fig.1.1.b.

IMs elongate and enclose autophagic substrates into the double-membrane membrane fold, which is, from the point of completion of vesicle formation, called autophagosome. PI3P is recycled from sealed autophagosomes (Cebollero et al., 2012). Complete autophagosomes are of 0.5-1.5 μm diameter in mammals, and of neutral interior pH (Mizushima et al., 2002). Autophagosomes fuse with other autophagosomes (Moreau et al., 2011), as well as with late endosomes during their maturation. The fusion with late endosomes leads to the formation of amphisomes, a mildly acidic compartment, where autophagy joins the dynamic network of endocytic membrane transport, channeling extra- and intracellular degradation pathways to a common destination. The end of autophagosomal life cycle is the fusion between autophagosome and lysosome or between amphisome and lysosome (Lamb et al., 2013). These fusion steps are regulated by the translocation of Syntaxin 17 from the inner to the outer membrane of the autophagosome, where it interacts with the endosomal/lysosomal membrane protein VAMP8

12

(Itakura et al., 2012). Their cargo is degraded in single-membraned autolysosomes by the low pH and lysosomal enzymes. Lysosomal acidification is co-regulated with autophagy activation to ensure proper digestion (Zhou et al., 2013). An increase in the number of autophagosomes may signal an upregulation of autophagosome formation (Mizushima, 2007) or a downregulation of downstream membrane fusion effects (Klionsky et al., 2008).

More than 30 autophagy-related (Atg) proteins have been identified so far, and this number is steadily increasing. Atg proteins form macromolecular complexes that regulate each step of the autophagosomal life cycle (Fig.1.3.c). The Atg1/ULK complex is the integrator of main autophagy regulating pathways and is directly regulated by the mTOR kinase. The Atg14-Vps34-Beclin complex forms a class-III phosphatidylinositol-3-kinase (PI3K) complex, which generates phosphatidylinositol-3-phosphate (PI3P), an essential lipid component of the omegasome and isolation membrane (IM) (Kihara et al., 2001, Polson et al., 2010, Herman and Emr, 1990). PI3P is recognized by the protein complex of Atg2-Atg18/WIPI; and also implicated in tethering Atg5 to the IM (Romanov et al., 2012). Atg2-Atg18/WIPI recruits Atg9 positive vesicles: these membrane structures are currently of incompletely understood function and origin, which probably supply membrane elements from the endosomes, trans-Golgi-network and mitochondria.

The isolation membrane elongates and closes into itself, facilitated by the Atg12-Atg5-Atg16 and LC3-phosphatidylethanolamine (PE). These two complexes are formed by so called ubiquitination-like reactions, due to the remarkable similarity to the catalytic steps during ubiquitin-proteasomal degradation. Atg7, a ubiquitin-activating (E1)-like enzyme forms a thioester bond with the C-terminal glycine residue on Atg12 or LC3-I, respectively (proLC3 is cleaved by Atg4b to expose the C-terminal glycine). In the next step the ubiquitin-conjugating (E2)-like enzymes Atg10 and Atg3 facilitate the binding of the activated glycine to an internal lysine of the target protein (Atg5), or to the amino-group of PE (Mizushima et al., 1998). Atg5-Atg12 conjugates interact with Atg16 on the IM (Mizushima et al., 2003). The

ubiquitin-ligase (E3)–like action of the Atg5-Atg12-Atg16 complex is the final step to regulate phosphatidylethanolamine (PE) binding of LC3-I (Fujita et al., 2008). While LC3-I is cytosolic, the LC3-PE-conjugate is membrane bound, and referred to as LC3-II. LC3-II remains on the cytosolic surface of the completed autophagosomes, while the Atg5-Atg12-Atg16 complex dissociates. LC3 (or its yeast homologue Apg8) was the first autophagosome marker identified, and fluorescent tagged LC3 is now conveniently used to visualise autophagosomes in cells (Mizushima et al., 2004b, Kirisako et al., 1999). LC3 can therefore identify isolation membranes, autophagosomes, amphisomes and autolysosomes.

1.1.2. Regulation of autophagy induction

When there is ample supply of nutrients, autophagy operates at a basal level, which is specific to the given tissue (Mizushima et al., 2004a). Autophagic turnover is tightly regulated in response to environmental factors, such as stress or lack of nutrient supplies. Several intracellular signalling pathways regulate autophagy in eukaryotes (Fig.1.2.a); most of them converge on the mTOR complex. mTOR is a mammalian homologue of the yeast autophagy regulator TOR (Target Of Rapamycin) protein (Sabatini et al., 1994, Brown et al., 1994). mTOR itself operates as the catalytic subunit of two multi-protein complexes: mTORC1 and the mTORC2. The composition of these two complexes as well as their cellular function is depicted in Fig.1.2.b. Regulation of autophagy cannot be isolated from other cellular functions of the mTORC1 complex; as mTOR activation is a decision which determines the cell's overall metabolic state and survival fitness.

Autophagy is controlled by insulin and growth factors in multicellular eukaryotes through a lipid phosphorylation cascade (Petiot et al., 2000). Class-I PI3 kinases generate PI(3,4,5)P₃, which in turn recruits Akt and PDK1 to the plasma membrane

(not to be confused with PI3P, an essential component of the autophagosome precursor membranes generated by class-III PI3 kinase (Axe et al., 2008). TSC1/2 (tumor suppressors, mutated in tuberous sclerosis) and Rheb are downstream effectors of these pathways (Findlay et al., 2005).

Sufficient amount of amino acids is a prerequisite for mTORC1 activation by growth factors. Amino acid starvation has long been known to induce autophagy in cell culture, yet our understanding of amino acid signalling is far from complete. Rag-GTP-ases have been identified as intracellular amino acid sensors by regulating mTOR complex, in an inside-out mechanism that starts from within the lysosome (Sancak et al. 2008; Kim et al. 2008). Amino acid content of the lysosomal lumen is sensed by the vacuolar H⁺-ATPase, which interacts with Ragulator, a trimeric protein complex that anchors Rag-GTPases to the lysosomal membrane (Zoncu et al., 2011). If lysosomes are filled with amino acids, a vATP-ase-Ragulator mediated conformation shift ensues and an active RAG-complex is formed (Sancak et al. 2008; Kim et al. 2008). RAGA/B heterodimer binds GTP as RAGC/D heterodimer hydrolyses GTP to GDP. RAGA/B and RAGC/D GTP-ases have been identified as intracellular amino acid sensors in the regulation of mTOR complex as they promote binding of mTORC1 complex to RHEB-enriched membranes (Sancak et al., 2010).

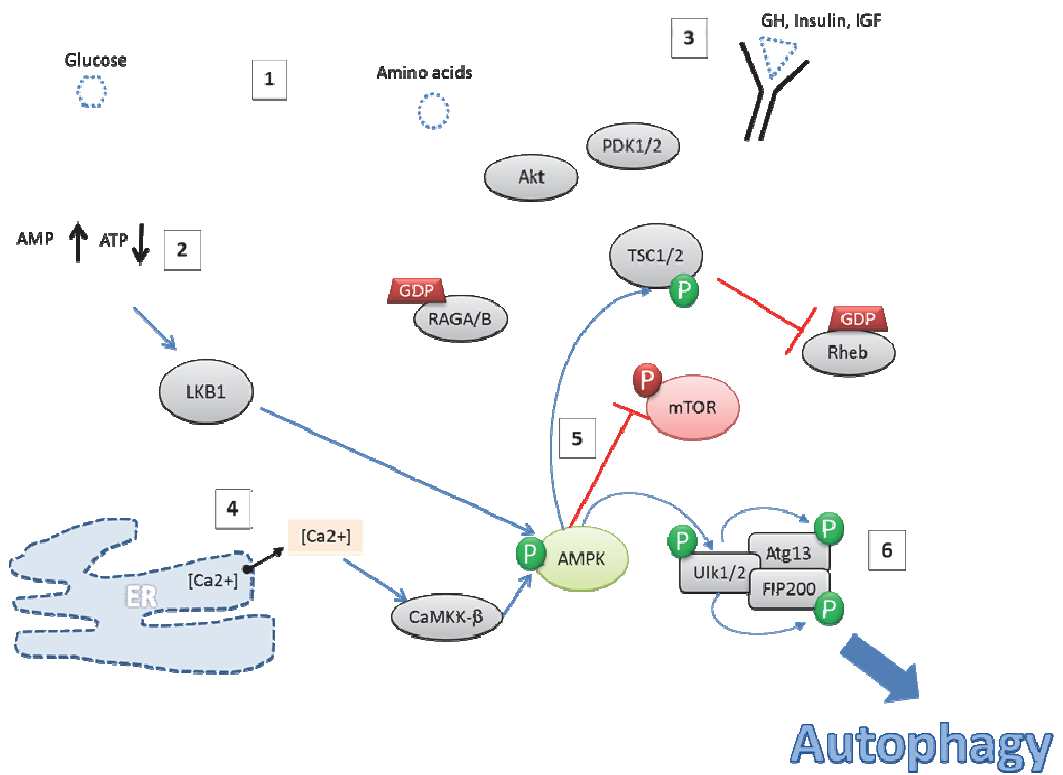
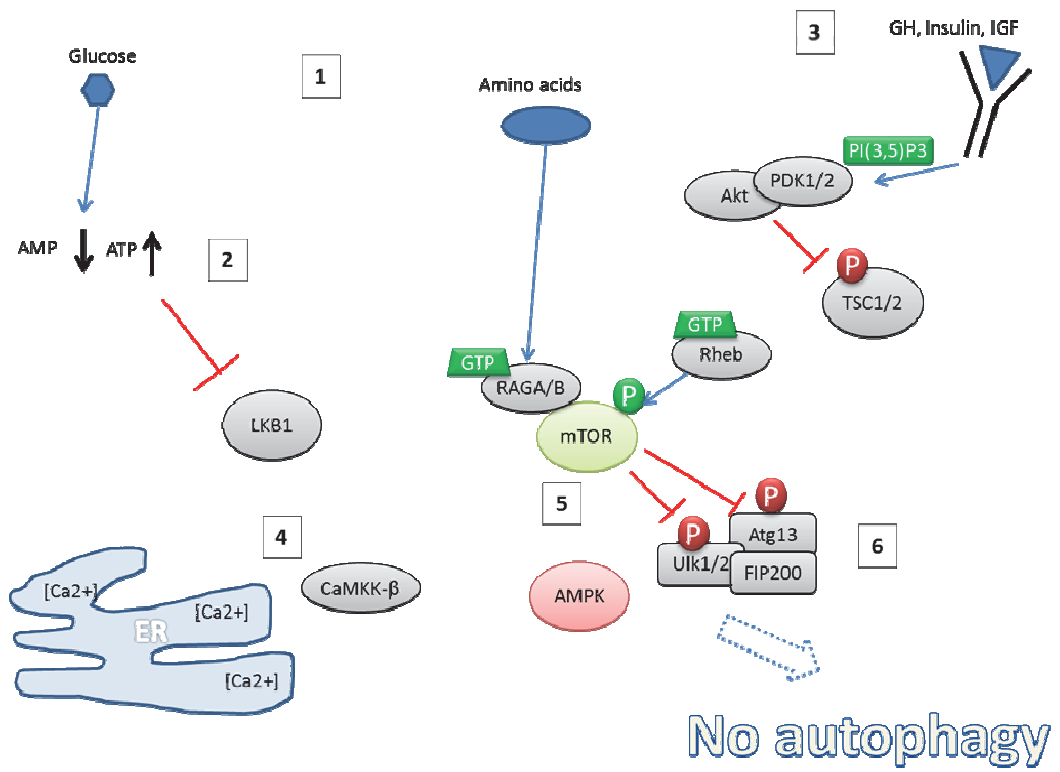
Autophagy eventually generates energy; hence its regulation by the cellular energy status appears evident. AMPK (AMP-activated protein kinase) is an evolutionarily conserved sensor, activated in response to low ATP vs. high AMP levels. AMPK inactivates mTOR and thereby induces autophagy. AMPK itself has multiple signalling inputs: the ATP/AMP ratio; which is transmitted by an upstream kinase, LKB1 (Shaw et al. 2004); the ER-stress-sensor Ca²⁺/calmodulin-dependent protein kinase kinase- β (CaMKK- β) and Sirtuin-1 (SIRT1) (Høyer-Hansen et al., 2007, Shaw et al., 2004, Cantó et al., 2010).

AMPK-phosphorylation has multi-pronged effect on autophagy-induction; by phosphorylation of TSC1/2 (Inoki et al., 2003), mTOR (Gwinn et al., 2008) and Ulk1/2 (Egan et al. 2011). AMPK may have an opposite effect by binding Ulk1/2 in the presence of adequate nutrient supply, facilitating its phosphorylation by mTOR (Shang et al., 2011).

The last gatekeeper of autophagy is the Ulk1/2 protein complex, as mTOR-dependent and -independent cascades are relayed by Ulk1/2 phosphorylation status (Shang et al., 2011, Egan et al., 2011, Kim et al., 2011). Activated Ulk1/2 phosphorylate their primary substrates, Atg13 and FIP200 to induce autophagy (Hosokawa et al., 2009, Jung et al., 2009, Ganley et al., 2009). Notably, the Ulk1/2-Atg13-FIP200 complex is formed even in the absence of autophagy, but its binding to the isolation membrane is mTOR dependent (Ganley et al., 2009). The physiological substrates of this macromolecular complex remains to be elucidated, a most recent study has detected direct interaction between FIP200 and Atg16L1 (Gammoh et al., 2013a).

There is growing evidence for alternative pathways, which circumvent mTOR and other autophagy initiator proteins (Nishida et al., 2009); as glucose deprivation or to ammonia may activate autophagy in an mTOR and Ulk1/2-independent manner (Cheong et al., 2011).

a



b

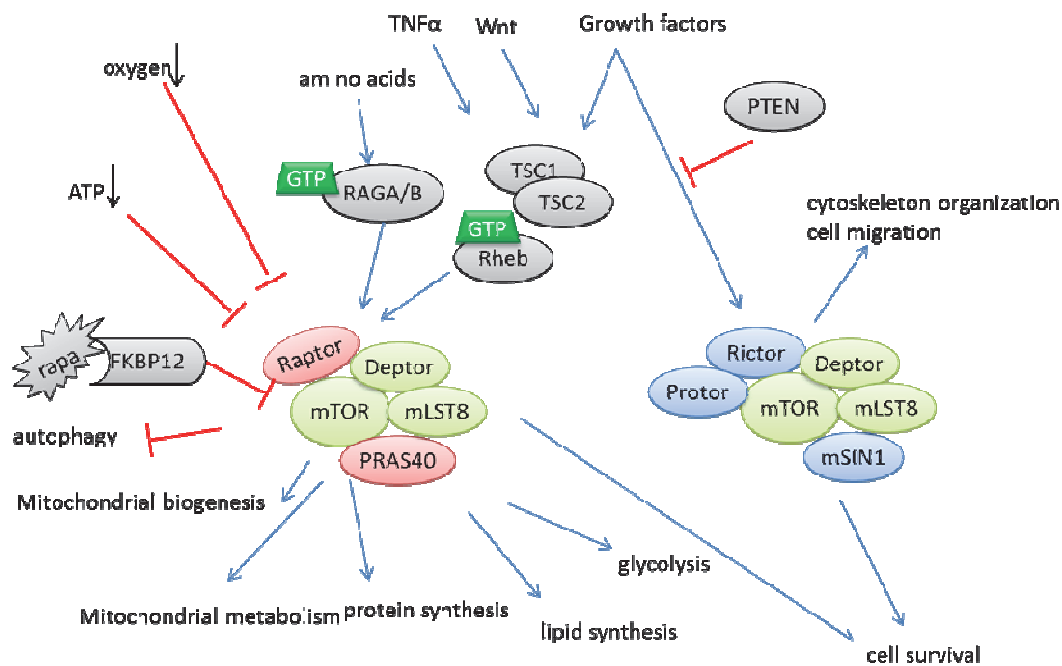


Fig. 1.2. a) Regulation of autophagy by environmental factors. Cells respond to the availability of 1) nutrients, 2) energy status and 3) growth factors as well as to 4) intracellular stressors through autophagy regulating pathways. 5) Signals are integrated by the tandem activity of the AMPK and mTOR enzyme complexes to 6) ensure inhibition or activation of autophagy through phosphorylation of the Ulk1/2 complex. **b) mTORC1 and mTORC2 complexes:** core components of both mTOR complexes are mTOR, mLST8 (mammalian lethal with Sec13 protein and Deptor (DEP-domain-containing mTOR-interacting protein). mTORC1-specific mTOR-binding partners are Raptor (regulatory-associated protein of mTOR; which binds directly to 4EBP1 and p70 α); and PRAS40 (proline-richAKT substrate 40 kDa). Another interacting protein, FKBP12 (FK-binding protein 12) is the direct binding partner of Rapamycin, which only inhibits mTOR in mTORC1 (Hara et al., 2013). The mTORC2 complex is distinguished by the mTOR-interacting units Rictor (rapamycin-insensitive companion of mTOR); mSIN1 (mammalian stress-activated protein kinase interacting protein) and Protor-1 (protein observed with Rictor-1). Upstream control pathways of mTORC1 include growth factors, nutrients, energy supply and inflammation (Laplanche and Sabatini, 2009). mTORC1 is not only involved in autophagy inhibition but is essential for distinct cellular functions: cell survival and proliferation, and various anabolic pathways including protein and lipid synthesis, mitochondrial biogenesis, glycolysis and oxydative phosphorylation. (Cunningham JT, 2007, Cheng et al., 2014). As opposed to the vast number of signalling inputs of mTORC1, little is known about mTORC2 regulation, as growth factor signalling via PTEN appears as a putative upstream pathway. (Guertin et al., 2009, Shrestha et al., 2015). mTORC2 is involved in cell survival, metabolism and cytoskeletal organization pathways (Jacinto et al., 2004, Sarbassov et al., 2005). rapa: Rapamycin

1.1.3. Substrate selection for autophagic degradation

Cells invest a great deal of energy to regulate protein homeostasis, by ensuring the correct level of proteins in the cell; not only by controlling protein production but also their degradation. Proteomic studies revealed a wide range of protein stability, from seconds to months (Doherty et al., 2009). The Ubiquitin-Proteasome System (due to the broad complexity of ubiquitination-dependent pathways, a misnomer, by itself) regulates degradation of short-lived proteins by directing them into the proteasome for degradation. UPS substrates are proteins that regulate cell cycle or signalling events, and misfolded proteins, when they are unable to be corrected by chaperones after translation. Autophagy, in turn, degrades long-lived proteins, protein aggregates or entire cellular compartments like mitochondria; or even invading pathogens – like bacteria or viruses. While first described as a non-selective mechanism of protein degradation; autophagy has an important role in selectively degrading appropriately tagged (primarily, but not exclusively K63-polyubiquitinated) proteins. We are just about to understand the principles of reading the ubiquitin code: p62, NBR1, OPTN, NDP52 are adaptor proteins that interact with ubiquitinated substrates as well as with LC3/GABARAP autophagosome proteins via their Ub-associated (UBA) and LC3-interacting (LIR) motives (Kirkin et al., 2009b; Shaid et al., 2012).

While the original concept of autophagy has been a stochastic and bulk degradation of substrates, recent studies have shown targeted degradation of ubiquitinated proteins, ribosomes, mitochondria, peroxisomes, and intracellular pathogens by autophagosomes. Cargo-selective autophagy types are named according to the sequestered content: xenophagy (intracellular bacteria and viruses), aggrephagy (protein aggregates), pexophagy (peroxisomes) and mitophagy (mitochondria) (Lamb et al., 2013). Mounting evidence suggests that the ubiquitination pattern and

ubiquitin binding autophagic adaptor proteins determine the substrate specificity for selective autophagy (Kirkin et al., 2009b).

Ub is a small, 8.5 kDa, globular protein, which has a ubiquitous role in regulation of protein trafficking and degradation. The first ubiquitin is covalently attached via its C-terminal glycine to the ϵ -NH₂ group of a lysine in the target substrate, or to the α -NH₂ group of its N-terminus. Successive ubiquitination steps may link Ub to another Ub acceptor residue on the substrate (multi-monoubiquitination) or to a previously attached Ub (polyubiquitination). Ub possesses seven lysine residues (K6, K11, K27, K29, K33, K48 and K63) and all of which is able to bind another Ub. However, successive addition of Ub preferentially occurs on the 48. and 63. lysine residues. Although it is difficult to determine the fate of protein from the ubiquitination pattern, cellular pathways preferentially use substrates with specific configuration of ubiquitin linkages. Monoubiquitination is involved in DNA repair and gene expression (Jackson and Durocher, 2013, Shilatifard, 2006), and also regulates receptor endocytosis e.g. in the case of growth factor receptors (Haglund et al., 2003b; Haglund et al., 2003a). Polyubiquitination through K48 (Chau et al., 1989) or less commonly through K11 results in proteasomal degradation, whereas a K63-linked Ub chain is preferentially recognized by autophagy (Kirkin et al., 2009b). Ubiquitination pathway is further complicated by deubiquitination, homotypic and heterotypic (mixed K48 and K63 inter-Ub-linkages) as well as branched ubiquitin chains; which add to the complexity of Ub-signalling network and aid the specificity of intracellular protein allocation (Komander and Rape, 2012, Sadowski et al., 2012).

Hence, ubiquitination is a tightly regulated post-transcriptional modification, which has a crucial role in determining the fate of the protein. A basic scheme of ubiquitination involves three stages (Fig.1.3.a). First, the C-terminal Gly of Ub forms a thioester bond with the catalytic cysteine of a Ub-activating (E1) enzyme. Next, Ub is transferred from the E1 to the catalytic Cys of the Ub-conjugating (E2) enzyme. E2 together with a Ub-ligase (E3) enzyme then transfer the Ub to the

specific residue of the substrate. Substrate-binding, and the Ub-chain configuration is achieved by the selectivity of E3 enzymes. E1-, E2- and E3-enzymes form an enzymatic cascade, with only a few E1s, some 40 E2s and hundreds of E3 enzymes (Berndsen and Wolberger, 2014).

The topology of ubiquitin linkages determines protein clearance by the ubiquitin-proteasomal or the autophagosomal degradation pathway (Fig.1.3.b). K63-linked polyubiquitin chains might serve as an “eat me” signal for autophagosomes (Tan et al., 2008) for a contrarian view please see here: (Riley et al., 2010). Intense K63-linked polyubiquitination does not necessarily lead to enhanced degradation of protein aggregates, and upregulation may promote accumulation (Tan et al., 2008). K63-polyubiquitin motifs are recognized by p62 (also known as A170/SQSTM1) and NBR1 (neighbour of BRCA1 gene 1) adaptor proteins that attach to the autophagosome protein LC3, so that their substrates are incorporated and degraded in the autophagosome (Bjørkøy et al., 2005, Kirkin et al., 2009a). Autophagy adaptor proteins are themselves autophagy substrates, hence their intracellular levels (assuming a constant level of their production) signal the rate of autophagic degradation, the autophagic „flux” (Bjørkøy et al., 2005, Kirkin et al., 2009a).

An accumulation of p62 together with K63-polyubiquitinated protein inclusions have been observed in autophagy deficient animal models (Hara et al., 2006) (Komatsu et al., 2005, Komatsu et al., 2007). Intriguingly, the knockdown of p62 suppressed liver injury in autophagy deficient mice, but did not improve their neurodegeneration phenotype (Komatsu et al., 2007).

1.1.4. Atg16(l1): at the crossroads of autophagy and inflammation

Atg16l1 is a mammalian counterpart of the yeast Atg16 protein: the N'-terminal coiled-coil domain shows weak homology with the yeast Atg16; the C'-terminal WD40 repeat and a linker region between these domains is absent in yeast (Mizushima et al., 2003). Atg16l2 is another mammalian Atg16 homologue, as yet without a confirmed role in the autophagosome assembly (Ishibashi et al., 2011).

For the sake of brevity, Atg16l1 will be referred to as Atg16 in the text below.

This protein is ubiquitously expressed in mouse tissues, the distribution of spliced isoforms is tissue specific: liver, kidney, spleen, thymus and testes contain a 63kDa and a 71 kDa form, while the brain, heart and skeletal muscles express a 75 kDa isoform (Mizushima et al., 2003).

Atg16 is attached to a pre-formed cytoplasmic Atg5-Atg12 complex to form an 800 kDa octamer of Atg5-Atg12-Atg16 on the isolation membrane (a minor form of 400 kDa four-set complex has also been identified). This protein complex performs an E3-like ligase reaction in LC3 lipidation (Hanada et al., 2007). The most N'-terminal region provides a platform both for the interaction with Atg5 and for the homo-oligomerization with other Atg16 molecules (Mizushima et al., 2003). Atg16 binds Atg5 via its most N-terminal region (aa 1-79), this region together with the coiled-coil domain (aa 1-276) is necessary to form homo-oligomers with other Atg16 molecules (Mizushima et al., 2003). The internal part of the coiled-coil region (aa 141-265, aa207-230 and aa 229-242, respectively) takes part in the interaction with the Golgi-resident small GTPase-s Rab33A and Rab33B (Itoh et al., 2008), with the WD-repeat PI(3)P effector protein WIPI2b (Dooley et al., 2014) and FIP200 (Gammoh et al., 2013b). The role of the C'-terminal WD40-repeat domain (aa 320-607) is much less understood, being dispensable for functional autophagy (Fujita et

al., 2009). Although the WD40 propeller structure is a conserved protein binding platform to form multiprotein complexes (Neer et al., 1994), the only direct binding partner of the Atg16 WD40 domain is TMEM59, a transmembrane protein that recruits autophagosomes upon *Staphylococcus aureus* infection (Boada-Romero et al., 2013) (Fig.1.3.c).

Atg16 is an important negative regulator of inflammation, which dampens the effect of LPS and other TLR4 agonists on macrophages. Loss of Atg16 leads to an overproduction of IL-1 β and IL-18, and macrophage sensitisation for apoptosis (Saitoh et al., 2008). Autophagosomes control IL-1 β release by sequestering pro-IL-1 β (Harris et al., 2011), thus anti-inflammatory function of Atg16 (especially in the context of intestinal inflammation) is closely linked to its role in autophagy. Atg16 is also involved in autophagy-independent cellular functions, by regulating neuropeptide-Y (NPY) secretion via Rab33A binding (Ishibashi et al., 2012).

Atg16 has come in the focus of autophagy research since a genome-wide association study identified a variant (T300A) overrepresented in patients with Crohn's disease (CD) (Rioux et al., 2007). The low penetrance of the disease and the high frequency of the susceptibility allele in the healthy population ($f=0.60$ in CD patients vs $f=0.53$ in healthy individuals) (Hampe et al., 2007) suggests that multiple environmental and genetic factors contribute to the disease pathogenesis. The T300A allele of ATG16, which is associated with the increased susceptibility to Crohn's disease, is located near the C'-terminal of the linker region between the coiled coil and the WD40 repeats. The T300A polymorphism, as part of a caspase-cleavage motif, potentiates caspase-3 and caspase-7 mediated degradation of Atg16, and increases IL-1 β production as a response to invading bacteria (Lassen et al., 2014, Murthy et al., 2014). ATG16 T300A harbouring HeLa and CaCo-2 cells are less effective in mounting autophagy in response to starvation; while intracellular clearance of *Salmonella typhimurium* (Kuballa et al., 2008) and *Yersinia enterocolitica* (Murthy et al., 2014) is also impaired.

A fraction of Atg16 associates with Nod1 and Nod2 on the plasma membrane (Travassos et al., 2010). Nod1 and Nod2 proteins recognize bacterial peptidoglycans and induce the recruitment of ATG16 to the site of bacterial entry, which triggers autophagy. Notably, Atg16 interacts with Nod1/2 in the absence of Atg5 and also in the absence of bacteria. The interactions with Nod1/2 or with TMEM59 respectively are both suggested links between intracellular bacterial detection and autophagy activation (Travassos et al., 2010, Boada-Romero et al., 2013).

Atg16 hypomorphic mice (Atg16HM, with low expression rate) have been previously studied in context of autophagy and inflammation (Cadwell et al., 2010). Having a direct role in the control of inflammasome activation, decreased expression in hypomorphic mice results in exacerbated intestinal inflammatory response, when induced by dextran sulphate sodium (Saitoh et al., 2008) or by murine norovirus (MNV) infection (Cadwell et al., 2010). Loss of Atg5 and decreased Atg16 expression lead to a similar impairment of Paneth cell lysozyme secretion (Cadwell et al., 2010), implicating a selective vulnerability of Paneth cells to autophagy-dysregulation in the intestine.

Constitutive and conditional knockout animal models represent a valuable tool to elucidate the role of specific proteins in the autophagy pathway. Currently existing autophagy-gene defects in mice are summarised in Table 1.1. (Kundu et al., 2008), (Sou et al., 2008, Read et al., 2011, Klionsky et al., 2012, Komatsu et al., 2005, Kuma et al., 2004, Fimia et al., 2007, Gan et al., 2006); (Saitoh et al., 2008) (Cadwell et al., 2010, Nemazanyy et al., 2013, Jaber et al., 2012) (Kojima et al., 2015, Zhang et al., 2013, Cann et al., 2008).

gene (homologous gene in mice)	characteristics, function in autophagy	loss-of-function mutant phenotype in mice
Atg1 (Ulk1/2)	Ser/Thr kinase, integrates upstream signalling pathways in the induction of autophagy	ULK1 $-/-$: viable, no defect in autophagy, reticulocytosis, transient defect in organelle clearance in erythrocytes
Atg3	E2-like enzyme, facilitates LC3-I conjugation to PE	Atg3 $-/-$: neonatal lethal, autophagy defect, decrease in plasma amino-acid levels in cesarean-section born starved neonates
Atg4b	cystein protease to cleave the microtubule-associated protein 1 (MAP1) light chain 3 (LC3), also to aid recycling of LC3 from autophagosomes	Atg4b $-/-$: viable, spheroid bodies in the deep cerebellar nuclei and in the vestibular nuclei, motor impairment
Atg4c	cystein protease to cleave the microtubule-associated protein 1 (MAP1) light chain 3 (LC3), also to aid recycling of LC3 from autophagosomes	Atg4c $-/-$: viable, decreased autophagy and locomotor activity upon starvation, increased susceptibility to carcinogen-induced fibrosarcoma
Atg5	autophagosome expansion, forms complex with Atg12 and Atg16	Atg5 $-/-$: neonatal lethal, autophagy defect, decrease in plasma amino-acid levels in cesarean-section born starved neonates Atg5 cKO in CNS: neurodegeneration, accumulation of ubiquitinated protein aggregates
Atg6/Vps30 (Becn1)	Beclin-1, component of the PI3K complex	Atg6 $-/-$: embryonic lethal by E7.5 with defects in proamniotic canal closure, Atg6 $+/-$: heterozygous mice spontaneously develop tumours

Atg7	E1-like enzyme, facilitates Atg12–Atg5 and Atg8–PE formation	Atg7 $-/-$: neonatal lethal, autophagy defect, decrease in plasma amino-acid levels in cesarean-section born starved neonates, Atg7 cKO in CNS: neurodegeneration, accumulation of ubiquitinated protein aggregates
Atg8 (Map1lc3)	Ubiquitin-like protein, cleaved from microtubule-associated protein 1A/1B light chain 3B (MAP-LC3b), conjugated to PE to elongate and seal the PAS / isolation membrane into an autophagosome	Map1lc3 $-/-$: no defect in basal autophagy, normal phenotype
Atg8 (Gabarap)	GABA-A-receptor-associated protein, conjugated to PE to elongate and seal the PAS / isolation membrane into an autophagosome	Gabarap $-/-$: no defect in basal autophagy, altered epithelial ion transport in renal brush-border membranes; increased mortality in sepsis models
Atg9a	integral membrane protein of unknown function, located at various intracellular membranes	Atg9a $-/-$: neonatal lethal, autophagy defect; enhanced production of IFN- β in Atg9a-knockout MEFs upon dsDNA stimulation
Atg16	autophagosome expansion, forms complex with Atg5 and Atg12	Atg16 $-/-$: neonatal lethal, Atg16 attenuated (low expression) and Atg16 cKO in Paneth cells: impaired innate immunity
Atg17 (FIP200)	forms a protein scaffold with Atg29 and Atg31 for pre-autophagosomal structure (PAS) or isolation membrane (IM) formation, binds Atg13	FIP200 $-/-$: embryonic lethal by E16.5 due to heart and liver malformation, FIP200 osteoblast cKO: terminal osteoblast differentiation impaired
Vps15	Ser/Thr kinase, component of the PI3K complex	Vps15 $-/-$: lethal before E7.5, Vps15 muscle KO: myopathy,

		accumulation of lysosomes and autophagosomes, glycogen accumulation in muscles
Vps34 (PIK3C3/VPS34)	protein sorting to the lysosome-like vacuole in yeast, the only PI 3-kinase in eukaryotes	PIK3C3 cKO in sensory neurons: viable, canonical autophagy defect but noncanonical autophagy functional, motor impairment, sensory neuron degeneration accumulation of ubiquitinated protein aggregates
n.k. in <i>S. cerevisiae</i> (Ambra1)	required for Becn1–Vps34 interaction, link to microtubules	Ambra1 gene-trap mutants (Ambra1 gt/gt): embryonic lethal, autophagy defect, neural tube defect, excessive apoptosis in various CNS areas

Table 1.1. Autophagy mutant mice. Selective loss of autophagy pathway components lead to a diverse array of phenotypes.

1.2. Semliki Forest Virus infection in Atg16 KO mouse tissues

1.2.1. Semliki Forest Virus (SFV): overview, epidemiology

Semliki Forest Virus (SFV) is an enveloped, positive single-stranded-RNA virus and is a member of the family *Togaviridae*, genus *Alphavirus*). SFV, together with its phylogenetically closest relatives Chikungunya and Ross River viruses is a member of the Old World Alphavirus group. All alphaviruses are arthropod-borne viruses (arboviruses); able to multiply both in vertebrates and insects (arthropods); and transmitted to man via insect bite. Man is generally considered to be a dead end of infection; however, urban surroundings and human-biting mosquitoes create a favourable environment for human to human transmission. Alphaviruses are clinically subtyped into Old and New World alphaviruses (Fig.1.4.a). Rash, fever, fatigue and arthralgia are characteristic symptoms of Old World alphavirus infection, while encephalitis is typically caused by New World alphaviruses (Fields et al. 2007). These two subgroups have evolved separately in the postglacial age, and the adaptation to host species has resulted in different replication strategies. Old World alphaviruses, like SFV and Sindbis virus (SINV) results in nearly 100% mortality of infected cells, due to the toxic effect of its non-structural protein nsP2, which inhibits host cell transcription as part of an immune evasion strategy. Conversely, New World alphaviruses, like Eastern equine encephalitis virus (EEEV) and Venezuelan equine encephalitis viruses (VEEV) use a capsid-dependent transcriptional interference, which results in a milder cytopathology and persistence of the virus in the host cell (Garmashova et al. 2007; Akhrymuk et al. 2012).

Alphaviruses continue to be of public health concern, as epidemic encephalitis outbreaks in the Western hemisphere may affect humans and livestock (Garmashova et al. 2007). A large-scale Chikungunya virus (CHIKV) epidemic occurred in Africa and India between 2004-2008, causing significant morbidity, and a number of mortalities in some populations (Staples et al. 2009). Sindbis virus and Ross River virus, endemic in Northern Europe and in Australia, cause epidemic polyarthritis (Laine et al., 2004). SFV infection is mostly asymptomatic or benign in humans. An exception to that was a single documented epidemic in the Central-African Republic; marked by fever, myalgia, arthralgia and headache as well as long-lasting sequelae (arthritis) in some patients (Mathiot et al. 1990). A single fatality in a laboratory worker was also documented (Willems et al. 1979), possibly due to inhalation of virus containing aerosol and with immunodeficiency in the patient history. Notwithstanding this incident, SFV is safe to use, and has been used in thousands of labs around the world; as a model system for virus infection studies and a potential vector for gene delivery.

The prototype SFV was isolated in 1942 from pooled mosquitoes in Uganda (Smithburn et al., 1946), followed by other isolations. Laboratory strains are derived from this virulent strain (designated as L10) and from the avirulent isolate, designated as A7 (McIntosh et al., 1961). Over many passages in cell cultures, the L10 strain has lost its original virulence, probably due to accumulated mutations (Atkins, 2013). Further research was greatly aided by the reconstruction of a highly infectious SFV strain using in vitro transcription from a cDNA clone of L10. As this cDNA clone pSP6-SFV4 appeared to have the highest infection yield (PFU/ μ g of RNA) in BHK cells, since then, this SFV strain (SFV4) has been designated as the prototype virus in many experimental protocols (Liljeström et al., 1991). Throughout this thesis, SFV4 strain will be referred to as SFV.

In contrast to humans, SFV infection causes rapidly progressing, lethal encephalitis or persistent infection in laboratory mice. The virulence of SFV is age-dependent, all strains causing lethal encephalitis in neonatal and suckling mice, up until the 12th

postnatal day. From postnatal day 14, the experimentally used strains SFV4, L10, V13 and Osterrieth strains are virulent, while A8, A7, A7(74), as well as MRS MP 192/7 strains are avirulent (Fazakerley 2002). All SFV strains are able to replicate in different types of muscles (skeletal, smooth, and cardiac muscle tissue), as plasma titer peaks within 24 h. The virus (independent from strain virulence) then passes the blood-brain barrier. Virulent SFV rapidly escapes perivascular foci by infecting neurons and oligodendrocytes. Viruses from an avirulent (e.g. A7(74)) strain remain confined to perivascular foci, as infection is only productive in maturing neurons undergoing axonogenesis and synaptogenesis (Fazakerley 2002). Restricted virulence can be experimentally overcome by the gold compound myocrisin (sodium aurothiomalate), which induces the formation of smooth-membrane vesicles in neurons, necessary for the virus replication (Pathak and Webb 1983; Scallan and Fazakerley 1999).

SFV strains in tissue cultures do not differ in their cell tropism as they successfully infect neurons and oligodendrocytes, while sparing astrocytes. *In vivo*, viral replication of the avirulent A7(74) strain is restricted to neurons and occurs at a relatively low multiplication rate, while the virulent L10 strain proliferates rapidly both in neurons and oligodendrocytes – hence, the extensive cytopathic damage reaches a lethal threshold. Loss of neuropathogenicity has been attributed to a mutation in the non-structural protein nsP3 of A7(74) (Tuittila and Hinkkanen, 2003) however, the exact mechanism remains to be elucidated. Reportedly, SFV-induced apoptosis is mediated by the intrinsic apoptosis pathway; leading to a loss of mitochondrial membrane potential, cytochrome-c release, and caspase activation, with no evidence for the involvement of death receptors or ligands (Urban et al., 2008). Virus proteins contribute to apoptosis by inducing ER-stress (Barry et al., 2010b).

1.2.2. Semliki Forest Virus structure and life cycle

The SFV virion particle consists of a 40 nm icosahedral nucleocapsid; surrounded by a glycoprotein envelope with 80 protruding, petal-shaped spikes; together with a diameter of 70 nm. The spikes are composed of a heterotrimer of E1, E2 and E3 glycoproteins, and mediate host receptor recognition and viral entry. 240 copies of the capsid protein encapsulate the 11.7-kb positive ssRNA genome, containing a 7-methylguanosine cap at its 5' end and a polyadenylate chain at its 3' terminus. The virus genome encodes four nonstructural proteins (nsP1-4), the capsid protein C and the E1, E2, E3 envelope glycoproteins. The virion proteins are translated from a 26S subgenomic RNA (Fields et al., 2007).

Alphaviruses enter the cells by endocytosis (Kielian et al., 2010), the exact mechanism, however, still holds many unanswered questions. Various membrane proteins and glycosaminoglycans have been hypothesised to serve as receptors of the E2 envelope glycoprotein, to facilitate the ingestion of SFV into clathrin-coated endocytic vesicles (Helenius et al., 1978, Smit et al., 2002). The E1 envelope protein regulates the fusion of virus and host cell membranes, and the acidic environment of endosomes leads to the dissociation of the E1-E2 complex (Kielian et al., 2010). Cholesterol and sphingolipids of endosomal membrane are also essential for the fusion step (Wilschut et al., 1995), which is followed by the release of the nucleocapsid into the cytosol. 60S ribosome subunits are essential for the uncoating and release of viral RNA (Singh and Helenius, 1992). Due to its positive polarity, the genomic RNA functions as the messenger RNA for the translation of the replicase polyprotein, which is cleaved to yield the nonstructural proteins (nsP1-4). Once transcribed, combinations of the four nsPs form replication complexes for the synthesis of the negative-strand template, the positive-strand genomic and subgenomic RNAs (Kääriäinen and Ahola, 2002). Endosomal and lysosomal

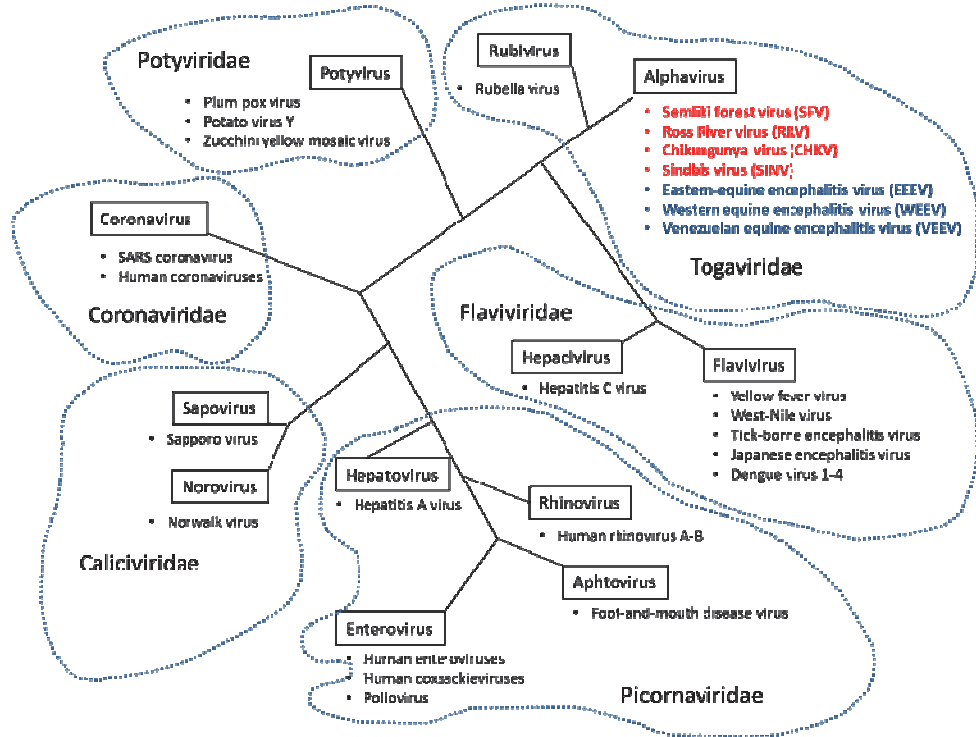
membranes bind nsPs and rearranged to form type I cytopathic vacuoles, the sites for the virus replication (Peränen et al., 1995, Kujala et al., 2001).

SFV replicates via its negative-stranded intermediate, that also yields a 3' end subgenomic messenger RNA (also capped and polyadenylated) for the translation of the polyprotein precursor the structural proteins. The capsid protein, cleaved immediately after translation of the structural polyprotein, forms complex with the ribosome and recognizes the 5' end packaging signal on the viral genomic RNA (Leung et al., 2011). The E2-E3 glycoprotein precursor p62 forms a heterodimer with the E1 glycoprotein and are inserted into the ER with the help of the E3 signal sequence, transported via the Golgi to the cell surface, where it is cleaved into E2 and E3 (note the difference between virus p62 and the p62/SQSTM1 in host cells). The viral 6K membrane protein is necessary for the budding step to release the virus from the infected cell (Liljeström et al., 1991). The budding virion incorporates the capsid-ensheathed genomic RNA; the membrane glycoproteins E1, E2, a small amount of 6K, and – uniquely among the known alphaviruses – E3 as well (Garoff et al., 1974). For an overview of SFV life cycle see Fig.1.4.c.

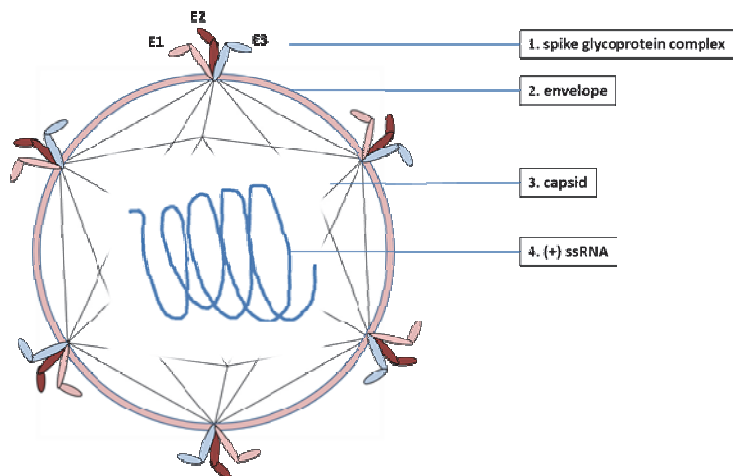
1.2.3. Autophagy in Semliki Forest Virus infection

Our understanding of the contribution of autophagy to Alphavirus infection and antiviral defence is rather limited. Chikungunya virus (CHIKV) has been shown to trigger oxidative stress in host cells together with unfolded protein response (UPR) in the ER. Both mechanisms contribute to autophagy induction; which, in the case of CHIKV infection, is cell-protective by inhibiting apoptosis and tissue-protective by reducing viral propagation (Joubert et al., 2012). In contrast to its evolutionary proximity to CHIKV, an interaction between SFV infection and autophagy induction has not been confirmed. The only study in the literature that tested SFV infection in

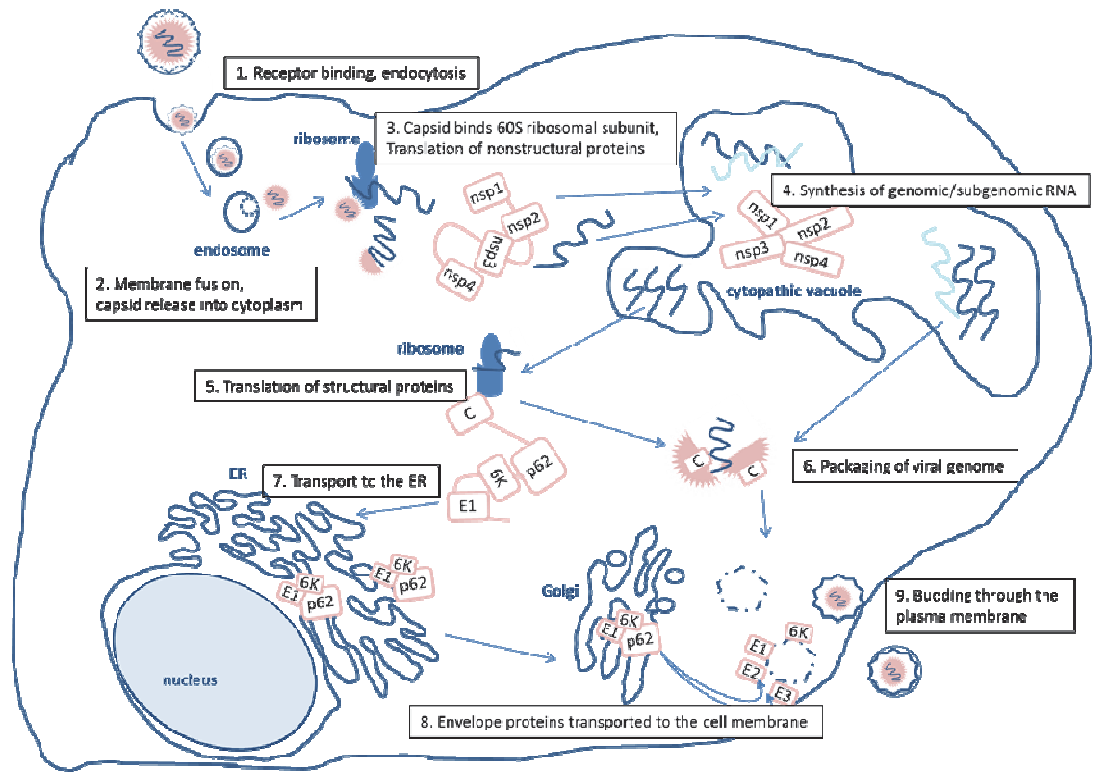
a



b



c



d

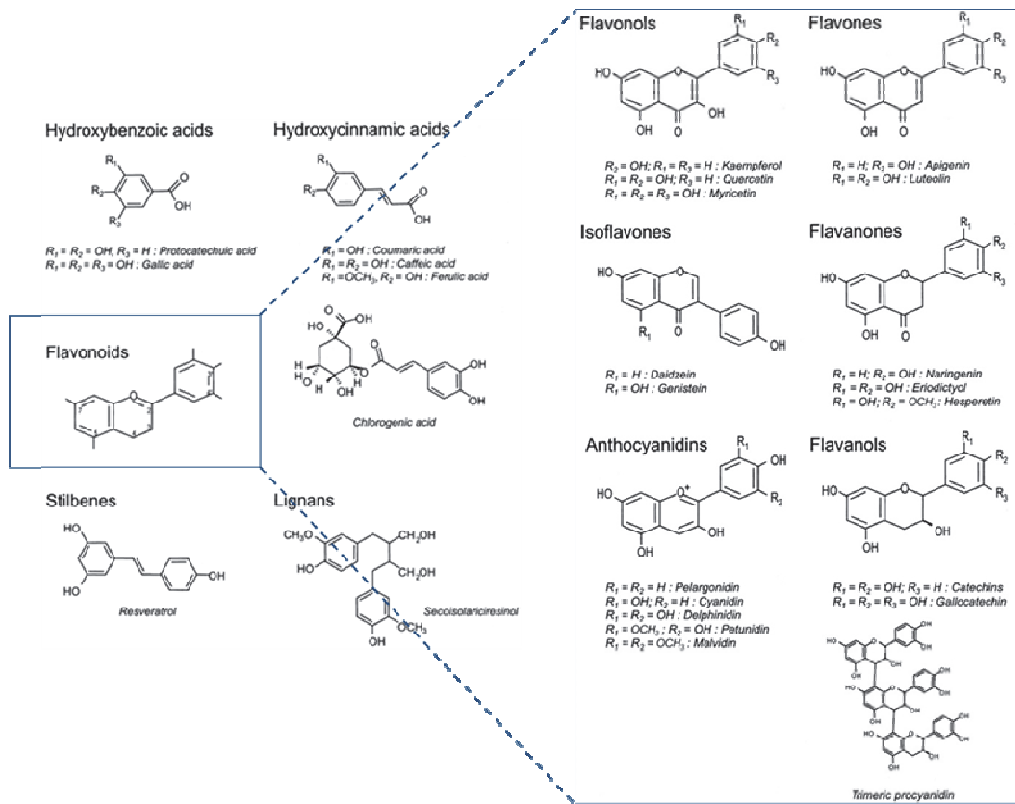


Fig. 1.4. a) Phylogenetic tree of (+)-strand RNA viruses. red : old-world alphaviruses; blue: new-world alphaviruses **b) Schematic model of SFV structure and c) SFV life-cycle** 1. receptor-mediated endocytosis 2. membrane fusion and capsid release 3. uncoating of viral RNA 4. translation of the non-structural polyprotein 5. synthesis of (-) strand RNA 6. synthesis of (+) strand genomic RNA 7. synthesis of (+) strand subgenomic RNA 8. translation and cleavage of the structural polyprotein 9. packaging of the genomic RNA into the capsid 10. transport of the envelope proteins into the ER and to 11. the Golgi 12. final virion assembly and release. (+)-strand RNA: dark blue, (-)-strand RNA: light blue. **d) Molecular structure of the four polyphenol classes: stilbenes, flavonoids lignans and phenolic acids.** Adapted from Manach and colleagues (Manach et al., 2004).

the context of autophagy found no effect on the mTOR pathway, and conversely, no effect of autophagy on viral entry or replication (Eng et al., 2012). This study identified the inhibitory effect of the viral spike protein complex on autophagosome trafficking to the lysosome, leading to an accumulation of autophagosomes in human osteosarcoma cells and other cell lines (Eng et al., 2012). As brain is the primary target organ for SFV, of particular interest is the role of autophagy in the context of alphavirus infection in neuronal models.

1.3. Autophagy induction *in vitro* by red wine polyphenols

1.3.1. Dietary polyphenols: promises and pitfalls in disease prevention

The search for novel ways of therapy or prevention of age-related cardiovascular and neurodegenerative diseases highlighted the effect of nutritional elements, especially that of plant polyphenols (Del Rio et al., 2010). Characterized by multiple hydroxybenzyl moieties, over 8,000 different polyphenols have been found in the plant kingdom, and several hundred are part of the human diet (Rahman et al., 2006). According to the number of phenol rings and to the structural elements that bind these rings to one another, polyphenols are classified into five major groups: phenolic acids (hydroxybenzoic acids and hydroxycinnamic acids), flavonoids, stilbenes, and lignans (Fig.1.4.d). In addition, there are more polyphenols that don't fit into this classification like curcuminoids and the anticoagulant precursor 4-OH-coumarin (Perez-Jimenez et al., 2010). Flavonoids and phenolic acids are the most abundant polyphenols in the human diet (Perez-Jimenez et al., 2010).

The flavonol quercetin (3,3',4',5,7-pentahydroxyflavone, QRC) is highly concentrated in black elderberry (42mg/100g) and in dark chocolate (25mg/100g); approx. 4mg QRC aglycon and glucosylated forms are found in 100 ml red wine (Neveu et al., 2010). The most important sources are tea, onions and apples, the daily intake in Western diet is approximately 16 mg/day (Hertog et al., 1993). QRC bioavailability is highly variable and largely dependent on the glycoside form or the food matrix, with the highest plasma levels observed after wine consumption (Goldberg et al., 2003). QRC-glucoside is readily absorbed through the small

intestinal epithelium, compared to other forms (Manach et al., 2005). QRC conjugates QRC-3-*O*-glucuronide, 3'-*O*-methyl-QRC-3-*O*-glucuronide, and QRC-3'-*O*-sulfate can be found in human plasma after dietary intake, while the aglycon and the intact glycoside is absent (Day et al., 2001). A unique feature of QRC metabolites is their stability and long retention time in circulation: a baseline plasma level of 0.05 μ M can be obtained after overnight fast (Egert et al., 2008). Volunteers who took 150 mg QRC daily (equivalent to 5 non-processed white onions (Crozier et al., 1997)) retained micromolar plasma concentrations of QRC sulfates and glucuronides one day after the last ingestion.

The flavanol monomer (-)-epicatechin (EC) is found in red wine at concentrations of 3.78mg/100ml. The richest source in human diet are cocoa powder with up to 158mg/100g and dark chocolate with 70mg/100g EC, but milk chocolate may also contain 15mg/100g. Amongst fruits, cider apple stands out with its EC concentration of 29mg/100g, followed by blackberry with 11mg/100g (Neveu et al., 2010). Baseline levels of EC range between 0.01-0.08 μ M (Rein et al., 2000), concentration peaks at 0.2-0.8 μ M following the consumption of a chocolate bar (Rein et al., 2000, Baba et al., 2000) with high interindividual variability observed in both studies.

Anthocyanins occur most concentrated in the skins of berry fruits (Gao and Mazza, 1994) and significant quantities are consumed in red wine. The major red wine anthocyanins are malvidin-3-*O*-glucoside (Ma3G; 9.97mg/100ml), delphinidin-3-glucoside (1.06mg/100ml); peonidin-3-*O*-glucoside (Pe3G; 0.82mg/100ml) and cyanidin-3-*O*-glucoside (Cy3G; 0.21mg/100ml). Berry fruits have their specific anthocyanin profile: Cy3G is enriched in blackberry (139mg/100g) and black elderberry (794mg/100g); Pe3G is found at high concentrations in black grape (6mg/100g), lowbush blueberry (5.5mg/100g), lingonberry (4mg/100g) and American cranberry (4mg/100g). Pe3G is also found in human plasma as the major methylated metabolite of Cy3G (Kay et al., 2005). Ma3G is also concentrated in black grape (39mg/100g) and in lowbush blueberry (26mg/100g) (Perez-Jimenez et

al., 2010). Recent evidences also showed anthocyanin bioavailability even by relatively low intake (Milbury et al., 2010). Anthocyanins may peak at 0.2-0.5 μM range in serum and undergo extensive metabolism (Kay et al., 2004, Kay et al., 2005).

Resveratrol (RSV) (2,5,4'-trihydroxy-trans-stilbene), found in greater quantities in grape skin, is ingested mainly with red wine consumption (0.27mg/100ml); peanuts, red cabbage, blueberries and bilberries contribute to a lesser extent (Lyons et al., 2003, Siemann and Creasy, 1992, Crozier et al., 2009). Free RSV was detected at trace levels (20 nM) after ingestion of 600 ml red wine (approx. 3 glasses) in serum, while metabolites RSV 4-glucuronide and RSV 3-glucuronide add up to 2 μM (Vitaglione et al., 2005, Goldberg et al., 2003).

Proanthocyanidins (procyanidin dimers and trimers), found in significant quantities in red wine with mean concentrations of procyanidin dimer B1 4.14mg/100ml, procyanidin dimer B2 4.97mg/100ml, procyanidin dimer B3 9.47mg/100ml, procyanidin dimer B4 7.29mg/100 ml, procyanidin trimer C1 2.56mg/100ml and procyanidin trimer T2 6.71mg/100 ml. Altogether they are a relatively less studied group of polyphenols. Originally they were thought to be metabolised completely into monomers (flavanols), however some evidence suggest their absorption into plasma in their native form (Serra et al., 2010, Perez-Jimenez et al., 2010).

The aforementioned polyphenols are overrepresented in a proposed "neuroprotective diet", containing dark berries and red wine. Epidemiological evidence supports protective effect of red wine against Alzheimer's Disease and cognitive decline; as well as maintaining cognitive health and protecting against neurodegenerative, cardiovascular and cerebrovascular diseases by flavonoid-rich berry diet (Orgogozo JM, 1997, Lindsay et al., 2002, Nooyens et al., 2013). The protective role of RSV has also been demonstrated in other age-associated illnesses, like cardiovascular diseases with secondary effect on cognitive function (Baur and Sinclair, 2006). While a great number of *in vivo* and *in vitro* experiments

also demonstrated protective role in various form of cancer, epidemiological results are less convincing. A Swiss study found significant inverse association between breast cancer incidence and RSV intake from grapes, but not for wine (Levi et al., 2005). More epidemiological evidence have been gathered to link flavone and flavonol consumption to cancer protection (Bosetti et al., 2005).

Red wine is most commonly produced from cultivars of the grape species *Vitis vinifera* (and, less commonly from *V. labrusca*, *V. riparia*, *V. rotundifolia*, *V. aestivalis* and their hybrids). Polyphenols are extracted from grape during vinification: white vinification method separates the juice from the solid parts after crushing the grape, while red wine vinification leaves grape juice fermented up to 3 weeks in contact with the grape skin and seeds. Polyphenols are more concentrated in grape solids: fermentation allows more polyphenols diffusing in the juice, consequently, polyphenol content is higher in red wine than in white wine.

The average total polyphenol content of red wines is 216mg/100ml while only 32mg/100ml for white wine (Perez-Jimenez et al., 2010). Anthocyanins (22.7mg/100ml), proanthocyanidins (29.4mg/100ml), flavanol monomers (11.5mg/100ml) and flavonols are the most abundant flavonoids in wine. Glycosilated malvidin makes up approx. 70% of total anthocyanidins. The main red wine flavanols are (+)-catechin (6.8 mg/100 ml) and (-)-epicatechin (3.8 mg/100 ml); the major flavonols in red wine are QRC-3-O-rhamnoside (1.16 mg/100 ml) and QRC-3-O-glucoside (1.14mg/100 ml). Being the main dietary source for RSV, many studies focused on this polyphenol compound to explain the health benefits of red wine; notwithstanding that RSV is a relatively minor part of total phenolic content of red wine (0.27mg/100ml for RSV (aglycone) vs 0.62mg/100ml for RSV-3-O-glucoside).

1.3.2. Polyphenol bioactivity and autophagy induction

While experimental studies have been nearly unanimous about their benefits, less clear is how dietary polyphenols influence cell homeostasis. Initial studies on polyphenols attributed their protective effects against cardiovascular, neurodegenerative and malignant diseases to antioxidant properties (Waterhouse et al., 1996, Rice-Evans et al., 1996). Recent studies point to a bioactivity beyond scavenging reactive oxygen radicals (Spencer, 2009, Kroon et al., 2004, Hollman et al., Schewe et al., 2008), and an increasing evidence suggests an interplay with cellular signalling pathways; with implication to autophagy as a candidate target in these studies.

Autophagy activation has been demonstrated *in vitro* by various polyphenols, including RSV (Cantó et al., 2010, Vingtdeux et al., 2010, Morselli et al., 2010), QRC (Wang et al., 2011); apigenin (Tong, Smith et al. 2012), kaempferol (Huang WW, 2013), EGCG (Kim et al., 2013) and curcumin (Aoki et al., 2007, Shinojima et al., 2007, O'Sullivan-Coyne et al., 2009). Until now, RSV has been the only polyphenol with *in vivo* confirmed autophagy activation in *C. elegans* and in mouse heart (Gurusamy et al., 2010, Morselli et al., 2010). mTOR-dependent and –independent pathways have been both implicated in polyphenol-induced autophagy (Wang et al., 2011, Vingtdeux et al., 2010, Morselli et al., 2011, Xiao et al., 2013).

2. MATERIALS AND METHODS

2.1. Materials

Chemicals not specified were purchased from Thermo Fisher Scientific (UK), Sigma-Aldrich (UK), Roche (UK) and Melford (UK). Solutions and buffers were prepared as described in Molecular cloning: a laboratory manual by Maniatis et al. (Wood, 1983) unless specified elsewhere. Chemicals and other consumables are listed below as (Supplier #Product code).

DNA studies

dATP (Roche #1051440), dTTP (Roche #1051482), dGTP (Roche #1051466) and dCTP (Roche #1051458)

Taq DNA polymerase (Roche #1647687)

Taq polymerase "Taq-O-D" prepared by D.Divekar (U. Mayer lab)

10X Taq Buffer with KCl and 15 mM MgCl₂ (Thermo Scientific #B16)

Atg16 genotyping primers:

#224:CTGAACAGTTAAGTTCCTAG and

#226 CCAAGAGACACTGACATAGG

Agarose (Melford # MB1200)

Orange G loading dye (Sigma #O3756)

1kB plus DNA ladder (Life Technologies #10787-018)

Cell cultures

Chinese hamster ovary cells stably expressing GFP::LC3 (CHO GFP-LC3)

green monkey kidney epithelial cells (Vero)

human embryonic kidney cells stably expressing GFP::LC3 (HEK-293 GFP-LC3)

human neuroblastoma cells SH-SY5Y

mouse embryonic fibroblast WT

mouse embryonic fibroblast Atg5 (-/-)

mouse embryonic fibroblast Atg16 (-/-) harvested by Ms. Laura Vaux

Cell culture media

Dulbecco's Modified Eagle Medium (DMEM, with 1000mg/l glucose, Gibco #11885-076)
Eagle's Minimum Essential Medium (EMEM, Sigma #M2279)
Fetal bovine serum (FBS, Gibco #10270-106)
Ham's F-12 Nutrient Mixture (Sigma #N4888)
HBSS (Sigma # H1641)
L-Glutamine (Gibco #25030-081)
Na-Pyruvate (Sigma #S8636)
Neurobasal medium (Gibco #10888-022)
Nonessential amino acids (NEA, Sigma#M7145)
PBS Ca-and Mg-free (Life Technologies #10010-015)
Penicillin (100 U/ml), Streptomycin (100 µg/ml) (P/S, Gibco #15140-122)
Trypsin/EDTA (T/E, Gibco #R-001-100)

Virology studies

Crystal Violet (Sigma #C3886S)
SeaPlaque Agarose (Lonza #50100)
Semliki Forest Virus prototype strain SFV4 (Liljeström et al., 1991)

Autophagy and polyphenol studies

Bafilomycin (Sigma #1793)
Torin-1 (TOCRIS #4247)
Wortmannin (Sigma # W1628)
(-)-epicatechin (Fluka #68097)
cyanidin-3-O-glucoside (Sigma #52976)
malvidin-3-O-glucoside (Fluka #04288)
peonidin-3-O-Glucoside (Sigma #40796)
protocatechuic acid (Fluka #03930590)
quercetin (Sigma #Q49510)
resveratrol (Sigma #R5010)

Histology, Immunohistochemistry

Clearene (SurgipathMedical Industries #K855109)
Donkey Serum (Abcam, #ab7475)
DPX mounting medium (Thermo Scientific #10050080)
Eosin-Y (Sigma # 230251)
Hematoxylin Solution, Harris Modified (Sigma #HHS16)
Hoechst 33342 (Molecular Probes # H1399)
Normal Goat Serum (Gibco, # PCN5000)
OCT embedding medium (Thermo Scientific #12634077)
Toluidine blue (Sigma # 16030)
Vectashield® Mounting Medium (Vector Labs #H1000)

Antibodies

Antibodies used are detailed in Table 2.1. Mouse anti-SFV antibodies are in-house antibodies from the University of Tartu, received as a kind gift from Prof. Andres Merits (University of Tartu, Institute of Technology, Tartu, Estonia)

Other chemicals

Acrylamide/Bis Solution (30%, Acrylamide: Bis 37.5:1; Bio-Rad #161-0158)
cOmplete proteinase inhibitor (Roche #11836170001)
DMSO (Sigma #D2650)
Formalin solution 10%, neutral buffered (BDH # 9713.1000)
Paraformaldehyde prilled (Sigma #441244)
Precision Plus Protein™ Standards protein marker (BIO-RAD #161-0373)
Recombinant mouse α -Synuclein, produced in E.coli (ATGen Global #ATGP0619-03)
TEMED [N,N,N',N'-Tetramethylethylenediamine] (Melford #T3100)
Tween-20 (Sigma #P1379)

Antibody (# product code)	manu- facturer	dil. (IHC)	dil.(WB)	notes
mouse anti-Actin	Abcam	n.a.	1:2000	
rabbit anti-Atg5 #A0731	Sigma	1:200	n.a.	
mouse mAb anti-Atg16l1 #M150-3	MBL	n.a.	1:1000	clone 1F12
rabbit anti-Atg16l1 #PM040	MBL	1:200	1:2000	
rabbit anti-Atg16l1 #AP1817b	Abgent	1:200		
rabbit anti- α -Synuclein #AB5038	Chemicon	1:200	1:2000	
rabbit mAb anti- α -Synuclein #4179	CST	1:100	1:1000	clone D37A6
rabbit anti- α -Synuclein (NT) #bs-0009R-BSS	bioss	1:100	1:1000	
mouse mAb anti- α -Synuclein #610786	BD	no stain	1:1000	clone 42
mouse hybridoma supernatant mAb anti- α -Synuclein & β -Synuclein #H3C	DSHB	no stain	1:1000	clone H3Cp2A51d8
rabbit anti- β -amyloid (1-42) #AB5078P	Chemicon	1:200	1:2000	
rabbit anti-LC3 #ab51520	abcam	1:200	1:2000	
rabbit anti-LC3B #L7543	Sigma	1:200	1:2000	
guinea pig anti-p62 (CT)	Progen	1:500	1:2000	
mouse anti-dsRNA	in house, UEA	1:1000	n.a.	
rabbit hybridoma supernatant anti-SFV capsid	University of Tartu	1:1000	1:10000	
rabbit hybridoma supernatant anti-SFV nsP1	University of Tartu	1:1000	1:10000	
rabbit hybridoma supernatant anti-SFV nsP3	University of Tartu	1:1000	1:10000	
mouse mAb anti-Tau (Tau46) #4019	CST	1:200	1:1000	
rabbit Anti-phospho-Tau (pSer ^{199/202}) #T6819	Sigma	1:500	1:2000	
mouse mAb anti-TDP43 #MABN45	Chemicon	1:200	1:1000	clone 3H8
mouse mAb anti-mono- and poly-ubiquitinated conjugates #BML-PW8810-0100	Enzo	1:200	1:1000	clone FK2
mouse mAb anti-WIPI1 #WH0055062M2	Sigma	1:1000	n.a.	clone 3C1
Alexa Fluor [®] 594 donkey anti-mouse IgG (H+L) # A21203	Molecular Probes	1:500	n.a.	
Alexa Fluor [®] 488 donkey anti-rabbit IgG (H+L) #A21206	Molecular Probes	1:500	n.a.	
Alexa Fluor [®] 594 donkey anti-rabbit IgG (H+L) #A21207	Molecular Probes	1:500	n.a.	
Alexa Fluor [®] 647 donkey anti-mouse IgG (H+L) #A31571	Molecular Probes	1:500	n.a.	
Alexa Fluor [®] 647 donkey anti-rabbit IgG (H+L) #A31573	Molecular Probes	1:500	n.a.	
Alexa Fluor [®] 488 goat anti- guinea pig IgG (H+L) #A11073	Molecular Probes	1:500	n.a.	
Alexa Fluor [®] 594 goat anti- guinea pig IgG	Molecular	1:500	n.a.	

(H+L) # A11076	Probes			
Alexa Fluor® 488 goat anti-mouse IgG (H+L) # A11029	Molecular Probes	1:500	n.a.	
Alexa Fluor® 594 goat anti-mouse IgG (H+L) # A-11005	Molecular Probes	1:500	n.a.	
Alexa Fluor® 680 AffiniPure Goat Anti-Mouse IgG (H+L) # 115-625-166	Jackson Immuno Research	n.a.	1:10000	
Anti-Mouse IgG (whole molecule)–peroxidase # A9044	Sigma	n.a.	1:1000	Dot blot
Alexa Fluor® 488 goat anti-rabbit IgG (H+L) # A-11008	Molecular Probes	1:500	n.a.	
Alexa Fluor® 594 goat anti-rabbit IgG (H+L) # A-11012	Molecular Probes	1:500	n.a.	
IRDye® 680LT Goat anti-Mouse IgG (H + L) #926-68020	LI-COR	n.a.	1:10000	
IRDye® 800CW Goat anti-Mouse IgG (H + L) #926-32210	LI-COR	n.a.	1:10000	
IRDye® 680LT Donkey anti-Rabbit IgG (H + L) #926-68023	LI-COR	n.a.	1:10000	
IRDye® 800CW Goat anti-Rabbit IgG (H + L) #926-32211	LI-COR	n.a.	1:10000	

Table 2.1. antibodies used in this doctoral research

Buffers, solutions

Coomassie stain: 0.1% (w/v) Coomassie blue R350, 20% (v/v) methanol, and 10% (v/v) acetic acid.

Crystal violet stain: 0.5% crystal violet dissolved in 25% (v/v) methanol

5x Laemmli's sample buffer for SDS-PAGE: 1 ml Tris 1M (pH 6.8), 3.2 ml Glycerol, 3.2 ml SDS 10%, 0.8 ml 2-mercapto-ethanol was mixed and kept on room temperature

Ponceau stain: 0.5% (w/v) Ponceau S, 1% (v/v) acetic acid

PBS/cOmplete: 1 tb cOmplete proteinase inhibitor in 50 ml 1xPBS

PBS-T0.1: 1xPBS, Tween 0.1 % (m/m)

4%PFA/PBS: 4g Paraformaldehyde (prilled) was added to 1xPBS, heated while stirring in a chemical fume cupboard

Tissue lysis buffer for DNA extraction: 0.1 M Tris/HCl, 0.2 M NaCl, 0.2 % (w/v) SDS, 5 mM EDTA, 0.1 mg/ml Proteinase K

TBS-T0.1: 1xTBS, Tween 0.1 % (m/m)

TBS-T0.5: 1xTBS, Tween 0.5 % (m/m)

TBS-T0.5-milk: 5g skimmed milk powder dissolved in 50 ml 1xTBS, Tween 0.5 % (m/m)

Kits, ready-made buffers

BCA Protein Assay Kit (Thermo Scientific #23225)
Bio-Rad Mini PROTEAN Tetra System (Bio-Rad #165-8000)
Coomassie Plus Protein Assay Kit (Thermo Scientific #23236)
DeadEnd™ Fluorometric TUNEL System (Promega, #G3250)
Luminata Classico Western HRP substrate (Millipore # WBLUC0500)
Pierce® Protein-free T20 (TBS) Blocking Buffer (Thermo Scientific #37571)
T-PER Tissue Protein Extraction Reagent (Thermo Scientific #78510)

Other specified lab equipment

ACCU-CHEK® Compact Plus meter system
Cell culture dishes, multiwell plates and trays (Cellstar #690-160, Cellstar #657-160,
Nunc #156499, Thermo Scientific #178883)
Mr. Frosty™ Freezing Container (Thermo Scientific #5100-0001)
FUJIFILM Luminescent Image Analyzer LAS-3000
GMI Microm HM 520 cryostat
Leica semi-automated Rotary Microtome (Leica #RM2245)
Leica vibrating blade microtome (Leica #VT1000 S)
LI-COR Odyssey CLx Infrared Imager
Zeiss Axioplan-2 upright epifluorescent microscope
Blot Absorbent Filter Paper (Bio-Rad #170-4085)
Immobilon-FL PVDF membrane (Millipore # IPFL00010)
Schleicher and Schuell Membrane Filters (Krackeler #32-10404112)

2.2. Methods

Cell cultures

Vero, MEF, HEK-293 and CHO/GFP-LC3 cells were grown at 37 °C under humidified 5% CO₂ atmosphere in Dulbecco's Modified Eagle Medium (DMEM); supplemented with 10% (V/V) fetal bovine serum (FBS), 100 U/ml Penicillin, 100 µg/ml Streptomycin (P/S), For HEK-293 cell line this medium was supplemented with 1% nonessential amino acids (NEA), in addition to the NEA contained in DMEM. For growing SH-SY5Y cells, the following culture medium was used: a mix of 50% Eagle's Minimum Essential Medium (EMEM) - 50% Ham's F-12 Nutrient Mixture (F-12), supplemented with FBS (10% V/V), P/S (100 U/ml - 100 µg/ml), 2mM L-Glutamine and 1mM Na-Pyruvate. Stock cultures were grown in 25cm², 75cm² and 175cm² dishes, and split at sub-confluency using Trypsin/EDTA. For immunocytochemical analysis, cells were grown on non-gelatinized coverslips. Cells were grown in 6 well plates for preparation of lysates and for virus plaque assays.

Autophagy assays

Autophagy was induced either by amino-acid starvation in HBSS (Sigma), treatment with Torin-1 (TOCRIS) or treatment with the polyphenols detailed in the appropriate section. Control samples were incubated in fresh growth medium. DMSO concentration was kept constant (0.1% when only one DMSO-soluble reagent vs. 0.2%, whenever more than one DMSO-soluble reagents were tested). Autophagy activation was monitored by LC3 immunofluorescence or by LC3-GFP fluorescence. Experiments where autophagosomes were abundant in control samples were excluded from study results.

Autophagy induction

HBSS or Torin assays were used as positive controls for autophagy induction.

1. amino-acid starvation assay

HBSS is an amino acid-free culture medium. Growth medium was removed; wells were washed with PBS; then Hank's Balanced Salt Solution (HBSS, Sigma) was added and cultures were incubated for 3 vs. 6 h.

2. Torin assay

Torin-1 is a potent and selective inhibitor of mTORc1 or mTORc2 kinase function, while not affecting other kinases in the autophagy pathway at low concentrations

(Thoreen et al., 2009). Growth medium was replaced with fresh growth medium containing 250nM Torin-1 and cultures were incubated for 3 vs. 6 h.

Autophagy inhibition

Autophagy was blocked either at the early stage, by inhibiting autophagosome formation or at the late stage by inhibiting autophagosome-lysosome fusion.

1. Wortmannin assay

Wortmannin (Wm) was used to inhibit the upstream membrane trafficking steps. Wm is a specific phosphoinositide 3-kinase (PI3K) inhibitor, used to deplete phosphatidylinositol-3,4,5-trisphosphate (PI(3)P) an indispensable component of the isolation membranes. Wm was dissolved in DMSO and added to the autophagy inducing medium to yield 40 nM final concentrations. In previous studies (Blommaert et al., 1997) higher concentrations were used, while high Wm concentrations were shown to interfere with the endosomal membrane traffic pathways (Reaves et al., 1996). An equally effective inhibition of starvation-induced autophagy can be achieved using 40 nM Wm (unpublished observations).

2. Bafilomycin assay

Bafilomycin A1 (baf-A) is a downstream autophagy inhibitor, which inhibits the autophagosome-lysosome fusion by blocking the vacuolar H⁺ATPase (Yamamoto et al., 1998). baf-A was dissolved in DMSO and added to the medium at concentrations of 100 nM.

Polyphenol treatment

Resveratrol, quercetin, (-)-epicatechin, cyanidin-3-O-glucoside, peonidin-3-O-glucoside and malvidin-3-O-glucoside were dissolved in DMSO. Protocatechuic acid was dissolved in ddH₂O, then filter-sterilized. Polyphenols were used at 0.01 uM to 100 uM final concentrations in the specified culture medium. Incubation time was set to 6 h, DMSO concentration was kept constant throughout the experiments.

Qualitative protein studies

1. Cell fixation

Cells on coverslips were rinsed with PBS and fixed with 4% PFA/PBS for 20' on room temperature, followed by repeated PBS washes. Virus-infected cells were fixed for 6h. Cells were then incubated in 0.5M glycine/PBS for 15' to quench unreacted formaldehyde groups from the PFA fixative; followed by repeated PBS washes. Cells were permeabilized with 0,5% Triton X-100/PBS, followed by repeated PBS washes.

2. Immunostaining

Nonspecific binding epitopes were pre-blocked in a blocking buffer containing 5%NDS/1xPBS or 5%NGS/1xPBS (serum harvested from the host species of the secondary antibody). All dilutions of primary and secondary antibodies were made in 2% serum/1xPBS (serum harvested from the host species of the secondary antibody, for application details see Table 2.1). Stainings were done by flipping the coverslip upside down, immersing the cells into a droplet (10 μ l) of the antibody solution. Coverslips were washed in mix of 2% serum/1xPBS-T0.1 for 3x5' after the incubation in the primary antibody staining. After secondary antibody staining, coverslips were washed in 1xPBS for 5', then stained with 2 μ g/mL Hoechst in PBS for 15'. Coverslips were then washed briefly with 1xPBS, dried by dabbing with a soft paper tissue and mounted on microscope slides using Vectashield[®] Mounting Medium (Vector Labs), dried briefly at room temperature, sealed with nail varnish; then slides were stored horizontally in a dust cover at 4°C.

Semi-quantitative protein studies

1. Preparation of cell lysates

Cells cultured in 6-well plates were washed with 1xPBS and dissociated from the plate using Trypsin/EDTA for 5' (100 μ l / well). Trypsinisation was stopped with ice-cold PBS/cOmplete (400 μ l/well).

Cell suspensions were then pipetted into Eppendorf tubes and centrifuged at 1000 rcf for 4' at 4 °C. Supernatants were discarded, pellets were lysed then in 200 μ l 5x Laemmli buffer (5' at 95 °C) and stored at -20 or -80 °C.

2. SDS-PAGE

Electrophoresis followed Laemmli's SDS-PAGE methods (Laemmli, 1970). For gel casting and for electrophoresis a Bio-Rad Mini PROTEAN Tetra System was used. Gel formulation is detailed in Table 2.2:

	Stacking gel 5%	Separating gel 6%	Separating gel 15%
dH ₂ O	1.4 ml	2.6 ml	1.1 ml
Tris 1M pH 6.8	250 μ l	-	-
Tris 1.5M pH 8.8		1.3 ml	1.3 ml
30% Acrylamide/Bis Solution 37.5:1		1.0 ml	2.5 ml
SDS 10%	20 μ l	50 μ l	50 μ l
APS 10%	20 μ l	50 μ l	50 μ l
TEMED	2 μ l	4 μ l	4 μ l

Table 2.2. composition of stacking and separating gels (calculated for 1 gel)

The sample buffer of cell/tissue lysates (containing 20 μ g protein) were heated to 95 °C for 5', then spun down briefly, added to the stack slots and resolved at 150 V.

Precision Plus Protein™ Standards protein marker was used to estimate the molecular weight of protein bands. Resolved proteins were then transferred to Immobilon-FL PVDF membrane in a wet transfer system on 200 mA for 14 h. To make sure complete transfer of protein bands, the separating gel was stained with Coomassie-blue stain and the PVDF membrane was stained with Ponceau-red stain.

3. Western blot

PVDF membrane was washed in TBS-T0.5 until Ponceau stain was removed, and then pre-blocked in TBS-T0.5-milk or in Pierce® Protein-free T20 (TBS) Blocking Buffer (Thermo Scientific). Immunoblots were performed with primary antibody diluted in a 50%-50% mix of blocking buffer and TBS-T0.1. PVDF membrane was then washed 3-times with TBS-T0.5 for 10', and then blotted with the appropriate secondary antibody diluted in TBS-T0.1-milk (for IR-Dye 680nm conjugated antibodies) or in a 50%-50% mix of Pierce blocking buffer and TBST0.1 (for IR-Dye 800nm conjugated antibodies). PVDF membrane was washed copiously with TBS-T0.5, then with PBS, and protein bands were visualized in Odyssey Infrared Imager (LI-COR Biosciences). Special notes on appropriate membranes, buffers and techniques are described in Odyssey Manuals: <http://biosupport.licor.com/index.jsp?&menu=&spec=Manuals>. Western blot densitometric analysis was performed using Image Studio Lite Ver. 4.0 (LI-COR).

4. Dot-blot

Schleicher-Schüll nitrocellulose membrane (pore size 0.2 μ m) was blocked in Pierce® Protein-free T20 (TBS) Blocking Buffer (Thermo Scientific) then placed on top of a double layer of pre-wetted blotting paper in a dot-blot chamber. 20 μ g eq. of tissue homogenates were diluted to 200 μ l in T100-homogenate buffer; then pipetted into the wells of the dot-blot chamber. Samples were sucked through the membrane using a water-pump system. The nitrocellulose membrane was then

immunoblotted using primary antibodies diluted in T20 protein-free blocking buffer (Pierce) for 1h on RT, washed 3-times with TBS-T0.5 for 10'. The nitrocellulose membrane was then blotted with HRP-conjugated secondary antibodies, diluted in T20 protein-free blocking buffer. Chemiluminescence was induced by dabbing the membrane into Luminata Classico Western HRP substrate (Millipore) and detected by FUJIFILM LAS-3000 Luminescent Image Analyzer.

Semliki Forest Virus (SFV) propagation

A frozen stock of the highly virulent SFV-4 strain was used, derived from the cDNA clone of the original isolate (designated as SFV-L10) (Liljeström et al., 1991) for the initial infection of Vero cells to grow an SFV stock. All SFV works were done in a Class 2 Biological Safety Cabinet. Infected and non-infected cultures were strictly separated. SFV stocks were propagated in Vero cell cultures, grown in a 75 cm² culture flask in growth medium until ~85% confluency. Growth medium was exchanged with 200 µl SFV solution, carefully distributed by tilting the flask to form an even layer on top of the cells. Cells were then incubated in a humidified chamber for 1 h, shaking the flask every 10' to ensure a homogenous fluid film. After 1 h 10 ml the following infection medium (with reduced FBS content) was added: Dulbecco's Modified Eagle Medium (DMEM); supplemented with 2% (V/V) fetal bovine serum (FBS) and P/S (100 U/ml - 100 µg/ml). Virus growth was monitored by checking for cytopathic effect under microscope. Medium was collected for freezing when infected cells detached. SFV infection experiments in MEF cultures were done following a similar procedure. Medium was collected for freezing at 4h, 8h, 12h and 24h p.i. (*post inoculation*) as outlined below.

Freezing and thawing SFV

Virus containing medium was collected in a Falcon tube, spun down at 1000 rcf for 5', then supernatant was pipetted into cryogenic tubes, and transferred to -70°C in a Mr. Frosty freezing container (Thermo Scientific). Virus containing medium was thawed up rapidly in a water bath, pre-heated to 37°C.

SFV quantification by plaque assay

2 ml-s of growth medium was added to each well in 6-well culture plates. Vero cells (from a healthy culture, grown to 100% confluence within 3 days) were diluted to a density of 7.5×10^5 /ml in growth medium, from which 1 ml was pipetted to each well. To reduce evaporation, seeded plates were placed in a plastic box, and incubated at 37°C in a humidified atmosphere of 5% CO₂ until sub-confluent density was reached.

Doubling serial dilutions of SFV working stock were prepared in Vero infection medium (with reduced FBS content). The composition of infection medium was as follows: Dulbecco's Modified Eagle Medium (DMEM); supplemented with 2% (V/V) fetal bovine serum (FBS), 100 U/ml Penicillin, 100 µg/ml Streptomycin (P/S).

Growth medium was decanted from the cells after which 500µl inoculum from each virus dilution were added to the wells in duplicate. Cells were incubated with SFV for 1 h at 37°C, in a humidified atmosphere of 5% CO₂, with rocking every 15'. Two wells were mock-infected with 200 µl Vero infection medium alone and acted as negative controls.

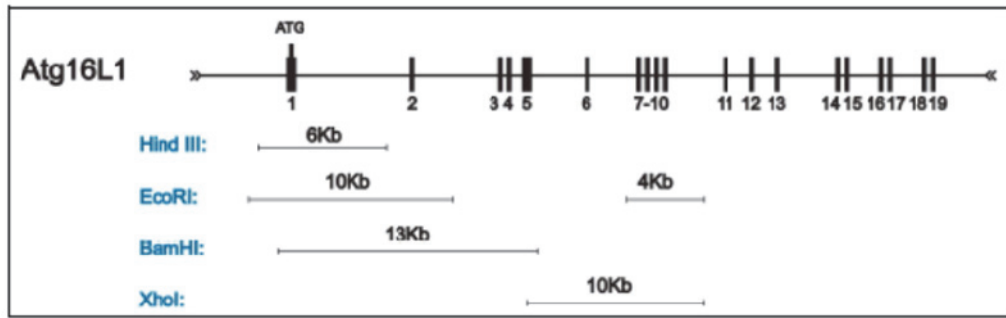
Equal amounts of 2% SeaPlaque Agarose (autoclaved, heated up then kept liquid at 37°C) and DMEM were mixed, and added on top of the inoculum to a final volume of 4 ml per well. When the agar had solidified (approx. 10' in the TC hood) the plates were incubated for 48 h at 37°C in a humidified atmosphere of 5% CO₂. When plaques were clearly visible (or by no later than 48 h) plates were flooded with 4%PFA/PBS and allowed to fix for 6 h, after which the fixative and agar were removed. Plates were briefly stained with crystal violet (Sigma), and then rinsed with running tap water. The plates were left to dry, plaques were counted against a dark background and viral titres were expressed as plaque forming units (PFU)/ml.

Mouse breeding and selection

All mice were kept, handled, tested and killed in accordance with Home Office guidance; regulated under the Animals (Scientific Procedures) Act 1986, (revised Jan. 2013). The housing room was maintained on a 12:12-h light-dark cycle. All mice were kept under specific pathogen-free conditions and provided with water and food provided *ad libitum*. Pups were weaned from their mother 21-28 days after birth, males and females were separated at weaning. Metal ear-tags were used for the identification of mice over the age of 14 days; younger pups were skin-marked with a pen. Mice for autopsies were killed by cervical dislocation, done with special care to avoid laceration of skulls. Atg16 KO (-/-) mice were generated by mating Atg16 heterozygous (+/-) mice, which had been previously backcrossed to C57/B6l background at least 3 times. The Atg16 (-) allele was generated by Cre-mediated excision of the Exon 2 of Atg16, which results in a frameshift in mRNA translation and a premature stop codon in the Exon 3. For the detailed description of generating the targeting vector, the recombinant Atg16 allele, generation of the first Atg16 fl/fl and Atg16 KO mice I refer to J.M. Arasteh's invaluable work on this project (Arasteh, 2012); which I briefly summarise here.

The genomic fragment containing the 5' fragment of Atg16 was isolated from the mouse PAC library RPCI21, constructed in Pieter de Jongs' laboratory (Osoegawa et al., 2000). Positive clones were screened by Southern hybridisation, using the Atg16 IMAGE clone cDNA (Image ID 6813377/AV130 A2, obtained from Geneservice). The selected clone #390-O24 was then digested with Eco RI restriction enzyme to obtain a 10 kb fragment ("Atg16-ER10") spanning the promoter and the 5' exons of the Atg16 gene; which was subcloned into a pBS-SK vector ("pBS-SK-Atg16-ER10") (Fig.2.1.a). As exon 2 is an integral part of every mouse Atg16 splice variants, a targeting construct was generated, containing loxP sites flanking exon. This floxed Atg16 targeting vector was used to transfect 129Sv-derived R1 embryonic stem cells to achieve homologous recombination. Embryonic stem cells were selected for neomycin resistance, screened via Southern hybridisation for homologous recombination of the targeted allele. To generate chimeric mice, positive cells were sent to the Transgenic Core Facility (Dresden, Germany) where injection into host blastocysts and implantation into pseudo-pregnant foster mothers were done. Chimeric mice were selected for a higher percentage of brown coat colour, then mated with C57BL/6 mice and offspring with a brown coat colour were tested for germline transmission. Heterozygous Atg16 floxed mice were then crossed with mice carrying the Cre recombinase transgene under the control of the ubiquitously expressed phosphoglycerate kinase (PGK) promoter (PGK^{Cre+}). Expression of Cre leads to the excision of the floxed Exon 2 sequence, which results in a frame shift and a premature stop codon in the Exon 3 (Fig.2.1.b). To achieve this, Atg16 fl/+ PGK-Cre+ mice were mated with wildtype mice to detect mice which were heterozygous (+/-) for the mutation and lacked PGK-Cre. The Neomycin resistance gene was removed by crossing heterozygous mice with mice expressing the Flp recombinase transgene (Fig.2.2.a).

a

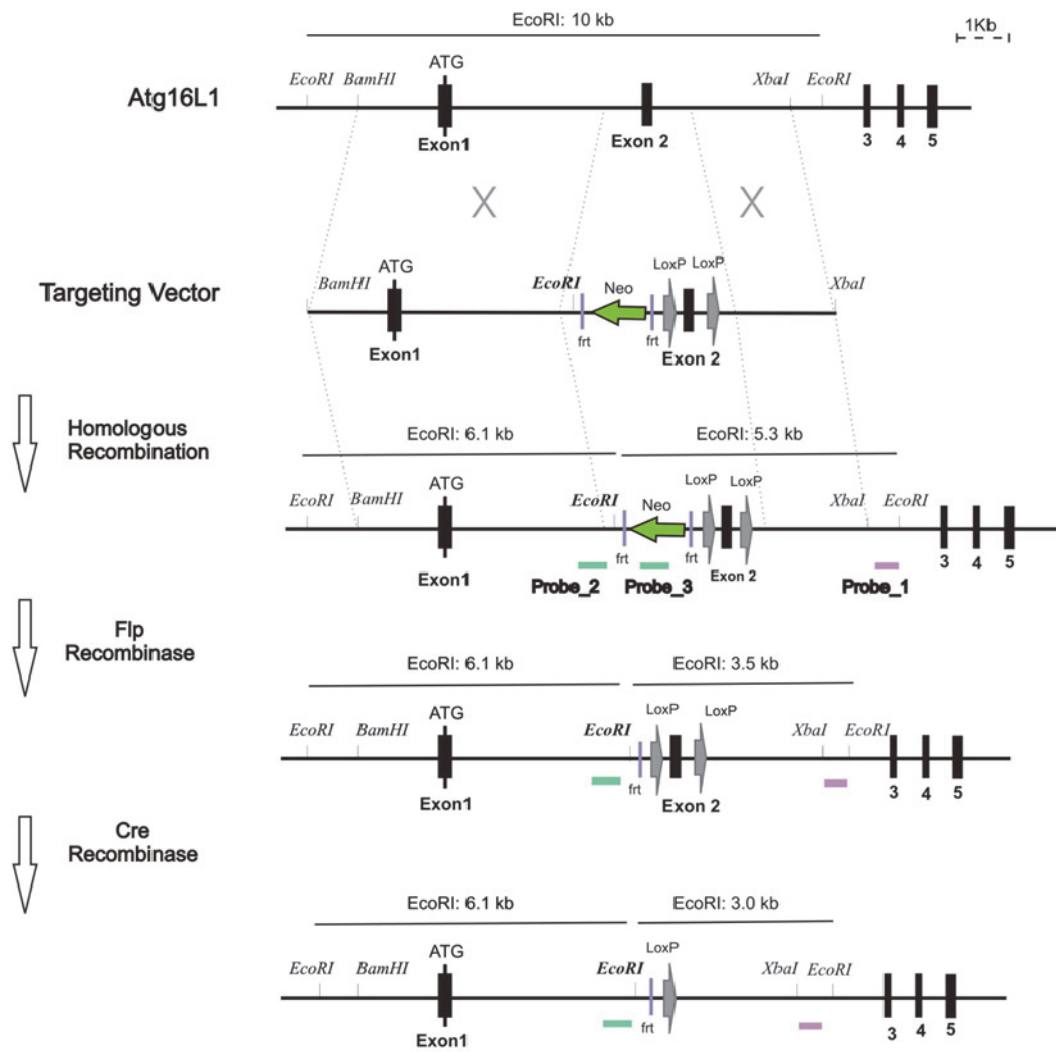


b

		5' UTR
ATG16 WT	DNA	61 CCCCCCAGTGTCCGGCACGGATCCGCCGCCCTGAGGCGCCGGGGCAGCGTTCGGCATGTCCG
	mRNAAUGUCG
	proteinM--S-
		121 TCCGGCCTGCGCGCCGACACTTTCGCCCTGGAAGCGTCACATCCCGAGGAACGAGG
		7 UCGGGCCUGCGCGCCGACACUUCGCCCGUGGAAGCGUCACATCCCGAGGAACGAGG
		3 -S--G--L--R--A--A--D--F--P--R--W--K--R--H--I--A--E--E--L--R--
		Exon 1
		Exon 2
		181 CGCCGGGACCGACTGCAGAGGCCAGGCCGTCGAGGAGATCATTCTGCAGTATACCAAGTTG
		67 CGCCGGGACCGACTGCAGAGGCCAGGCCGUCGAGGAGAUCAJUUCGAGUUAJACCAAGUUG
	23 -R--R--D--R--L--Q--R--Q--A--F--E--E--I--I--L--Q--Y--T--K--L--	
	241 CTGGAAAAGTCAGATCTTCATTGAGTATTGACCCAGAAACTACAAGCAGAAAAGCAT...	
	127 CUGGAAAAGUCAGAUUCUAUUCAGUUCUGACCCAGAAAACUACAAGCAGAAAAGCAU...	
	43 -L--E--K--S--D--L--H--E--V--L--T--Q--K--L--Q--A--E--K--H--...	
	5' UTR	
ATG16 KO	DNA	61 CCCCCCAGTGTCCGGCACGGATCCGCCGCCCTGAGGCGCCGGGGCAGCGTTCGGCATGTCCG
	mRNAAUGUCG
	proteinM--S-
		121 TCCGGCCTGCGCGCCGACACTTTCGCCCTGGAAGCGTCACATCCCGAGGAACGAGG
		7 UCGGGCCUGCGCGCCGACACUUCGCCCGUGGAAGCGUCACATCCCGAGGAACGAGG
		3 S G L R A A D F P R W K R H I A E E L R
		Exon 1
		Exon 3
		181 CGCCGGGACCGACTGCAGAGGCCAGGCCGTCGAGGAGATCATTCTGCAGTTCCTGGACATG
		67 CGCCGGGACCGACTGCAGAGGCCAGGCCGUCGAGGAGAUCAJUUCGAGUUAJACCAAGUUG
	23 -R--R--D--R--L--Q--R--Q--A--F--E--E--I--I--L--Q--F--L--D--M--	
	241 ATGTTGCTGGAATGATAGTCAACTACAAGAAATGGCCAGTTGAGSATCAAACAC...	
	127 AUGGU GCGUGGAAUGAUAACUACAAGAAAUGGCCAGUUGAGGAUCAAACAC...	
	43 -M--V--R--G--M--I--V--N--Y--K--K--V--P--S--stop-	

Fig. 2.1. a) Restriction endonuclease digestion patterns of the 5' end of mouse Atg16. A 10Kb EcoRI digestion fragment of the Atg16 gene was cloned into pBS-SK vector to generate pBS-SK-Atg16-ER10. b) Comparing Atg16 WT and KO Atg16 genomic DNA, mRNA transcript and translated peptide sequences. Adapted from J.M. Arasteh (Arasteh, 2012).

a



b

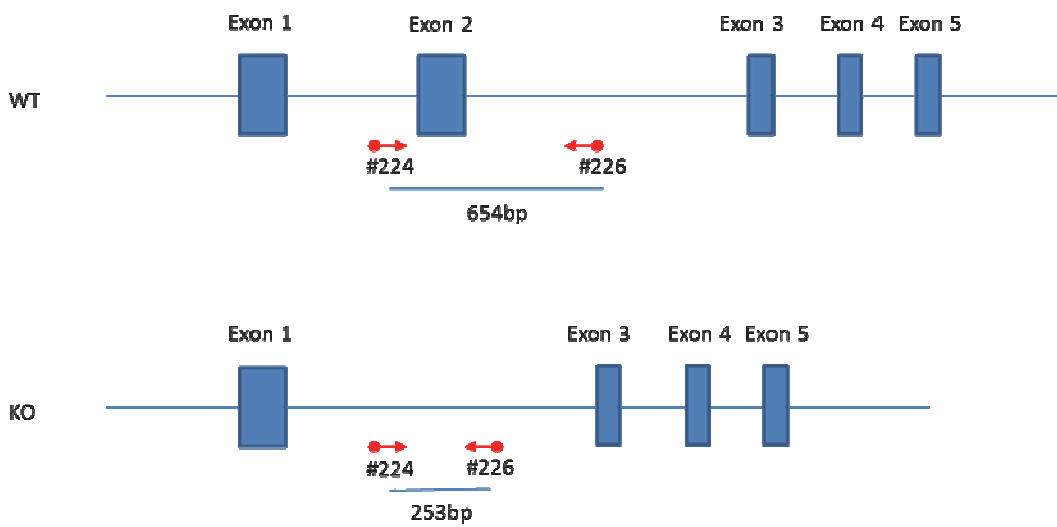


Fig. 2.2. a) Steps involved in generating the Atg16 KO mice. Floxed Exon2 is excised by Cre recombinase, Neomycin cassette is excised by Flp recombinase from the final sequence. Adapted from J.M. Arasteh (Arasteh, 2012) **b) PCR strategy for genotyping Atg16 WT and KO mice.**

Mouse genotyping

1. DNA extraction from tissues

Ear punch biopsies from living mice were obtained by an ear puncher, or tail tips from carcasses were cut by a scissor. All tools were sprayed with 70 % EtOH and wiped clean, to prevent cross-contamination. The tissue sample was lysed in 250 μ l Mouse Tissue Lysis Buffer (see below) at 55 °C in a benchtop rotating incubator, until completely dissolved. Tissue lysates were then immediately processed or stored at 55 °C. Composition of Mouse Tissue Lysis Buffer was as follows: Tris/HCl 0.1M (made from Tris/HCl 1M pH 8.5); NaCl 0.25 M; SDS 0.2 w/V %; EDTA 0.005M; Proteinase K 100 μ g/ml;

2. Genotyping PCR (Fig.2.2.b)

Tissue lysates were diluted 1:10 in dH₂O, and a PCR reaction mixture was prepared in a volume of 50 μ l as follows: 38.5 μ l dH₂O, 5 μ l 10X Taq Buffer with KCl and 15 mM MgCl₂ (Thermo Scientific #B16; final cc. for MgCl₂: 1.5 mM); 0.5 μ l dNTP mix consisting 0.25 mM dATP (Roche #1051440), dTTP (Roche #1051482), dGTP (Roche #1051466) and dCTP(Roche #1051458) (end cc 25 pM for each). 1 μ l of forward and reverse primers (100mM of primers #224 and #226, end cc: 20 pM); 2 μ l "Taq-O-D" in-house Taq DNA polymerase (concentration n.k.); 3 μ l of tissue lysate. Thermocycling was done using Touchdown PCR Programm as follows: 95 °C for 10', then a sequence of denaturing at 95°C for 1', annealing at 65°C for 1' (with 1 °C lower annealing temperature in each subsequent cycle) and extension at 72°C for 1'. Final extension was done at 72 for 10'. Amplified DNA fragments were separated on a 2% agarose gel using Orange-G loading buffer at 1x cc.; product size was verified using 1kb plus DNA ladder following incubation of the agarose gel in EtBr bath. Preparation of Orange G loading buffer (Sigma #O3756) and 1kB plus DNA ladder (Life Technologies #10787-018) was performed as follows:

5x Orange-G loading buffer: 7.5 ml glycerol was mixed with 100 mg Orange-G dye then topped up with dH₂O to 50 ml

1x 1kB plus DNA ladder: 50 μ l 1kB plus DNA ladder stock solution (1 μ g/ μ l) was dissolved in a mixture of 200 μ l 5X Orange-G Gel loading buffer + 750 μ l dH₂O (Final cc.: 0.1 μ g/ μ l.)

Behavioural phenotyping

When perinatal lethality was observed, neonates with milk spot were sacrificed and non-suckling mice were left in the cage. Alternatively, neonates were fostered with lactating BALB/c females. Maternal behaviour and behavioural bias towards pup genotype was tested by removing skin-marked pups from the nest and placing them one-by-one into a distant edge of the cage.

Blood glucose measurement

Mixed blood glucose level was measured from a drop of blood of decapitated animals using an ACCU-CHEK® Compact Plus device.

Glucose treatment

50 µl 30% glucose in PBS was filter sterilized, then injected subcutaneously under the subnuchal fold of mouse neonates

Tamoxifen treatment

Mice were weighed on a tabletop balance. 90ug/g Tamoxifen (diluted in corn oil) was injected a) intraperitoneally into pregnant females at 12-14 dpc (*dies post coitum*) b) intraperitoneally into lactating females at 5-10 dpp (*dies post partum*) c) subcutaneously under the subnuchal fold of mouse neonates. (All Tamoxifen regimes were cancelled following the observation of near 100% lethality of mouse pups – treated either directly or indirectly by Tamoxifen-treated lactating females.)

Post-mortem examination

Autopsy of dead neonates (either found dead or killed on the 1st postnatal day) were performed using microsurgical instruments from Fine Science Tools. Animals were weighed on a tabletop weighboard.

Preparation of brains

After cervical dislocation, mice were decapitated; the head was immobilized with pins on a polystyrol box-lid. Skin was removed from the top of the skull and the brain was exposed by cutting the skull shallowly from the foramen magnum to the level of the eye sockets using blunt-ended iris scissors, where the lateral incisions were done to reach the left and right orbitae. Using a spatula, the brain was flipped out of the skull (together with the olfactory bulbs), and cut alongside the midline, to separate the hemispheres and the left and right half of the brainstem. One half was immersed immediately into ice cold PBS, then fixed in 4%PFA/PBS. Fixation time was determined by calculating the penetration time of PFA through the entire tissue volume (1 mm/h). Fixed brains were washed in PBS and stored in PBS at +4 °C. The other half of the brain was snap-frozen by immersion into liquid Nitrogen, then transferred into an Eppendorf tube on dry ice, and stored at -80 °C.

Histological methods

Histological methods not specified here were taken from Bancroft's Theory and Practice of Histological Techniques (Bancroft, 2001).

1. Haematoxylin-Eosin staining

Paraffin sections were hydrated to water, placed in a Coplin jar filled with Hematoxylin Solution for 5', then washed with running tap water for 20' or until tissue structure was clearly visible. Sections were then transferred to a Coplin jar filled with Eosin-Y and incubated for 5'. Sections were then dehydrated by rapid immersion into EtOH of rising concentration.

2. Toluidine blue staining

0.1g Toluidine blue powder was dissolved in 1% sodium tetraborate to yield a 0.1% stain solution. Hydrated paraffin sections were stained with this solution in a Coplin jar for 10', dipped into dH₂O briefly, then differentiated in 50% EtOH for 30''. Sections were then dehydrated by rapid immersion into EtOH of rising concentration.

3. Bielschowsky silver staining was done following the modifications by Litchfield & Nagy (Litchfield and Nagy, 2001)

Paraffin sections were hydrated to water, and cooled to +4 °C. Sections were then incubated in pre-cooled 20% AgNO₃ at +4 °C for 20'; washed in dH₂O at +4 °C for 5'; incubated in ammonium saturated 20% AgNO₃ at +4 °C for 20'; transferred to ammonia-water (2 drops into 50 ml dH₂O) at +4 °C for 5', then transferred to dH₂O

at +4 °C for 5'. Staining was then developed at room temperature as follows: 50 µl Bielschowsky developer (see below) was added into 25 ml 20% AgNO₃ (ammonium saturated). Developer solution was dropped on top of the sections until background turned light brown. Sections were then washed in dH₂O, transferred to Hypo (see below) for 5', followed by a further dH₂O washing step.

Bielschowsky-developer: 0.5 g citric acid was dissolved in a mixture of 100 ml dH₂O + 20 ml Formalin + 1 drop of cHNO₃.

Hypo: 5g Na-thiosulfate was dissolved in 100 ml dH₂O

Sections were then counterstained with Eosin then dehydrated by rapid immersion into EtOH of rising concentration.

Formic acid pretreatment for Toluidine blue and Bielschowsky-stain:

Deparaffinized sections were hydrated to H₂O; immersed into 85% Formic acid for 10min; washed with tap water for 5'; immersed into a mix of 75%EtOH + 25 % Acetic acid (glacial) for 10min, then washed again with tap water for 5'.

Na-citrate retrieval

Deparaffinized sections were hydrated to H₂O; sections were incubated for 5' in 0.1 M PBS (pH 7.4); then transferred to 10 mM sodium citrate buffer (pH 6.0) preheated to boiling in a microwave oven. Sections were heated repeatedly to boiling for 2' in microwave, while citrate buffer was replaced. Sections were then allowed to cool to room temperature, and rinsed 3x5' in PBS (pH 7.4 -or pH 3.0 for subsequent TUNEL assays.)

Paraffin embedding and preparation of microtome sections

Fixed tissue samples were dehydrated through a series of graded alcohol washes as follows; 30% (v/v) alcohol for 1 h, 50% (v/v) alcohol for 1 h, 70% (v/v) alcohol for 1 h, 85 % (v/v) alcohol for 1 h, 90% (v/v) alcohol for 1 h, 95% (v/v) alcohol for 1 h, 100% (v/v) alcohol for 2x1 h, then immersed in Clearene (Surgipath Medical Industries #K855109) for 1 h. Samples were immersed in 65 °C paraffin wax overnight and mounted onto blocks on the following day. 4 µm thick sections were cut using a microtome, dried briefly at room temperature and stored at 4°C.

OCT embedding and preparation of cryosections

Fixed tissue samples were incubated in 5% sucrose / 1x PBS then 25% sucrose / 1xPBS (each for 24 h on RT shaker) and immersed into an OCT-filled aluminium foil cone to ensure cryoprotection. OCT-embedded samples were frozen by immersing the aluminium foil cone into a beaker with pre-chilled isopentane for 1'. The beaker with isopentane was placed into an ice-bucket with liquid N₂, and stirred constantly throughout the freezing procedure.

Dehydration of fixed samples for paraffin embedding:

PFA or glutaraldehyde fixed samples were placed in 1x PBS, then into rising concentrations of EtOH as follows: EtOH 30% (30min) - EtOH 50% (30min) - EtOH 70% (1h) - EtOH 80% (1h) - EtOH 90% (1h) - EtOH 95% (1h) - EtOH 100% (1h) - EtOH 100% (1h). Samples were then washed in Clearene for 1h, followed by paraffin embedding and sectioning using a Leica Microtome.

Deparaffinization and hydration of paraffin-embedded sections

Paraffin embedded sections were collected on microscope slides, deparaffinised and rehydrated in the following series of solutions: Clearene (5min) - Clearene (5min) - EtOH 100% (2min) - EtOH 90% (2min) - EtOH 70% (2min) - EtOH 50% (1min) - EtOH 50% (1min).

Dehydration and mounting paraffin-embedded sections after histological staining

Stained sections were dehydrated in the following series of solutions: EtOH 70% (2sec) - EtOH 80% (2sec) - EtOH 95% (2sec) - EtOH 100% (2sec) - EtOH 100% (2sec) - Clearene (5min) - Clearene (5min). Excess clearene was dabbed off, and then slides were covered with DPX mount and coverslips. Slides were left to dry ON at RT.

Detection of apoptosis in tissues

Apoptosis was detected in paraffin embedded tissue sections (d=5µm), using the DeadEnd™ Fluorometric TUNEL System (Promega, #G3250). DNaseI (Ambion, #AM222) treated sections were used as positive controls to detect double-stranded DNA breaks. Before performing TUNEL assay, sections were deparaffinized, hydrated to H₂O and pre-treated as follows: microscope slides were placed in a Coplin jar with 0.01M Natrium Citrate buffer (pH 3.0) heated up in a microwave oven until boiling (5-10 times) and let to cool down to room temperature. Sections were treated with Proteinase K (supplied in the DeadEnd™ Fluorometric TUNEL Kit), and positive control sample was treated with DNaseI following the supplier's instructions, then TUNEL assay was performed following the manufacturer's protocol.

Preparation of tissue homogenates

Tissue homogenates from snap-frozen tissues (brain and liver) were prepared in a Homogenate buffer described by Waguri and Komatsu (Waguri and Komatsu, 2009); consisting of 0.25 M sucrose, 10 mM 2-[4-(2-hydroxyethyl)-1-piperazinyl] ethanesulfonic acid (HEPES), pH 7.4, and 1 mM dithiothreitol (DTT). A metal bearing ball and suitable volume of ice-cold Homogenate buffer were added to frozen tissues, which then were homogenized in a TissueLyser LT (Quiagen #85600), at 50 rpm, 2'. The homogenates were transferred into new tubes on ice, supplemented with Triton-x100, vortexed and centrifuged at 13200 rpm, 10'. The supernatant was transferred into a new tube on ice ("Tx100 fraction"), while the pellets were resuspended in room temperature Homogenate buffer, supplemented with 2 % SDS ("SDS fraction"). Both fractions were then sonicated, aliquoted and stored at -80°C.

Antigen retrieval methods and protein extraction methods were compared to optimize signal to background ratio. Fluorescent images displayed here are representative for brain sections after antigen retrieval with sodium citrate, immunoblot figures are representative brain homogenates extracted in Laemmli buffer, as indicated.

Preparation of organotypic brain cultures

Mouse neonates were culled by cervical dislocation in the morning hours, as soon as the litter was detected. After decapitation brains were quickly harvested, brainstem and olfactory bulbs were removed, and 400µm-thick coronal sections were prepared using a bench-top vibratome. Sections were collected in ice-cold, sterile, Ca²⁺- and Mg²⁺-free PBS (Life Technologies), washed in PBS and transferred onto a 0.4 micron Millicell inserts (Millipore #PICMORG50 6-well plate size) and the insert was placed on top of 1.1 ml Brain-slice Growth Medium (see below). Growth medium was replaced 24h after setting up the culture, then every 48h. Organotypic brain sections were cultured for at least 3 days before further experiments were performed.

Composition of Brain-slice Growth Medium (for 500 ml) was as follows: Neurobasal medium (#21103-049 Life Technologies) 440 ml + B27 supplement (#17504-044 Life Technologies) 10 ml + Horse serum (#16050-122 Life Technologies) 25 ml + 200 mM L-Glutamine (#25030024 Life Technologies) 5 ml [final cc. 2 mM]

SFV infection of organotypic brain cultures

Organotypic brain cultures were slices were infected with the Semliki Forest Virus prototype strain SFV4 (Liljeström et al., 1991). Ten-fold logarithmic serial dilutions of a SFV working stock were prepared in Brain-slice Infection Medium (see below). Brain-slice Growth Medium was carefully removed and brain slices were covered by 200 µl of the virus-containing Brain-slice Infection Medium. In general, it took approx. 10' until the medium reached the bottom of the plate. Brain slices were incubated for 1 h in the infection medium, rocking the plate a couple of times every 10'. The virus-containing medium was then removed, and adherent viruses were inactivated by washing the wells with mildly acidic PBS (pH 5.5). Fresh infection medium (without virus) was pipetted below the insert, and then collected immediately to quantify leftover inoculum. Brain slices were cultured further in 1.1 ml fresh infection medium, which was replaced and collected for freezing at 24h, 48h, 72h then every 48h p.i.

Composition of Brain-slice Infection Medium (for 500 ml) was as follows: Neurobasal medium (#21103-049 Life Technologies) 460 ml + B27 supplement (#17504-044 Life Technologies) 10 ml + Horse serum (#16050-122 Life Technologies) 25 ml + 200 mM L-Glutamine (#25030024 Life Technologies) 5 ml [final cc. 2 mM]

Viability assay of virus infected organotypic brain cultures

Various, commercially available cell viability assay kits measure the activity of mitochondrial dehydrogenases, which correlates with the number of viable cells. WST-1 cell proliferation reagent (Roche #11644807001) is used for the quantification of the overall activity of the mitochondrial succinate-tetrazolium reductase system (RS), by the colorimetric reaction of WST-1 to yield formazan dye. NAD⁺ is a coenzyme of the RS in this reaction. As SFV infection was found to interfere with the cell metabolism to generate NAD⁺ for the virus replication (Cassells and Burke, 1973b), this colorimetric assay quantifies NAD⁺ production rather than viability of infected cells. Measuring LDH concentration in culture media helps to distinguish between colorimetric changes attributable to loss of cell viability and virus-induced metabolic changes.

Digital imaging

Images were acquired using a 63x Plan-Aprochromat objective (of 1.4 numerical aperture) and processed using AxioVision® SE64 4.9.1 (Carl Zeiss Vision) with the modules Multichannel Fluorescence and Z-Stack. 5 sections were taken each time along the Z-stack, with a distance of 0.55 µm. Nearest-neighbour deconvolution module was used for detecting colocalization of intracellular structures.

Imaris® x64 7.2.3 was used for re-stacking sections to obtain 3D images. Surface and Spots functions were used for calculating nuclei and autophagosomes in images. Spots between 0.5-1.5 µm of diameter were classified as autophagosomes.

Statistical analysis

All statistical analysis were performed using SPSSv.22.0. Means of scale values were compared using two-tailed independent Student's t-test if sample data followed normal distribution. Whenever sample data deviated from normal distribution, one-way ANOVA was used to compare means. Shapiro-Wilk test was used to test normality assumption of sample data distribution, due to its better power than Kolmogorov-Smirnov test (Ghasemi and Zahediasl, 2012). Independence or relationship between categorical variables was analyzed using Pearson's Chi-square test.

3. RESULTS

3.1. Ubiquitinated protein aggregates in Atg16 KO mice

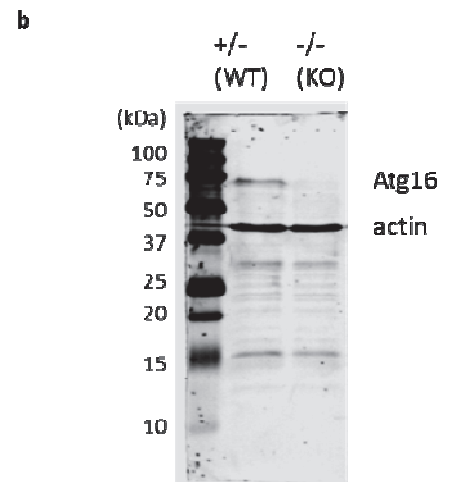
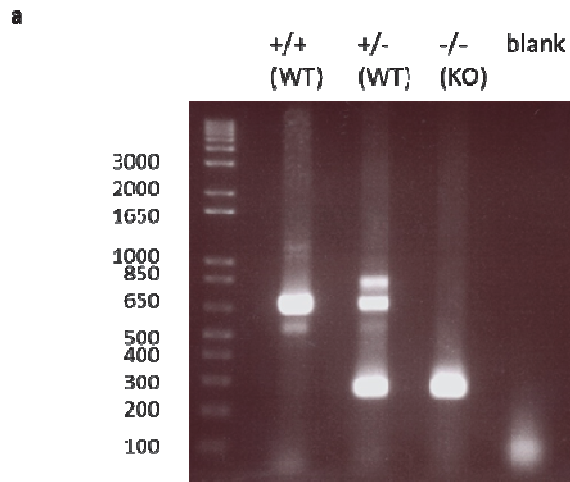
3.1.1. Study objectives:

Existing KO models of autophagy genes are characterized by the pathologic features of impaired starvation resistance; aggregation and ubiquitination of dysfunctional proteins and liver toxicity (see Table 1.1) (Komatsu et al., 2005, Kuma et al., 2004, Hara et al., 2006, Komatsu et al., 2007). The aim of this study was characterising the CNS phenotype of Atg16 KO (-/-) mice and generating a knockout animal model for further studies on the role of autophagy in neurodegenerative diseases and antiviral response.

3.1.2. Phenotype description of the Atg16 KO mice

Atg16 KO mice harbour a truncated Atg16 gene with no functional Atg16 protein expressed (Fig.3.1.a,b). Atg16 KO neonates were not viable beyond the first postnatal day. As pups were born during the dark period, their exact life expectancy was not determined more accurately. To avoid miscalculation of cannibalized pups, prepartum fetuses were harvested from pregnant mothers on day 18 p.c. Atg16 genotype of E18.5 fetuses from Atg16 heterozygous matings followed a Mendelian

distribution (Fig.3.1.c). When litters were collected later during the day, Atg16 KO pups were observed as they stopped spontaneous motion and turned cyanotic shortly before the onset of death; indicating a cardiopulmonary decompensation as an immediate pre-lethal condition. Most Atg16 KO neonates were found alive when collected in the morning (8am-10am). They appeared smaller, yet without parturition injuries (visible laceration or haemorrhage). KO neonates had normal body curvature and vigorous movement in the first hours, arguing against an overt neuromuscular dysfunction. The most apparent phenotypic difference between KO and WT pups was the lack of milk spot in KOs (Fig.3.1.d). Subsequent autopsies confirmed that Atg16 KO pups did not commence suckling, in spite of the continuity of their GI tracts. For further experiments newborn litters of Atg16 heterozygous mice were collected by 10 am. Neonates were sacrificed by cervical dislocation, without lacerating the skulls. Dead neonates were also collected. Autopsies were performed on carcasses, and genotype was determined from lysates. Autopsies found no visible abnormality, no malformation of the major viscera (liver, lungs, heart, spleen, kidney, thymus). Lungs and stomachs of KO carcasses were air-filled, which confirms that they were born alive, as pups were able to breathe and swallow (Fig.3.1.e). Histopathological analysis of the lungs and the heart found no structural abnormalities to explain the compromised vital functions of KO neonates (Fig.3.1.g), which made an underlying metabolic or neurogenic condition a conceivable hypothesis. Body weight and blood glucose levels in mutant neonates were significantly lower than in WT littermates (Fig.3.1.f). Peri-mortal KO neonates were successfully rescued by subcutaneous injection of 5% glucose. Glucose-injection prolonged their survival only for a short time, as KO mice failed to initiate suckling and were dead by the following day.



c

genotype	No of fetuses	Observed frequency (%)	Expected frequency (%)
+/+	32	25.2	25
+/-	69	54.3	50
-/-	26	20.5	25

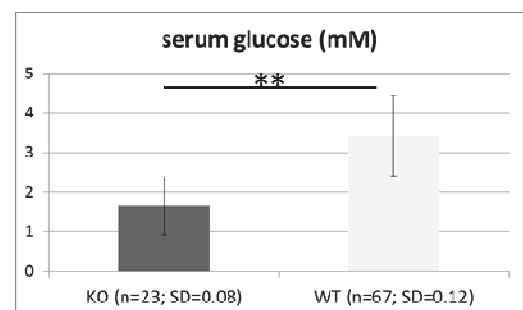
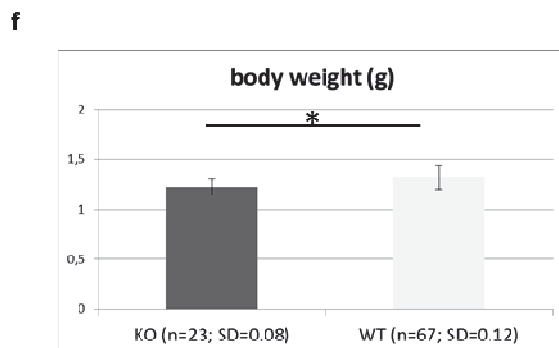
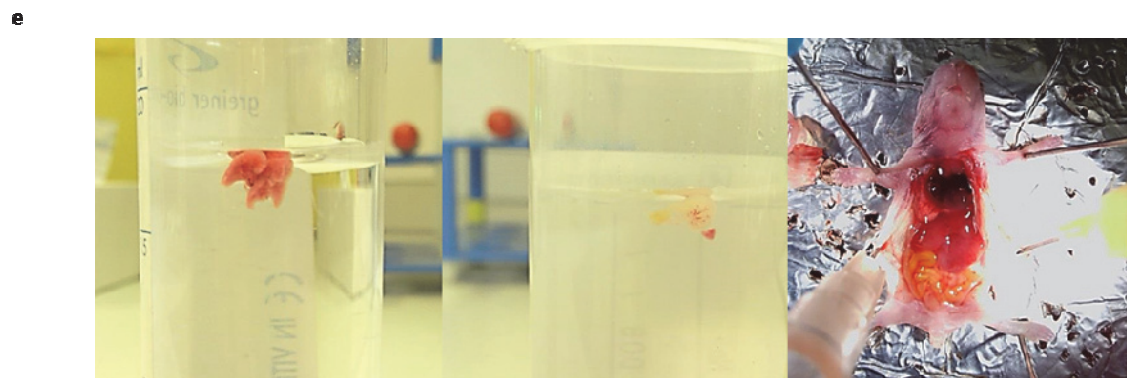
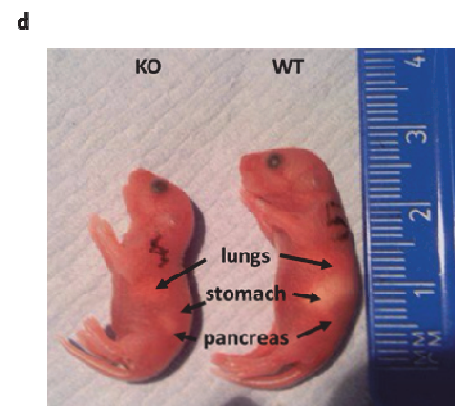
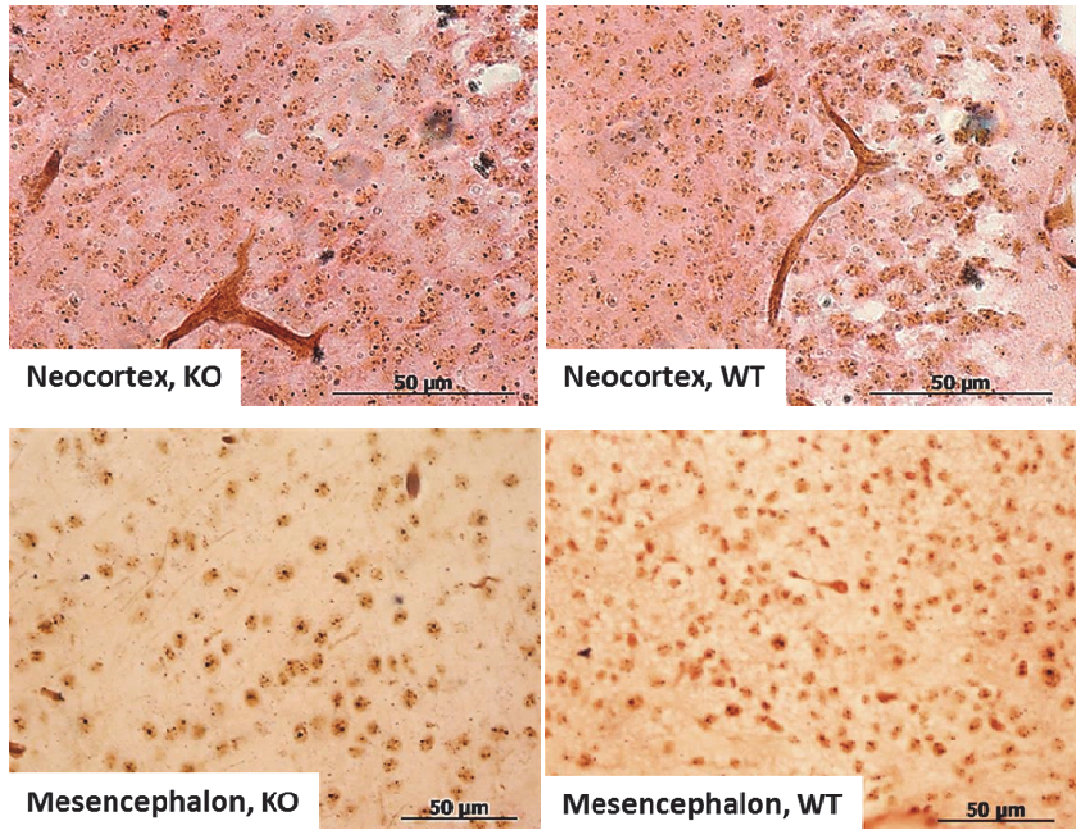


Fig. 3.1. a) Detection of Atg16 KO by PCR. KO allele: 253 bp band WT allele: 654bp band. In heterozygous mice a larger DNA band of 907 bp appears. **b) Detection of Atg16 KO by western blot (mouse brain lysates).** No Atg16 protein is expressed in KOs while the brain-specific 75 kDa Atg16 isoform is found in WT lysates. **c) Genotype distribution of prepartum fetuses show Mendelian distribution** (Chi-squared: 1.520, df: 2, p (two-tailed): 0.4677 n= 127.) **d) Phenotypic appearance of newborn mice.** Atg16 KO pups are typically smaller and have no milk spot (pancreas tagged for unambiguousness) **e) Autopsy findings of a representative Atg16 KO carcass** (found dead when litter detected). Air-filled lungs (left) and stomach (middle) floating in PBS verify that KO pups survived parturition and born alive. No gross congenital abnormality seen in the thoracic and abdominal viscera (right). **f) Atg16 KO neonates showed reduced body weight and reduced blood glucose levels as compared to WT littermates.** Densitometric values are represented graphically as mean \pm SD. Asterisk (*) indicates a significant difference between KO and WT samples; means compared by one-way ANOVA, *: $p < 0.05$, **: $p < 0.001$ **g) Haematoxylin-eosin staining of lung and heart sections of neonate mice.** Lung maturation entered the saccular stage both in Atg16 KO and in WT pups. Hearts showed no ischaemic, hyper- or hypertrophic signs.

3.1.3. Neuronal pathology of Atg16 KO mice

Newborn pups underwent macroscopical and microscopical analysis of the central nervous system. In the absence of gross anatomical deformity, neuronal layers were analysed by haematoxylin-eosin, toluidine blue and Bielschowsky silver stains. Abnormal cells or cell layers were not detected using these histological stains when WT and KO brains or spinal cords were compared (Fig.3.2.a). To investigate the presence of autophagosomes, immunohistochemical stainings were performed, using antibodies against the autophagosomal markers Atg5, and LC3; however autophagosome-specific staining was neither detected in autophagy-competent nor in Atg16 KO brain sections. Immunoblot studies showed a clear LC3-I/II conversion in WT brain lysates, while it was missing in KO brains. Simultaneously, p62 and polyubiquitinated autophagy substrates accumulated in KO brains in the absence of autophagy (Fig.3.2.b).

a



b

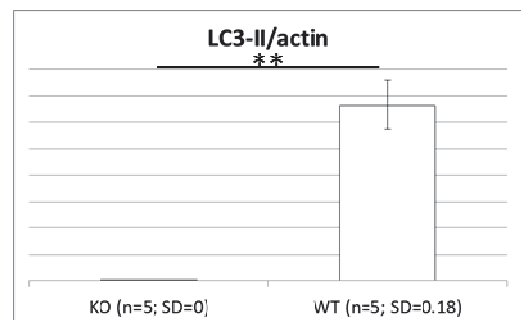
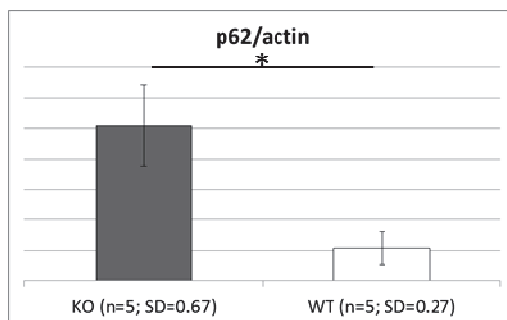
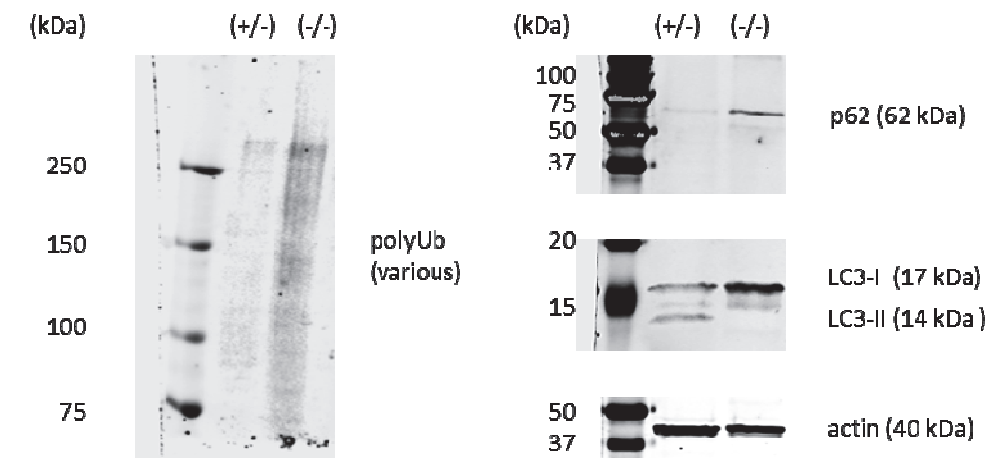


Fig. 3.2. a) Normal histological structure found in Atg16 KO brains. Neonate brain sections were stained with Bielschowsky silver (brown) and eosin (pink). Apparent damage or loss of neuronal layers was not detected. **b) Lack of autophagy results in accumulation of autophagy substrates in Atg16 KO mice.** Brain lysates were resolved in SDS-PAGE and immunoblotted with anti-polyUb, anti-p62, anti-LC3 and anti-actin antibodies. Atg16 KO brains accumulate high molecular weight polyubiquitinated proteins and p62, while LC3 I/II conversion was not detected. Densitometric values are represented graphically as mean \pm SD. Asterisk (*) indicates a significant difference between KO and WT samples; means compared by one-way ANOVA, *: $p < 0.05$, **: $p < 0.001$.

Autophagy has been implicated in the clearance of protein aggregates from neurons, as previous studies detected a polyubiquitin pathology in Atg5 and Atg7 KO mice (Hara et al., 2006). Brain slices were immunostained to detect the distribution of autophagy substrates: using antibodies against polyubiquitin chains and the p62 polyubiquitin-binding protein, an adaptor for K63-polyubiquitinated autophagy substrates (Bjørkøy et al., 2005). Extensive accumulation of protein aggregates, immunopositive for polyubiquitin chains as well as for p62, was detected in Atg16 KO brains (Fig.3.3.a). These protein aggregates were observed throughout the central nervous system (Fig.3.3.b) and in various other tissues of Atg16 KO mice (Fig.3.4.a). Extracerebral inclusions were most prominent in size in the sensory ganglia (dorsal root ganglia and ganglia of cranial sensory nerves); smaller aggregates were also detectable in the retinal pigment epithelium (RPE), in the liver and in the small intestine. These results indicate that loss of autophagy has a tissue-specific effect, and accumulation of polyubiquitinated substrates does not occur uniformly in the body.

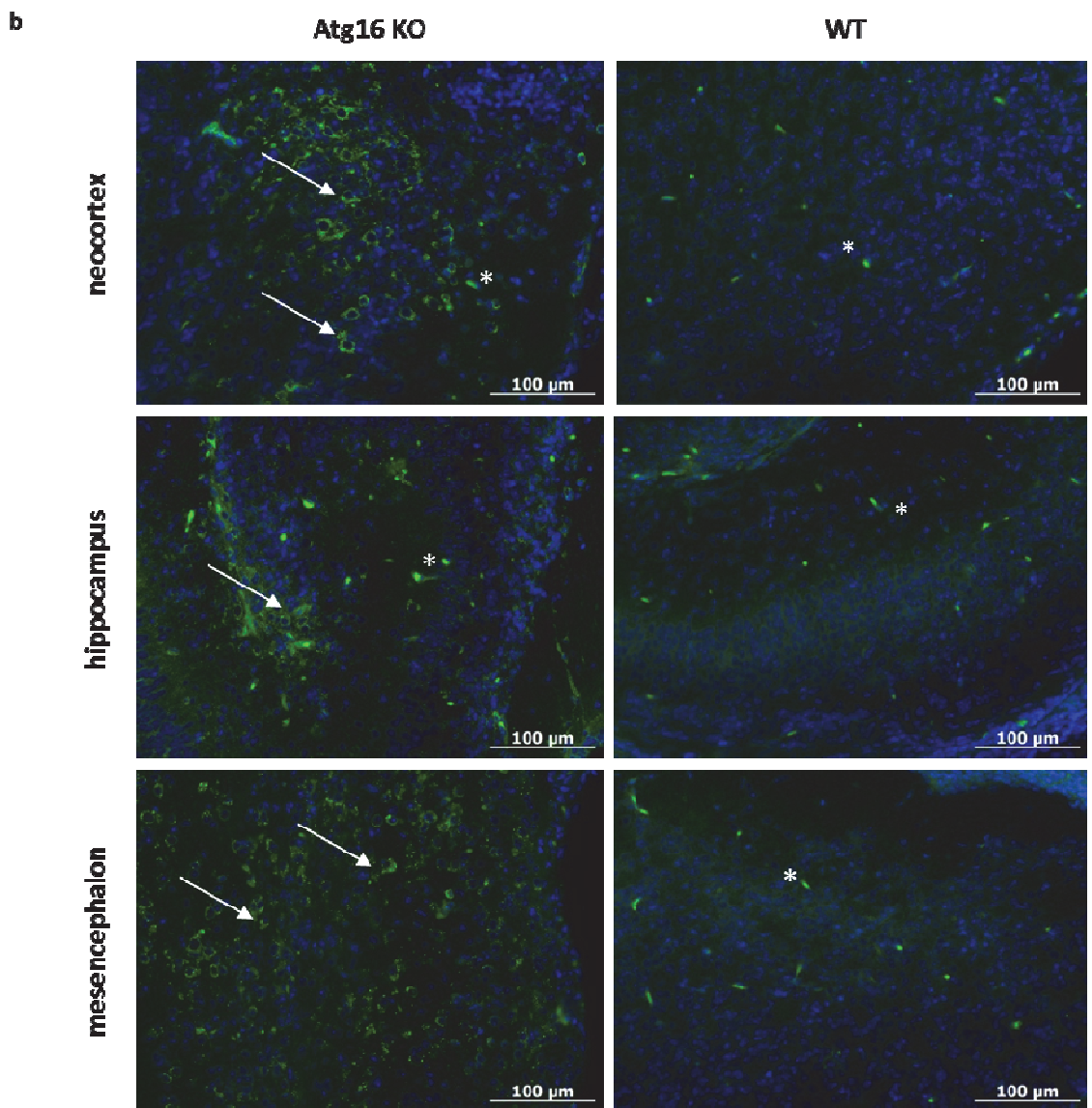
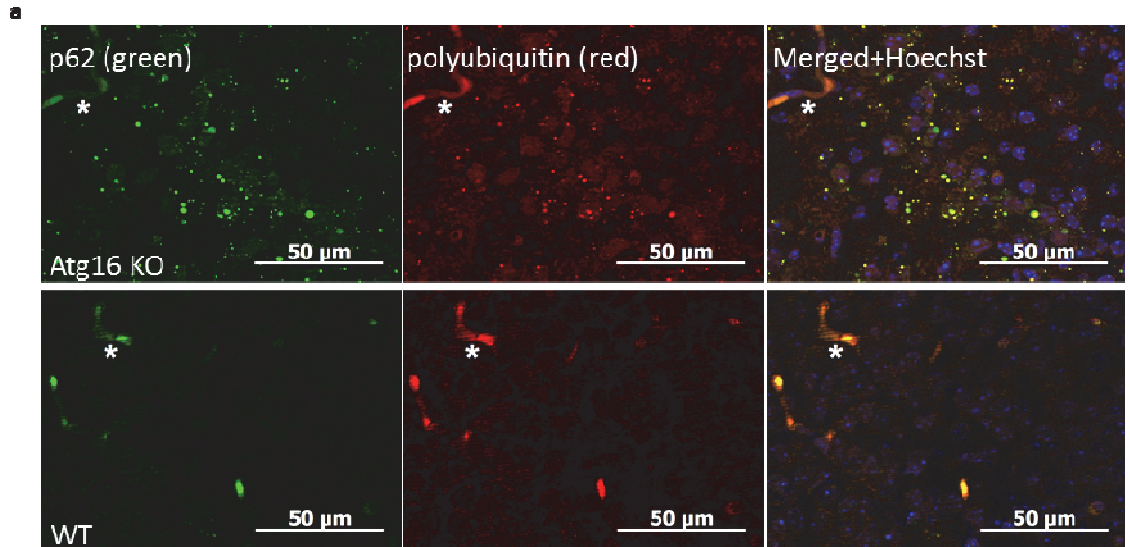
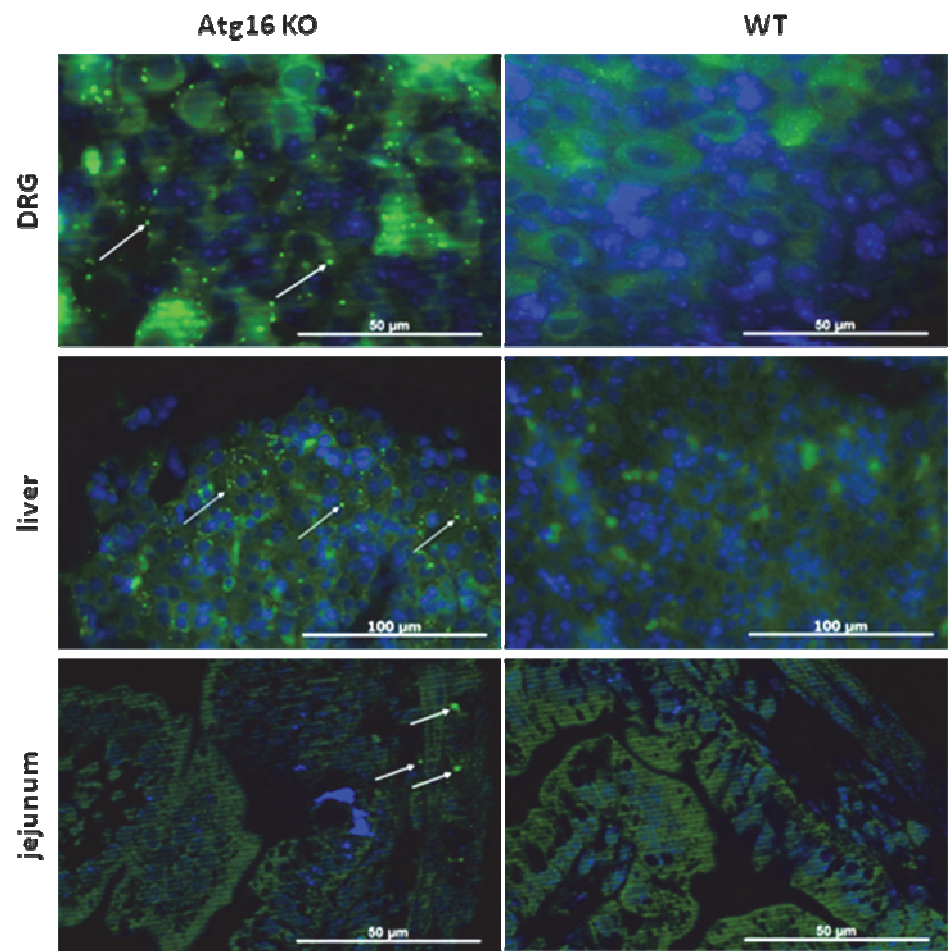


Fig. 3.3. a) p62 and polyubiquitin-positive protein aggregates appear in Atg16 KO brains. Midbrain section from an Atg16 KO neonate was stained with p62 (green) and polyUb-(red) specific antibodies and with Hoechst nuclear stain (blue). **b) Protein aggregates shown in various Atg16 KO brain regions.** Neonate brain sections were stained with anti-p62 (green) and Hoechst nuclear stain (blue). Non-specific signal from brain capillaries is labelled with asterisk (*) Aggregate-accumulating neurons labelled with arrow in low-magnification images.

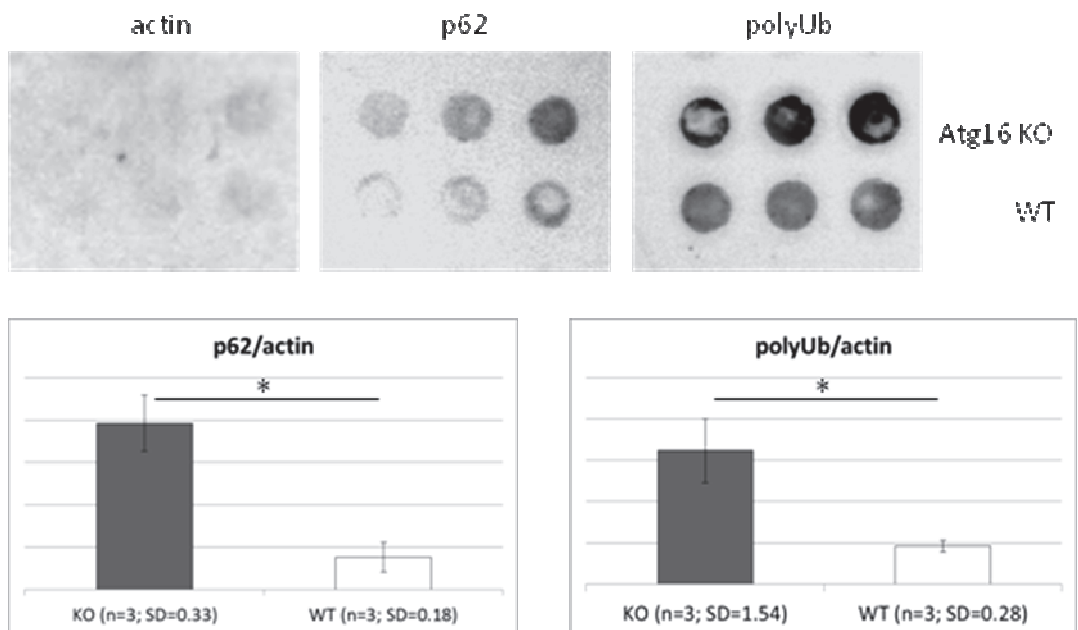
Polyubiquitinated protein inclusions appear in a range of human neurodegenerative diseases, and are characterized by their resistance to protein extraction, and require strong detergents to go into the soluble phase (Kazantsev et al., 1999). To test detergent-solubility, an aggregate-filtration method was applied, developed to detect Lewy-bodies in Parkinson's Disease (Kramer et al., 2008) by loading brain homogenates on a nitrocellulose membrane. Dot-blot polyUb probes showed strong signal in Atg16 KO compared to WT brain homogenates. PolyUb signal was reduced when homogenate was supplemented with SDS, confirming that protein aggregates in Atg16 KO mice are insoluble in non-ionic detergents (2% Triton-X100), but soluble in the presence of ionic detergents (2% SDS) (Fig.3.4.b).

Fig. 3.4. (see next page) a) Protein aggregates appear in Atg16 KO tissues, outside of the central nervous system. Cryosections from neonate dorsal root ganglia (DRG), liver and jejunum were stained with anti-p62 (green) and Hoechst nuclear stain (blue). Aggregate-accumulating cells are labelled with arrows **b) Polyubiquitinated aggregates are detergent-insoluble.** Anti-polyUb dot-blots were done on filtered neonate brain homogenates. Polyubiquitinated inclusions in Atg16 KO brains are Triton-insoluble but are readily dissolved in 2% SDS. Densitometric values are represented graphically as mean \pm SD. Asterisk (*) indicates a significant difference between KO and WT samples; means compared by one-way ANOVA, *: $p < 0.05$.

a

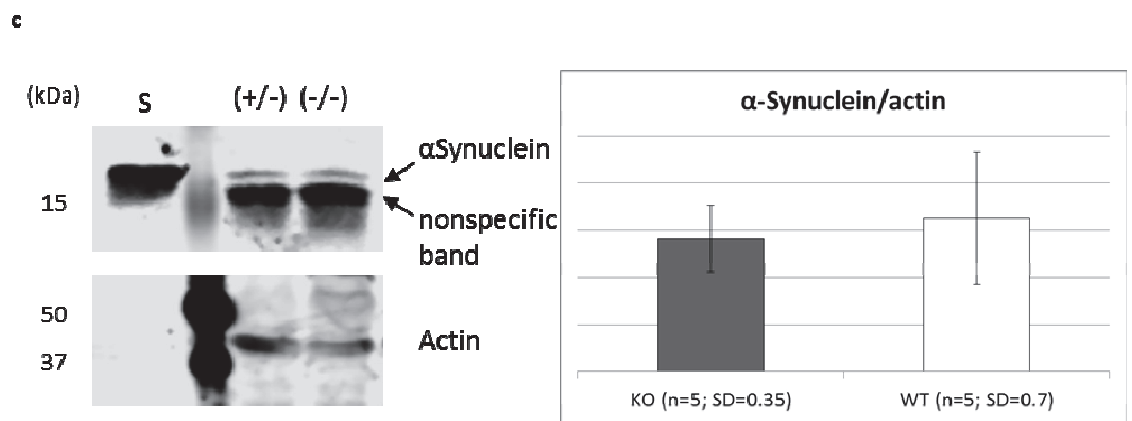
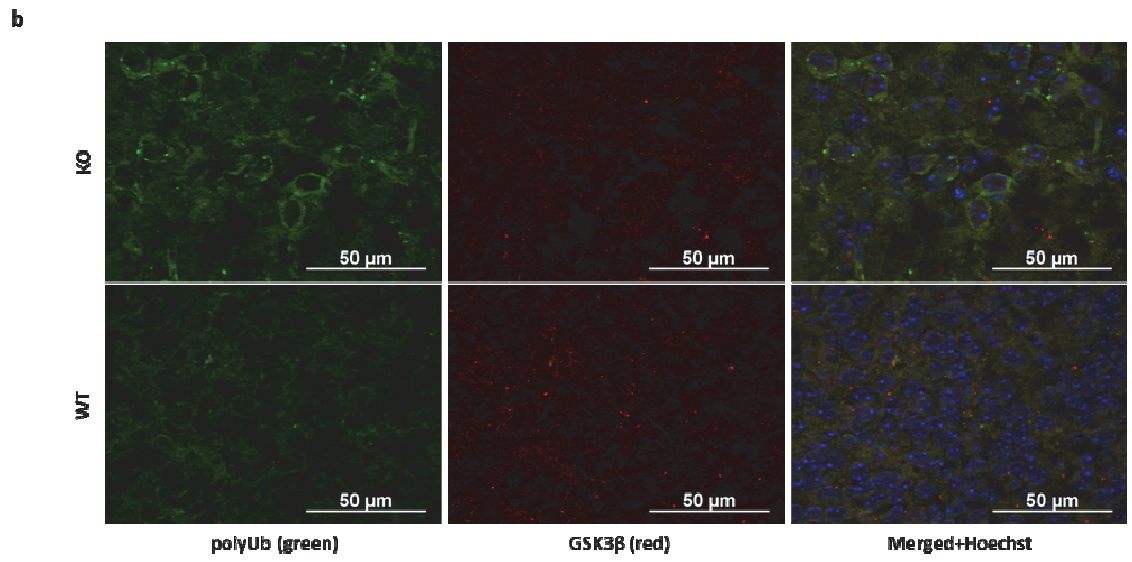
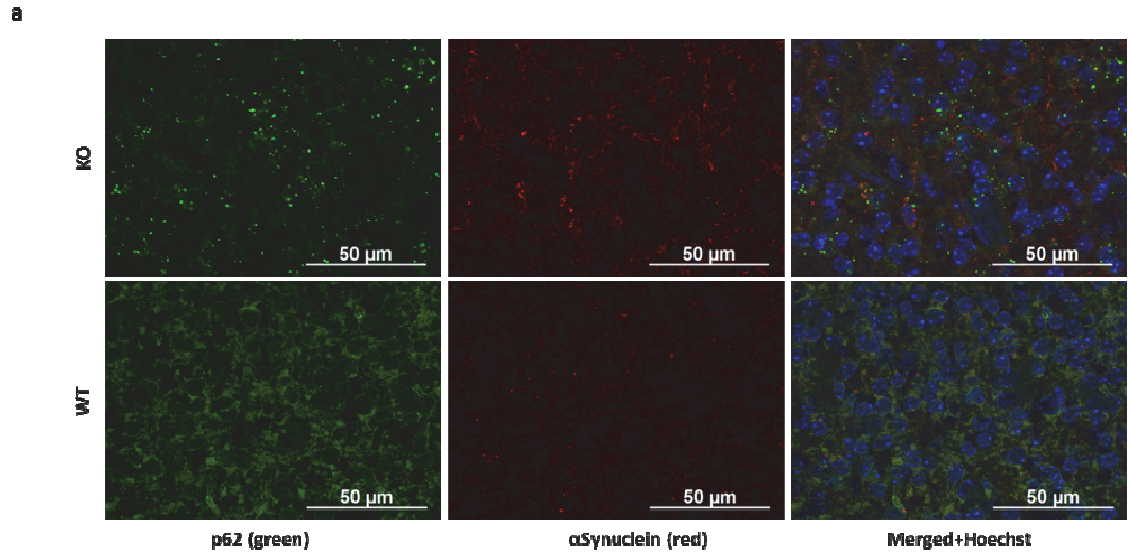


b



3.1.4. Polyubiquitinated aggregates are not associated with human neurodegenerative disease markers

Mice were then tested for the neurodegenerative disease markers beta-amyloid, Tau, α -synuclein, TDP-43 or GSK-3 β . These markers are used in diagnostic screens for taupathies, like Alzheimer's Disease (beta-amyloid 1-42, Tau, hyperphosphorylated Tau, GSK-3 β); synucleinopathies, like Parkinson's Disease, Dementia with Lewy-Bodies (alpha-Synuclein) or the FTL-ALS spectrum disorders (TDP-43) (Dickson et al., 2009, Tebbenkamp and Borchelt, 2009, Neumann et al., 2006, Hoozemans et al., 2009). Double immunostaining of brain sections for polyubiquitin (or p62) and selected neurodegenerative disease markers did not show colocalization. The neuronal distribution or CNS expression of these neurodegenerative disease markers was not affected by Atg16 KO (Fig.3.5.a,b,c,d). In conclusion, these experiments detected no structural correlate between the morphology of Atg16 KO brains and neuropathological lesions in human neurodegenerative diseases.



d

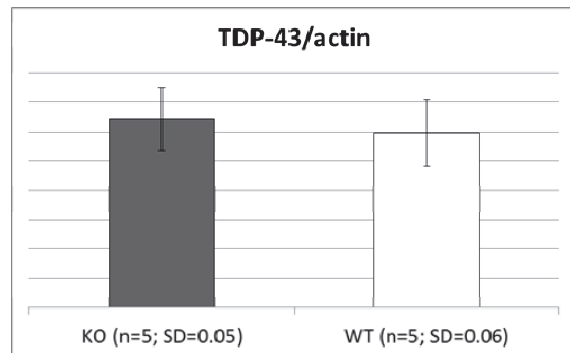
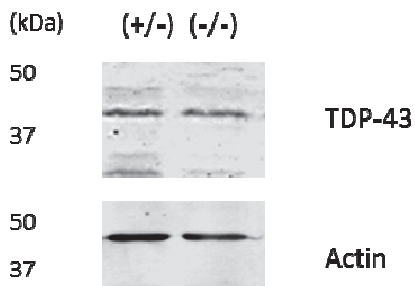
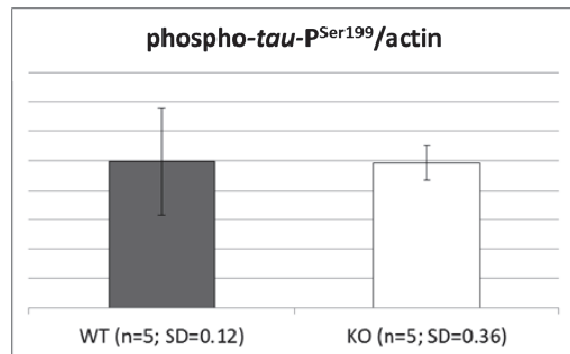
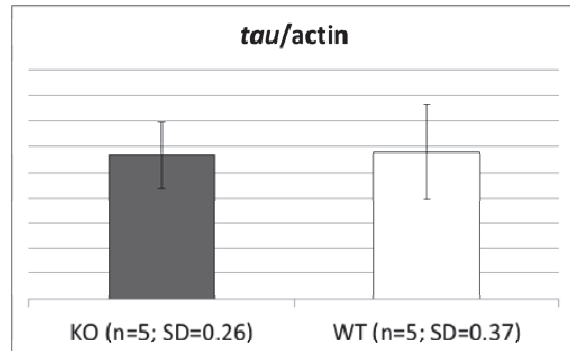
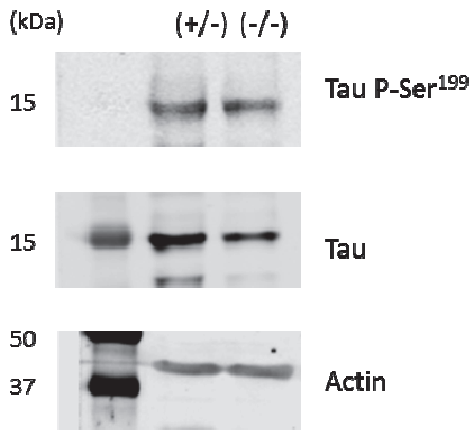
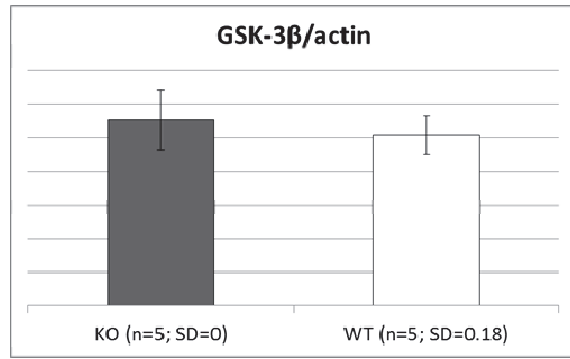
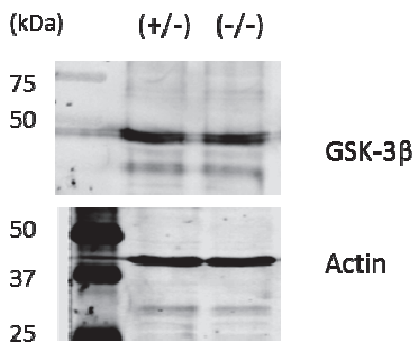
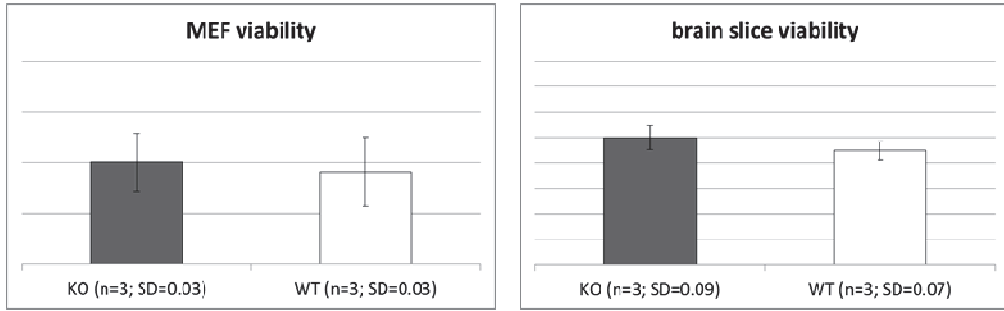


Fig. 3.5. a) α -Synuclein does not co-localise with the intraneuronal inclusions in Atg16 KO brains. Neonate midbrain sections were stained with anti-p62 (green), anti- α -Synuclein (red) and Hoechst nuclear stain (blue). No colocalisation (yellow puncta) detected. **b) GSK-3 β does not co-localise with the intraneuronal inclusions in Atg16 KO brains.** Neonate midbrain sections were stained with anti-polyUb (green), anti- GSK-3 β (red) and Hoechst nuclear stain (blue). **c) & d) Neurodegenerative disease markers are not elevated in Atg16 KO mice.** Immunoblotting of neonate brain homogenates, resolved in TPER or in 5xLeemml buffer: for anti- α -Synuclein, S: 500 ng purified mouse α -Synuclein as positive control; anti-GSK-3 β ; anti-Tau, anti-phosphoTau (P-Ser¹⁹⁹); anti-TDP-43. Densitometric values are represented graphically as mean \pm SD. Asterisk (*) indicates a significant difference between KO and WT samples; means compared by one-way ANOVA, *: p<0.05.

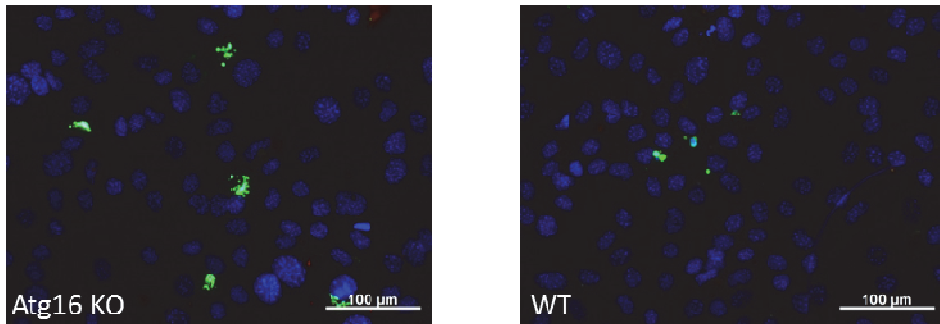
3.1.5. Cell death in Atg16 KO tissues

Viability of primary mouse fibroblasts (MEFs), harvested from E14.5 embryos, was quantified by WST-1 assay (Roche), a colorimetric test that measures the activity of mitochondrial dehydrogenases. Atg16 KO did not reduce viability of cultured mouse fibroblasts (Fig.3.6.a); however, apoptotic cell morphology was different in WT and Atg16 KO MEFs. Apoptotic WT MEFs had dense, small nuclei, while KO MEFs underwent abnormal apoptosis with irregular-shaped nuclei in TUNEL staining (Fig.3.6.b). Previous reports on autophagy defective mouse models showed cell loss in various neuronal layers, ultimately leading to limb paralysis, ataxia, and pathologic reflexes (Komatsu et al. 2006). To compare cell death in WT and Atg16 KO a TUNEL staining was done, which did not indicate accelerated apoptosis in Atg16 KO brains as compared to WT littermates (Fig.3.6.c). Notably, TUNEL-positive cells were always negative for protein inclusion markers, while surrounding cells usually displayed the polyubiquitin inclusion pathology (Fig.3.6.d).

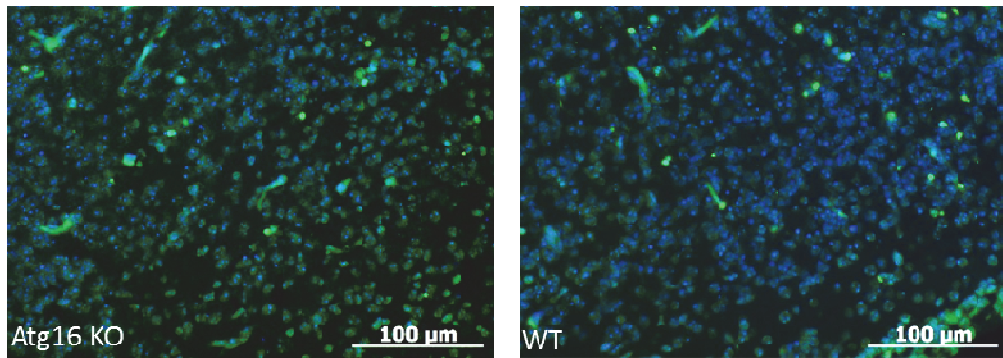
a



b



c



d

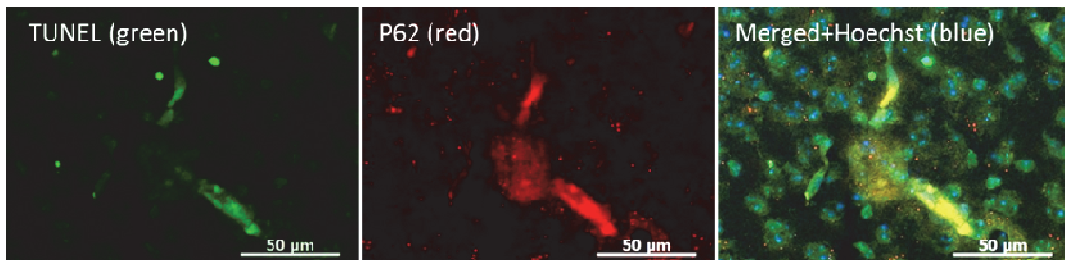


Fig. 3.6. a) Atg16 KO does not impair viability of primary MEFs and OBCs. No significant difference detected using WST-1-metabolism assay. (OD values are represented graphically as mean \pm SD; means compared by Student's t-test) **b) Abnormal cell death morphology in Atg16 KO MEFs.** WT and Atg16 KO MEFs (non-infected), stained with TUNEL (green) and Hoechst nuclear stain (blue). **c) Apoptosis in Atg16 KO brains is not accelerated as compared to brains of WT littermates.** Neocortex sections from WT and KO neonates, stained with TUNEL (green) and Hoechst nuclear stain (blue). **d) Protein aggregation does not lead to apoptosis in Atg16 KO mice.** Midbrain section from a P0 neonate; stained with TUNEL, anti-p62 antibody and Hoechst nuclear stain. No association detected between apoptosis (TUNEL) and protein aggregation (p62). Atg16 KO does not affect cell viability.

TUNEL staining of fixed brains may also be affected by the inadvertent asphyxia during cervical dislocation of animals. In order to avoid this, organotypic brain slices (OBCs), harvested from neonate mice were cultured on a semi-permeable membrane interface, then tested for viability using WST-1 assay (Roche), a colorimetric test that measures the activity of mitochondrial dehydrogenases. Atg16 KO did not reduce viability of cultured brain tissues (Fig.3.6.a), suggesting that polyubiquitinated protein aggregates are not causatively linked to neuronal cell death or to the mortality of Atg16 KO mice.

3.1.6. Summary

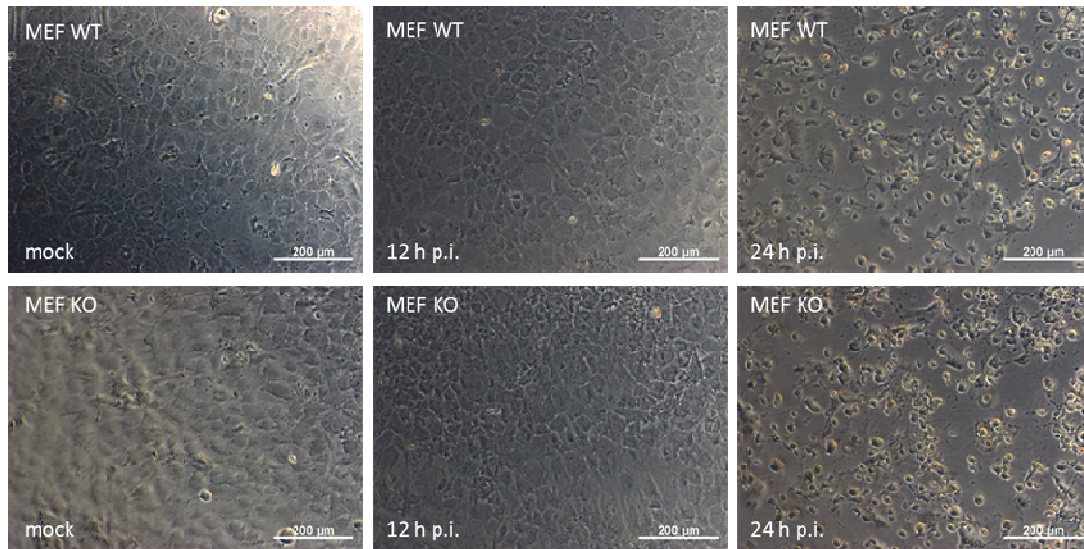
The above experiments confirm that Atg16 KO neonates recapitulate most phenotype characteristics of the Atg5 KO and Atg7 KO mice (Kuma et al., 2004, Komatsu et al., 2005). Neonate pups, however, fail to commence suckling in the presence of lactating mothers. Rapid exhaustion of nutrient supplies results in hypoglycaemia in Atg16 KO neonates, which – together with dehydration - is a feasible explanation of their mortality. Histopathological analysis revealed an accumulation of protein inclusions in the CNS of Atg16 KO neonates, immunopositive for polyubiquitin and p62. The importance of these observations lies in the fact that similar intraneural inclusions are commonly found in human neurodegenerative diseases (Kuusisto et al., 2008, Nakano et al., 2004). While polyubiquitinated aggregates are commonly associated with neurodegeneration, cell damage or accumulation of pathogenic proteins was not observed in the affected neurons. Apoptotic Atg16 KO cells are characterised by irregular-shaped nuclei; possibly due to an impaired phagocytosis of dead cells by neighbouring fibroblasts, as autophagy has been implicated in the phagocytic clearance of apoptotic debris (Qu et al., 2007).

3.2. Semliki Forest Virus infection in Atg16 KO mouse tissues

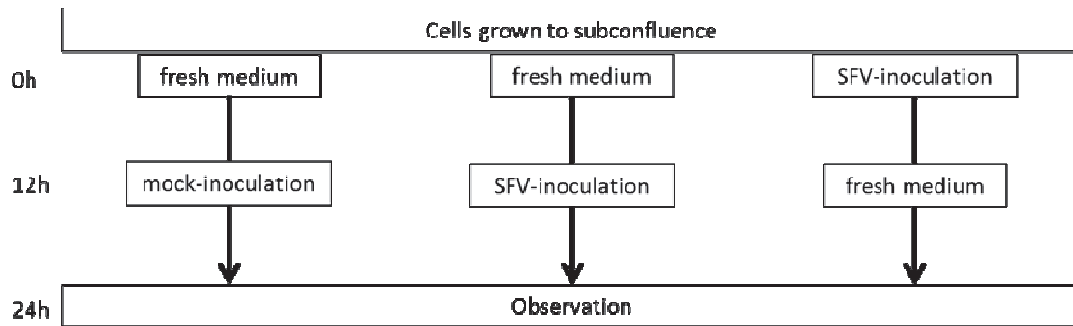
3.2.1. Study objectives:

Semliki Forest Virus (SFV) uses the endosomal-lysosomal pathway to infect host cells (Helenius et al., 1980, Froshauer et al., 1988), a pathway which is closely linked to autophagy. There is little evidence to implicate the role of autophagy in host cell defence against SFV infection or in viral exploitation of host cell function. The aim of these studies was to gain a better insight into the mechanism of SFV infection and autophagy, using a novel Atg16 KO model. Cultured cells and OBCs were inoculated with the highly virulent SFV-4 strain of Semliki Forest Virus, derived from the cDNA clone of the original isolate (Liljeström et al., 1991). SFV viruses were initially amplified on Vero cell monolayers, and virus containing cell culture supernatant was used to inoculate MEF culture monolayers (WT and Atg16 KO, harvested from E14.5 embryos) or OBCs (harvested from P0 neonates).

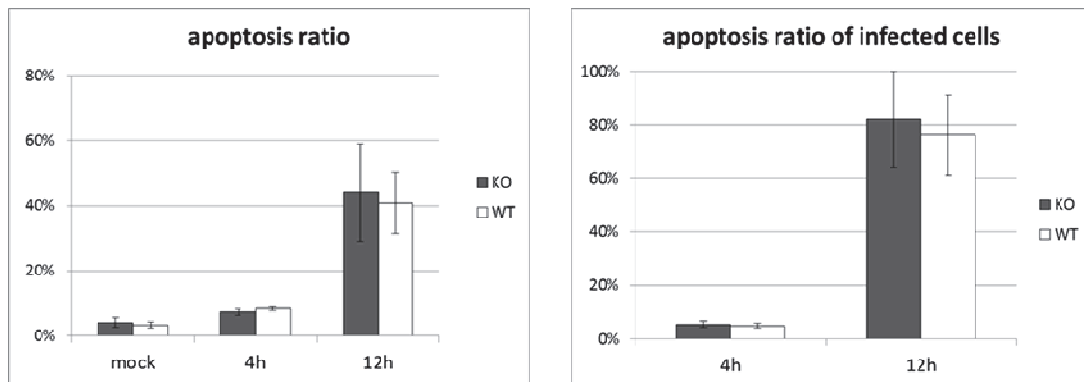
a



b



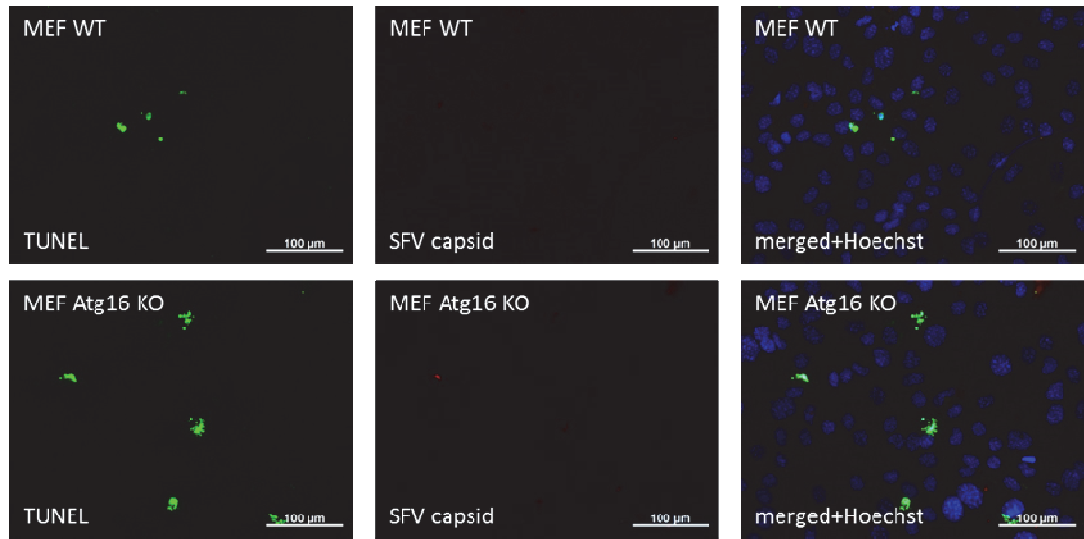
c



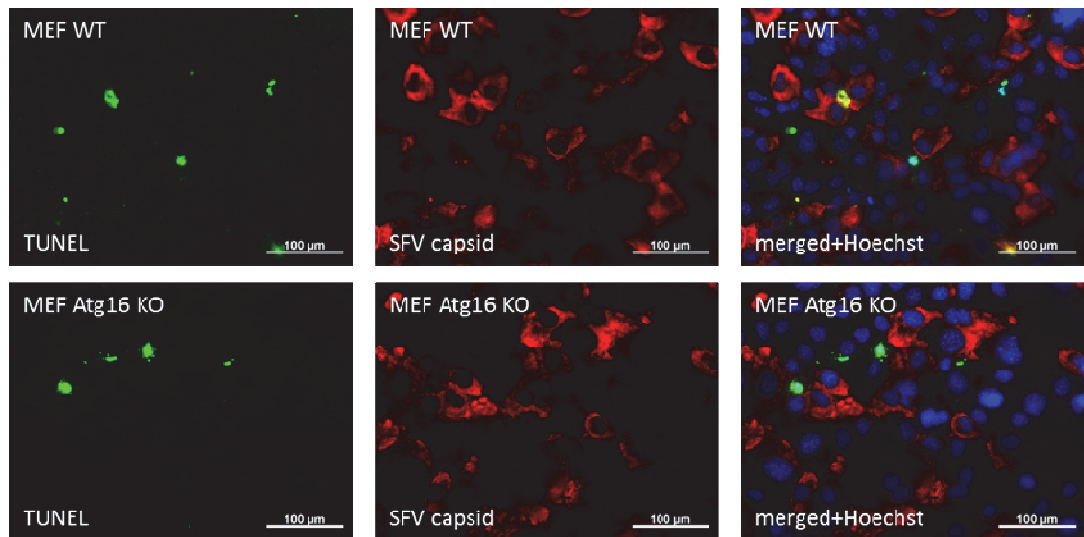
TUNEL (+) / total cells		
	avg	SD
KO mock	0,042	0,015
WT mock	0,034	0,009
KO 4h	0,073	0,010
WT 4h	0,084	0,005
KO 12h	0,439	0,149
WT 12h	0,408	0,094

TUNEL (+) SFV (+) / SFV (+)		
	avg	SD
KO 4h	0,055	0,012
WT 4h	0,049	0,009
KO 12h	0,82	0,18
WT 12h	0,76	0,15

d



e



f

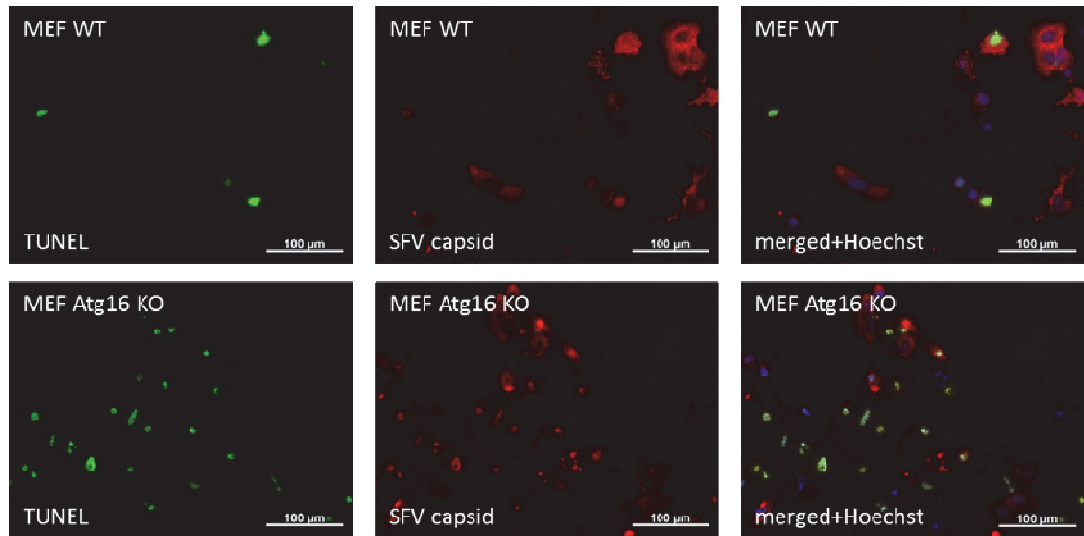
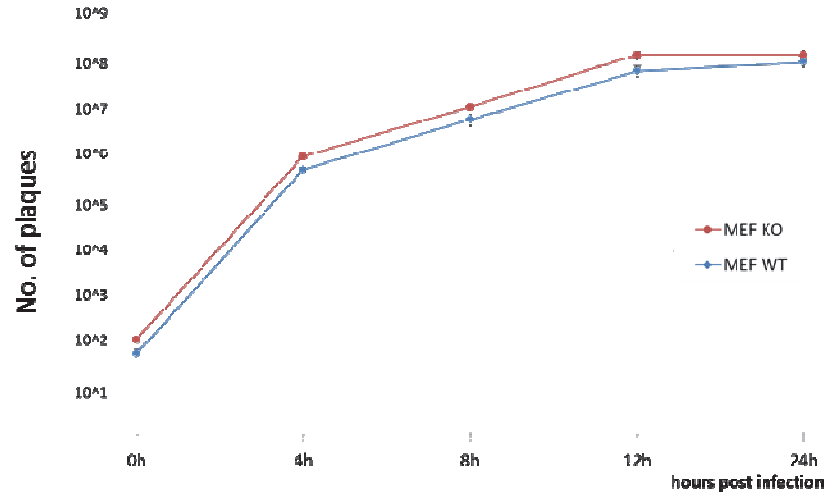
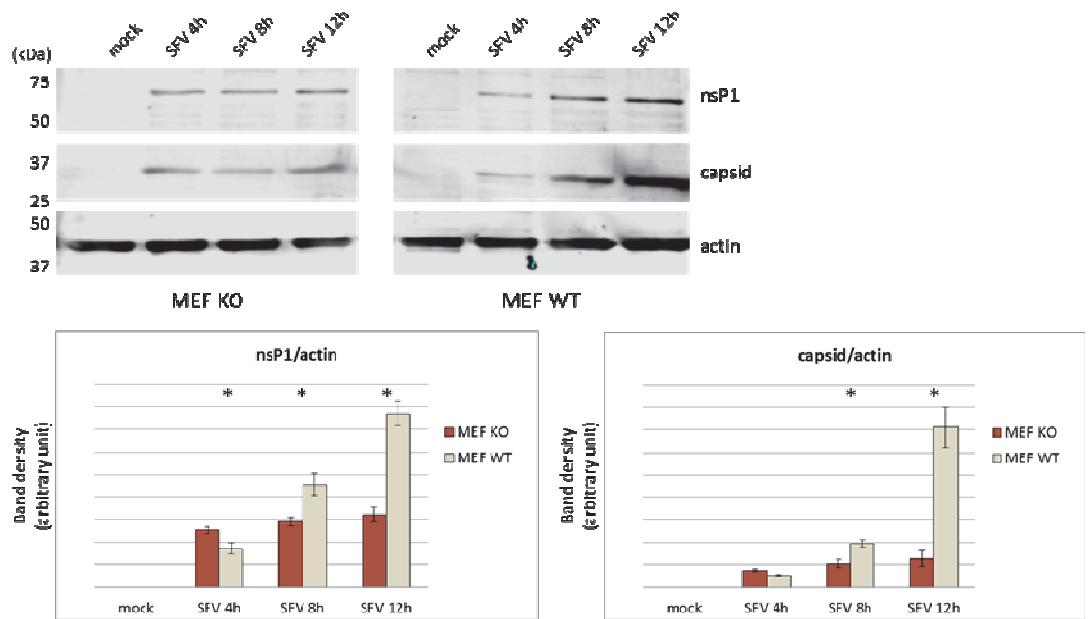
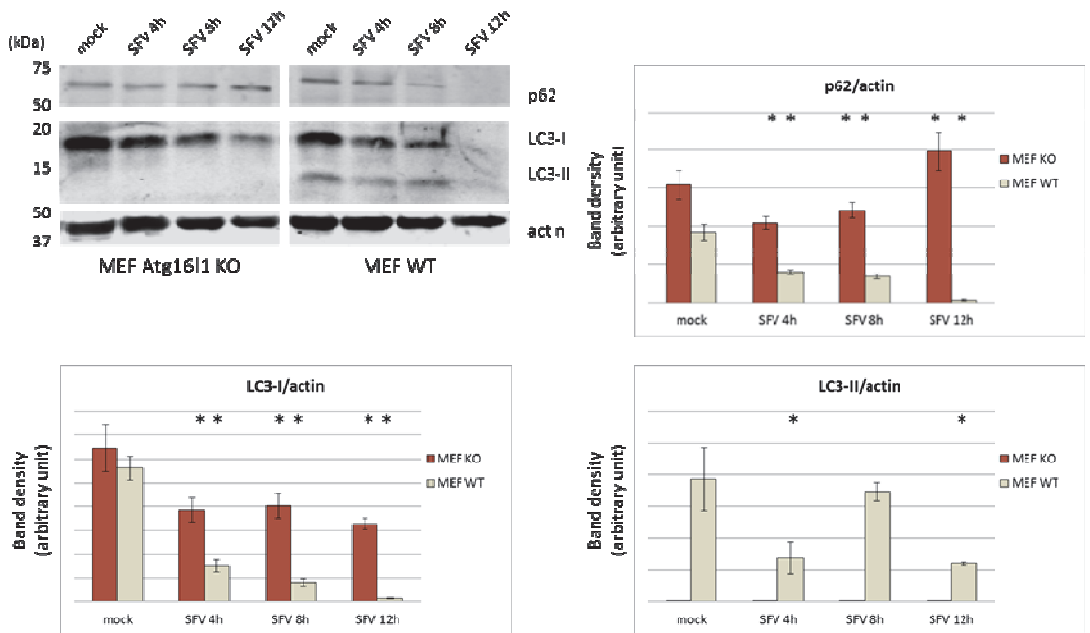


Fig. 3.7. a) Cytopathic effect of SFV infection is indistinguishable in Atg16KO and WT cultures. Bright field microscopy of WT and Atg16KO MEFs, infected with SFV (MOI: 0.5). Cytopathy is visible from 12h post inoculation, cells detach from the surface 24h post inoculation. **b) Flowchart of virus infection experiments** **c) WT and Atg16 KO MEFs are equally susceptible to SFV infection and apoptosis.** Apoptotic ratio (TUNEL pos. / total cells) is represented graphically as mean \pm SD; means compared by one-way ANOVA. Approx. 300 cells were counted from 5 fields for each condition tested. **d), e) & f) Infected MEFs commit apoptosis approx. 12hrs after SFV infection** Fluorescent microscopy of WT and Atg16 KO MEFs, infected with SFV (MOI: 0.5). Cells stained with TUNEL (green), anti-SFV-capsid antibody (red) and Hoechst nuclear stain (blue). d) mock e) 4 h p.i. f) 12 h p.i.

3.2.2. Semliki Forest Virus infection in monolayer cultures

WT and Atg16 KO MEF cultures were inoculated at low (0.5) or high (10) MOI as indicated and infection was monitored under a light microscope for morphological changes at given time points. As subsequent passages result in adaptation and accumulation of mutations, first the lytic effect of the SFV4 strain was confirmed in cell cultures. Cytopathic effect of SFV (cytoplasmic vacuolation and pyknosis) became evident in 12 h p.i. (post inoculation), and most MEFs detached from the surface within 24 h p.i. (Fig.3.7.a). Inoculated MEFs were fixed at various time points (Fig.3.7.b) then subjected to immunostaining with antibodies detecting SFV non-structural proteins (nsP1 and nsP3), SFV capsid and double-stranded RNA (dsRNA). Anti-capsid staining showed widespread, productive virus infection by 4 h p.i. TUNEL positive apoptotic cells, in turn, were sparsely detected up until 12 h p.i. (Fig.3.7.c,d,e,f). Their frequency in cell cultures was independent from Atg16 genotype at any time point. Notably, at initial stages of SFV infection, cells expressing SFV capsid were negative for TUNEL and TUNEL-positive cells did not display SFV markers. SFV infection had no effect on nuclear morphology in apoptotic cells, while Atg16 KO MEFs were characterized by an impairment of nuclear condensation (see in detail in chapter 3.1.5.).

a**b****c**

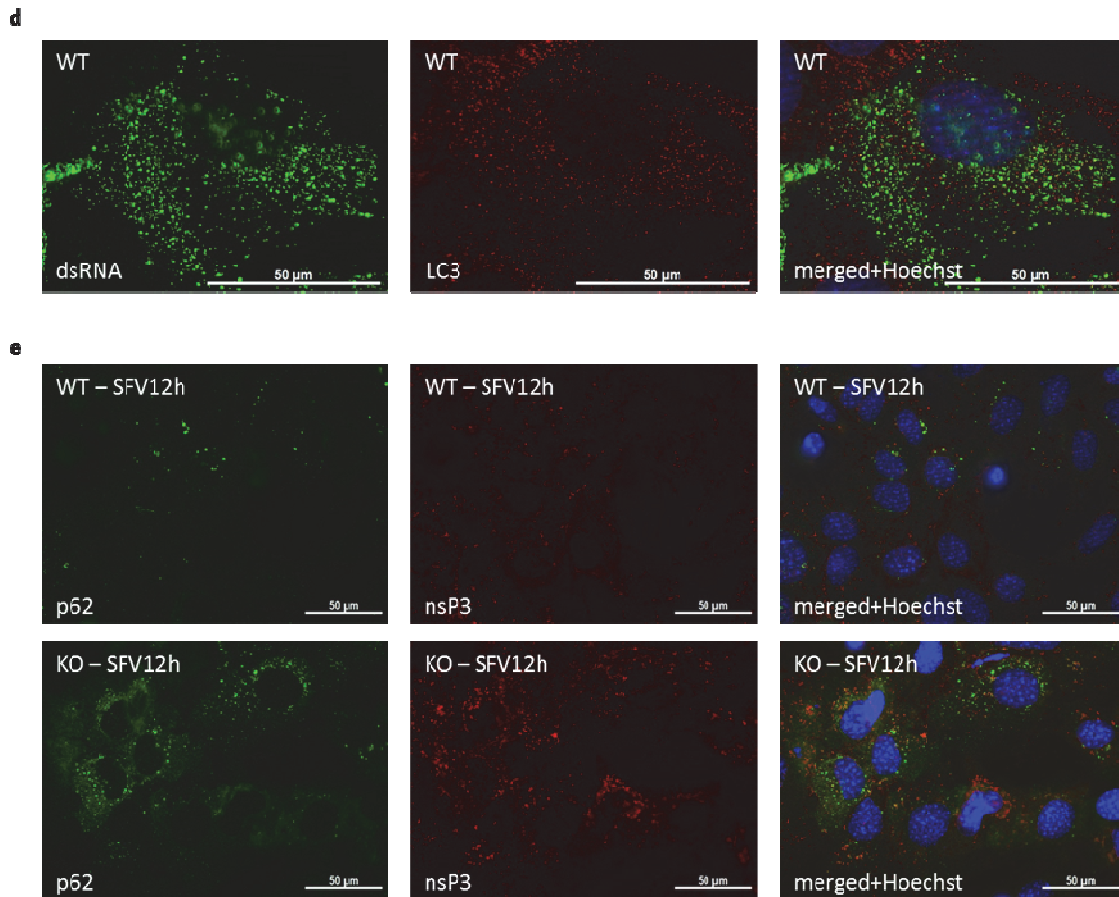


Fig. 3.8. a) No difference found between Atg16 KO and WT MEF SFV production. MEF-s cultured from wild type and Atg16 KO mice were infected with SFV. Infectious particle production was quantified by plaque assays in Vero cell monocultures. **b) Loss of Atg16 reduces viral protein expression in infected MEFs.** Infected WT and Atg16 KO MEF lysates immunoblotted for SFV-nsP1 or SFV-capsid. Densitometric values are represented graphically as mean from 3 independent experiments \pm SD. Asterisk (*) indicates a significant difference between KO and WT samples; means compared by one-way ANOVA, *: $p < 0.05$ **c) Effects of SFV infection on autophagy protein levels.** WT and Atg16 KO MEFs infected with SFV, immunoblotted for host LC3 and p62. Densitometric values are represented graphically as mean from 3 independent experiments \pm SD. Asterisk (*) indicates a significant difference between corresponding mock and infected samples; means compared by one-way ANOVA, *: $p < 0.05$ **d), e) Replicating SFV does not associate with autophagy proteins.** Fluorescent microscopy of WT and Atg16 KO MEFs, infected with SFV (MOI: 0.5). d) Immunostaining with antibodies recognizing dsRNA (green) or LC3 (red). Hoechst nuclear stain (blue). No colocalization observed (yellow dots absent). e) Immunostaining with antibodies recognizing p62 (green) or SFV-nsP3 (red). Hoechst nuclear stain (blue). No colocalization observed (yellow dots absent).

SFV virus production in Atg16 KO and WT MEF cultures was quantified by plaque assays. SFV infectious particles rised to high titers as early as 4 h after cell culture inoculation: infection was equally productive in Atg16 KO and WT MEF cultures as no significant difference in plaque numbers was detected (Fig.3.8.a). The effect of Atg16 KO on virus replication was further analysed by estimating the levels of viral replicase protein (nsP1 and nsP3) and capsid protein (C) production using western blots. SFV infected Atg16 KO MEFs expressed significantly lower levels of nsP1 and capsid proteins, compared to WT MEFs (Fig.3.8.b). The effect of virus replication on the conventional autophagy pathway was investigated by comparing LC3-I/LC3-II ratio and p62 levels in infected and mock-infected cells (Fig.3.8.c). Loss of autophagy increased p62 levels and blocked LC3-I/LC3-II conversion in Atg16 KO MEFs. SFV infection gradually decreased p62 in WT MEFs. In Atg16 KO MEFs an initial attenuation of p62 expression during the early phase of SFV infection was followed by an increase from 12h p.i. LC3-I levels were gradually decreased upon SFV-infection in WT and, similarly, in Atg16KO MEFs; hence, this effect was independent from autophagy. In WT MEFs, LC3-II was attenuated as SFV-infection progressed. LC3-II was missing in Atg16 KO MEFs. The localization of SFV replication was independent from autophagosomes as viral dsRNA or the replicase nsP3 did not co-localize with LC3, nor with the polyubiquitin-adaptor p62. Autophagosomes did not accumulate in infected cells (Fig.3.8.d,e).

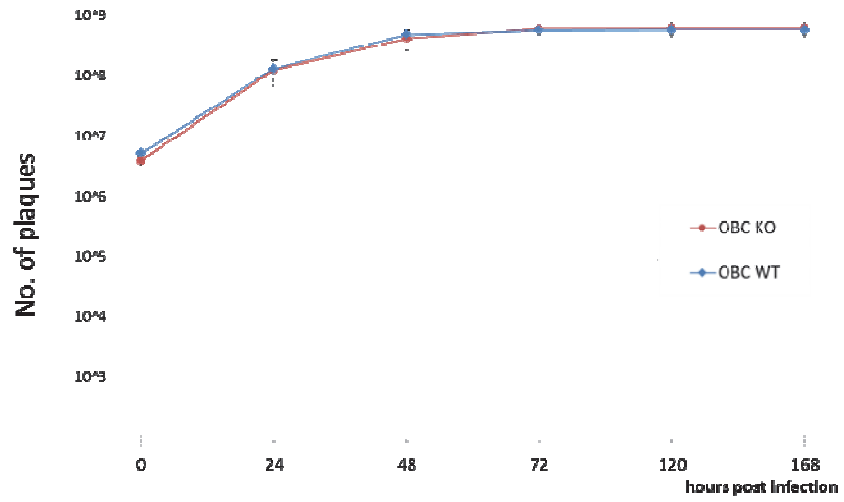
3.2.3. Semliki Forest Virus infection in organotypic brain cultures

The micro-environmental aspects of viral brain infection were recapitulated using organotypic coronal brain slices (OBCs). Each brain slice was inoculated with 10^7 infectious SFV particles on the 4th day after harvesting. Virus production was subsequently assayed by plaque assays in Vero cell monolayers. As OBCs detach easily from membrane, manipulation was minimized and residual virus load was calculated after removing the inoculum. Plaque assays showed a very low (~ 100 particles/2 days/brain slice), yet detectable production of SFV in brain cultures, even after 7 days (Fig.3.9.a). There was no significant difference of plaque numbers, and therefore no difference of SFV production in WT and Atg16 KO cultures. Viral protein production was quantified by western blots from OBCs lysed 5 days after inoculation. Capsid expression was non-significantly lower in KO cultures, while WT and KO cultures generated similar amounts of viral nsP1 (Fig.3.9.b). LC3-I/LC3-II ratio and p62 levels were assayed by western blots to study SFV-induced changes in autophagy (Fig.3.9.c). Similar to MEFs, Atg16 KO increased p62 levels and blocked LC3-I/LC3-II conversion in OBCs. An opposite tendency of p62 expression in WT and Atg16 KO OBCs was observed: p62 levels decreased in SFV-infected WT OBCs and increased in Atg16 KO OBCs. LC3-I and LC3-II levels were decreased in SFV-infected WT and Atg16 KO brain cultures. These virus induced changes did not reach a statistical significance. To examine the effect of Atg16 deficiency on the neurotoxicity of SFV a WST colorimetric assay was performed, commonly used to test cell viability (Fig.3.9.d). The results showed an increased sample absorption in SFV-infected OBC media (which would indicate an increased viability); however, it appears rather conceivable that WST-1 viability test was confounded by the metabolic effects of viral infection (Cassells and Burke, 1973a), SFV-infected OBCs were then analysed by TUNEL staining to detect apoptotic cells. The frequency of TUNEL-positive cells was not significantly higher in virus infected

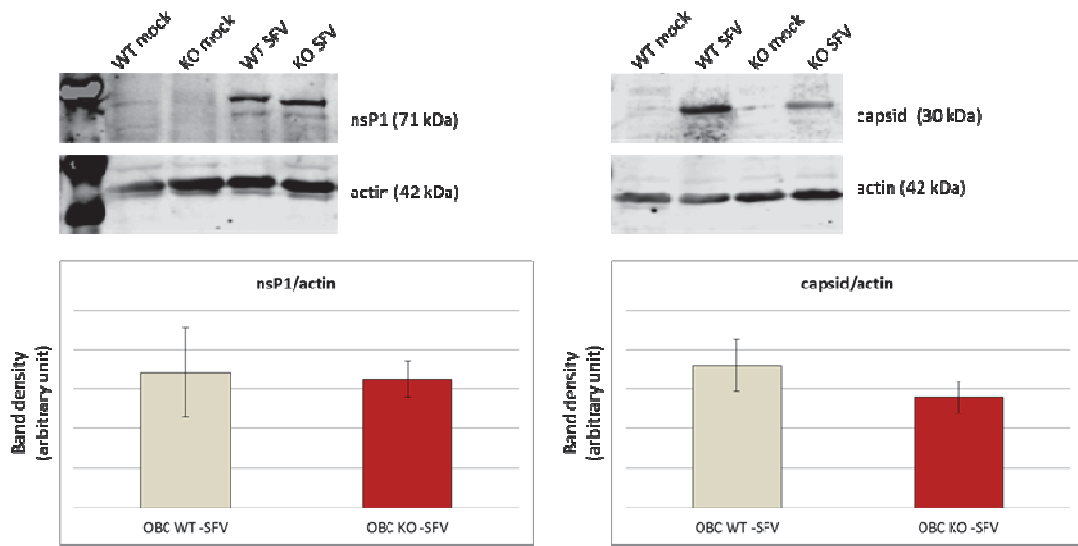
brain cultures, and independent from Atg16 genotype. Infected cells (expressing SFV-capsid) were negative for TUNEL, while apoptotic cells were negative for SFV markers (Fig.3.9.e,f).

Fig.3.9. (see next pages) a) Atg16 KO has no effect on SFV production. OBCs were cultured from WT and Atg16 KO mice and infected with SFV. a) Virus production was assessed by plaque assay in Vero cell monocultures. **b) lysates of infected OBCs immunoblotted for SFV-nsP1 and SFV-capsid.** Densitometric values are represented graphically as mean from 3 independent experiments \pm SD. Asterisk (*) indicates a significant difference between KO and WT samples; means compared by one-way ANOVA, *: $p < 0.05$ **c) Effects of SFV-infection on autophagy protein levels in OBCs.** OBCs were cultured from WT and Atg16 KO mice and infected with SFV. Lysates of infected OBCs immunoblotted for p62 or LC3. Densitometric values are represented graphically as mean from 3 independent experiments \pm SD. Asterisk (*) indicates a significant difference between KO and WT samples; means compared by one-way ANOVA, *: $p < 0.05$ **d) WST-1 assay in SFV-infected organotypic coronal brain cultures.** Organotypic coronal brain cultures from control or Atg16 KO mice were infected with SFV. Cultures were assayed for viability 5 days after inoculation using WST-1 (Roche). The biochemical background of WST-1 assay: NADH^+ -dependent cleavage of the tetrazolium salt WST-1 produces dark red formazan which is measured colourimetrically (picture adapted from the product description of WST-1 colorimetric assay (Roche)) OD values are represented graphically as mean from 3 independent experiments \pm SD; means of corresponding mock and infected samples were compared by Student's t-test *: $p < 0.05$ **e) Apoptotic cells (arrows) in brain cultures are SFV-negative.** Fluorescent microscopy of WT and Atg16 KO OBCs, infected with SFV. Cultures were fixed and processed for immunofluorescence 5 days post inoculation, then analyzed with TUNEL (green) and immunostained for SFV capsid (red). Hoechst nuclear stain (blue). **f) Apoptosis is not significantly increased in SFV-infected OBCs.** Apoptotic ratio (TUNEL pos. / total cells) is represented graphically as mean \pm SD; means compared by one-way ANOVA. Approx. 300 cells were counted from 5 fields for each condition tested.

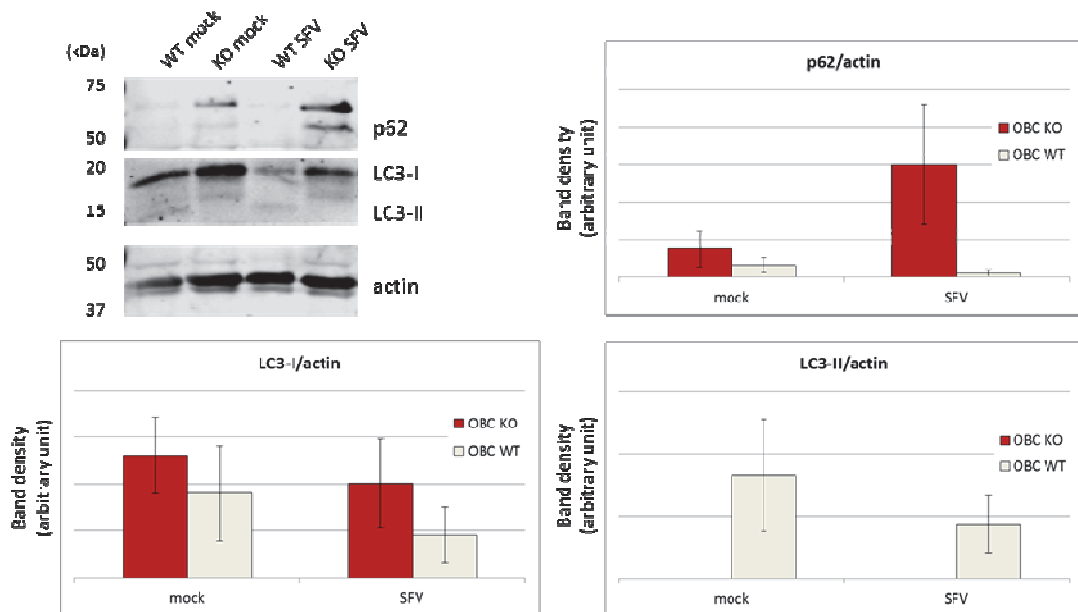
a



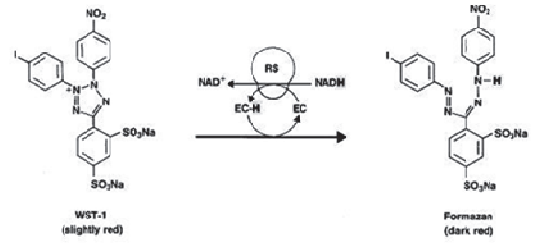
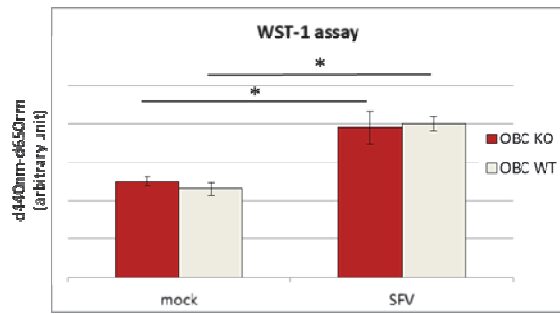
b



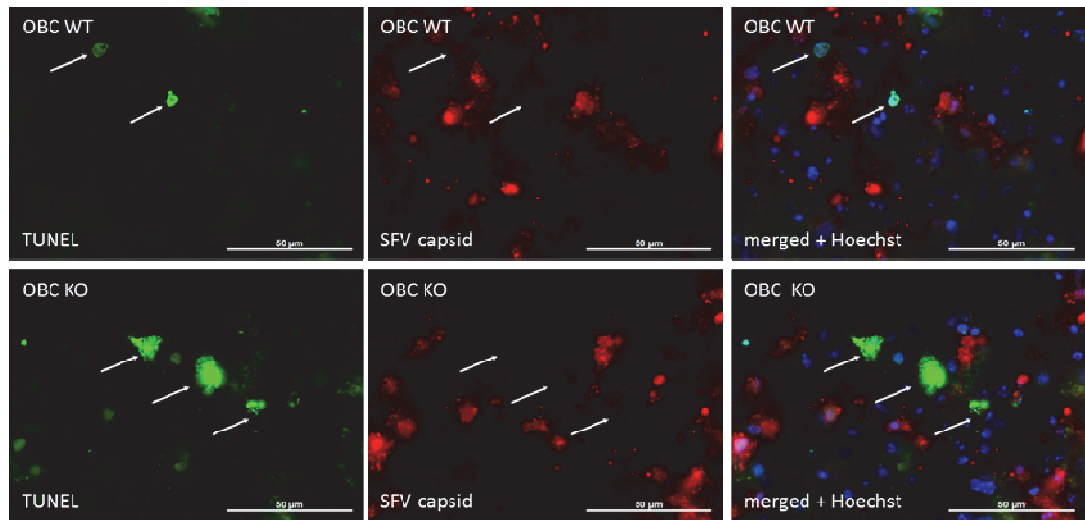
c



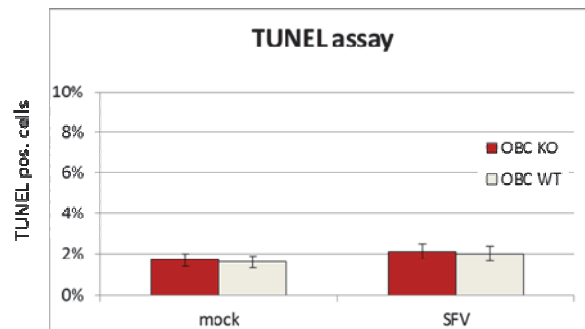
d



e



f



3.2.4. Summary

These studies investigated the interaction between autophagy and SFV infection using Atg16 KO and WT cell cultures as well as organotypic brain cultures. Lytic infection by SFV4 was observed in cell cultures as infectious particles rapidly rised to high titers, and viral protein expression was detected as early as 4 h p.i. in cell culture monolayers. In agreement with previous studies (Eng et al., 2012), SFV markers showed no colocalization with autophagosome proteins (LC3 or p62) in autophagy competent cultures. In contrast to the aforementioned paper, the above results do not confirm an accumulation of autophagosomes, neither as a result of their increased formation, nor by an impairment of their fusion with lysosomes. Replication kinetics, cytopathogenicity and extent of cell death in SFV infected cell cultures was not affected by Atg16 KO in MEFs and in OBCs. While Atg16 KO MEFs expressed relatively low nsP1 and capsid levels and similar (yet non-significant) tendency was found in Atg16 KO brain cultures, it did not interfere with SFV proliferation. Both in MEF cultures as well as in OBCs, the production of infectious SFV particles peaked on the first day after infection, followed by a rapid decrease. The similar pattern however, reveals a strikingly different infection kinetics: SFV proliferation in MEFs was only limited by the availability of viable cells. In OBCs, while SFV proliferation was demonstrated by the presence of viral dsRNA, non-structural and capsid proteins, infectious virus production decreased rapidly. As cells started to commit apoptosis 12 h p.i. in MEF cultures, and no association was found between apoptosis markers and SFV infection in OBCs, it appears a feasible explanation that apoptosis is not a direct sequelae of SFV infection, rather than cytokines secreted from infected cells.

3.3 Autophagy induction *in vitro* by red wine polyphenols

3.3.1. Study objectives:

Nutritional studies implied health benefits from wine and berry consumption (Orgogozo JM, 1997, Lindsay et al., 2002, Nooyens et al., 2013), which implicates a mechanism that depends on their polyphenol content and/or autophagy stimulation. Hence, investigating the feasibility of autophagy induction by dietary or pharmacological intake of polyphenols is of practical importance. Polyphenols enriched in dietary berries and red wine (Macheix et al., 1990), such as resveratrol (RSV), quercetin (QRC), (-)-epicatechin (EC), cyanidin-3-O-glucoside (Cy3G), peonidin-3-O-Glucoside (Pe3G) and malvidin-3-O-glucoside (Ma3G) were tested *in vitro* to establish their dose-response relationship with autophagy induction. A concentration range from 0.01 μM to 100 μM was selected to span the range of plasma concentrations following dietary consumption, or administration in the context of pharmacological studies (Manach et al., 2004, Goldberg et al., 2003).

3.3.2. Polyphenol studies in monolayer cultures

Mouse embryonic fibroblasts (MEF), human neuroblastoma (SH-SY5Y) cells and green monkey kidney epithelial cells (Vero) as well as GFP::LC3 transfected human embryonic kidney (HEK-293) and Chinese hamster ovary (CHO) cells were incubated in the specified culture medium enriched with polyphenols as outlined in the Materials and Methods.

WST-1 cell proliferation assays (formazan concentration directly related to the metabolic activity of the cells) showed no polyphenol-induced reduction of cell viability *in vitro* (Fig.3.10.a). Polyphenol induced changes in autophagy were tested by assessing the qualitative and quantitative differences of the autophagosome marker proteins LC3 and p62, as outlined in the most recent guidelines for autophagy studies (Klionsky et al., 2012). For positive controls, the mTORc1 agonist chemical Torin (250 nM, TOCRIS) was added to the culture media, or cells were exposed to amino-acid starvation in Hank's balanced salt solution (HBSS) (Klionsky et al., 2012). A dose-dependent autophagosome accumulation was observed in cells treated with the stilbene RSV or the flavonol QRC. For both polyphenols, supraphysiological doses ($\geq 10\mu\text{M}$) were necessary to detect autophagosome accumulation in cells (Fig.3.10.b,c,d).

The pro-autophagic effect of polyphenols was quantified by LC3 immunoblotting, as RSV and QRC dose-dependently increased LC3-I to LC3-II conversion in treated cells (Fig.3.11.a,b). LC3-II accumulation reached significance from 10 μM concentrations of RSV or QRC; below the concentration needed to increase autophagosome density in parallelly done LC3 immunostainings. As the number of autophagosomes and LC3 immunoblot density are defined by the rate of autophagosome formation and degradation, the lysosomal inhibitor baf-A was added to RSV or QRC to differentiate autophagy induction from lysosomal inhibition. RSV+baf-A or QRC+baf-A increased LC3-II conversion compared to baf-A alone. These

experiments indicate that RSV and QRC dose-dependently induce autophagic flux (formation of new autophagosomes), without blocking degradation in lysosomes. To substantiate the hypothesis on dose-dependent autophagy activation in polyphenol-treated cell cultures, levels of the autophagosome-substrate adaptor protein p62 were tested. Increasing RSV or QRC concentrations led to a bell-shaped curve of p62 levels; while p62 accumulation was near linear in the presence of the lysosomal inhibitor baf-A (Fig.3.11.c,d). p62 levels increased in the neuroblastoma cell line SH-SY5Y from as low as 0.01 μ M QRC. Induction of autophagy in positive controls (e.g. by starvation) cleared p62 from cells.

Corresponding immunostainings revealed an increase of p62 puncta in cells treated HBSS (amino acid starvation) and in cells treated with RSV or QRC. p62 puncta co-localized with autophagosomes (LC3 puncta) in starved cells or in the presence of high-dose (100 μ M) RSV/QRC. At lower concentrations however, RSV and QRC induced the formation of p62 puncta independent from autophagosome formation (Fig.3.12.a). Amino acid starvation induces canonical autophagy, which is regulated by Beclin-1/phosphatidylinositol-3-kinase III (PI3-K) complex and the presence of phosphatidylinositol-3-phosphate (PI(3)-P). Canonical autophagy is inhibited by wortmannin (Wm), a PI3-K inhibitor (Blommaert et al., 1997). To find out if RSV or QRC acts in a similar manner to starvation, autophagy induction was tested in the presence of Wm. As opposed to amino-acid starvation (HBSS), RSV or QRC-treatment was relatively insensitive to Wm (Fig.3.12.b) which implies a role of PI3-K-independent autophagy activation.

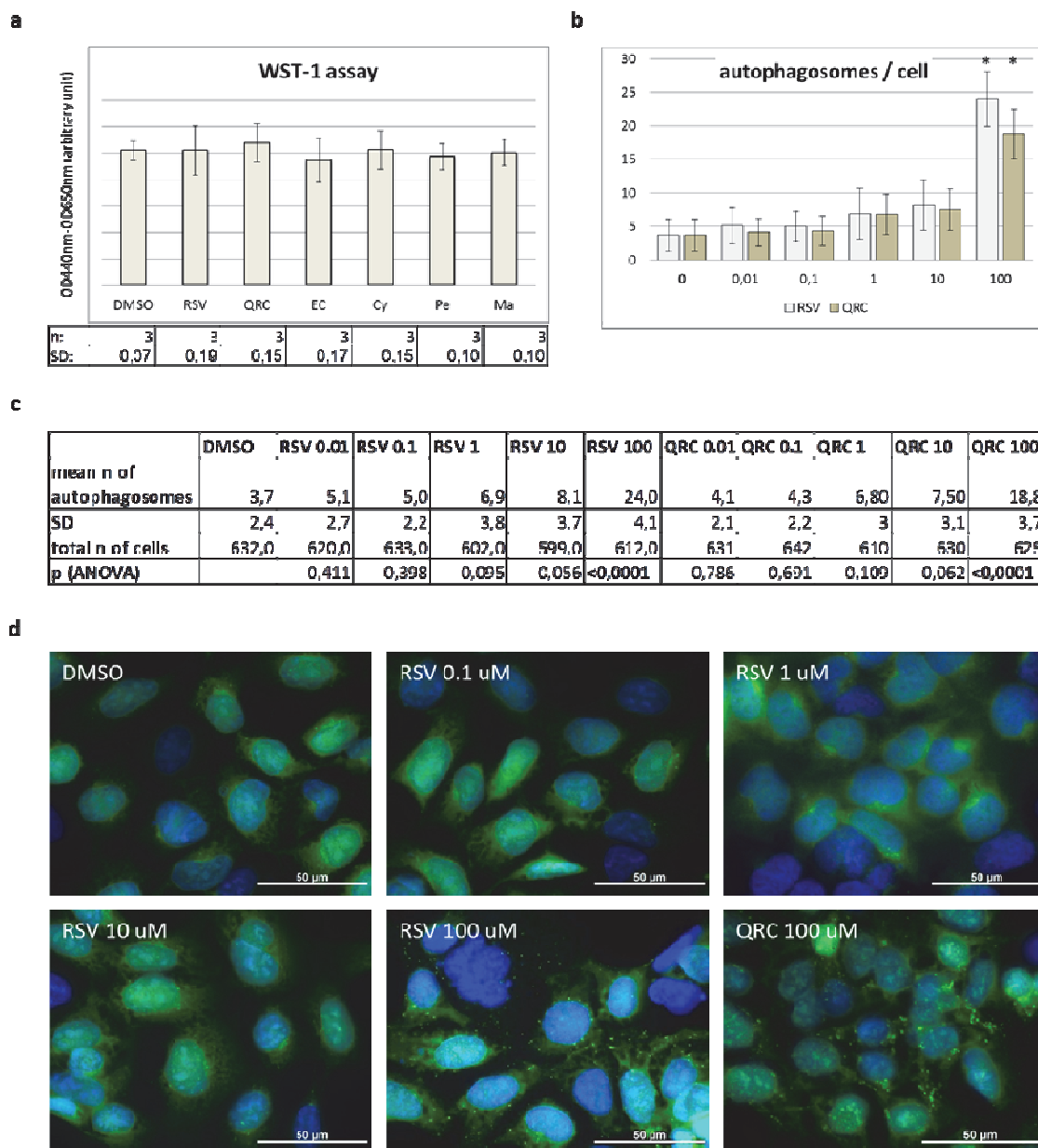
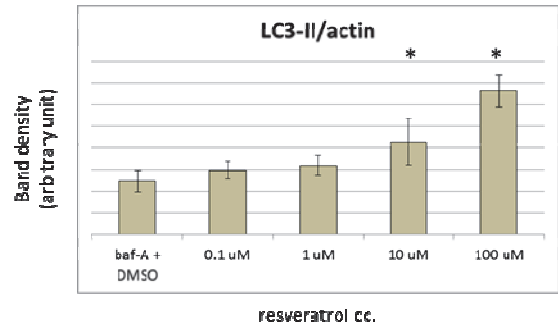
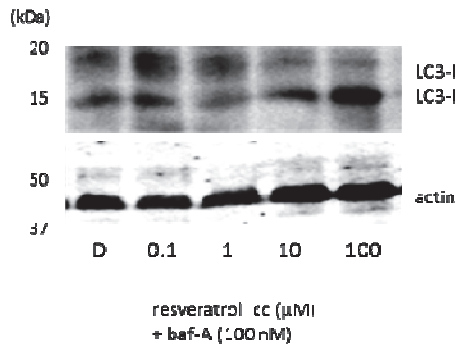
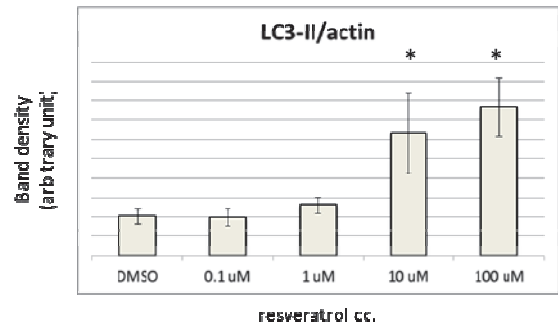
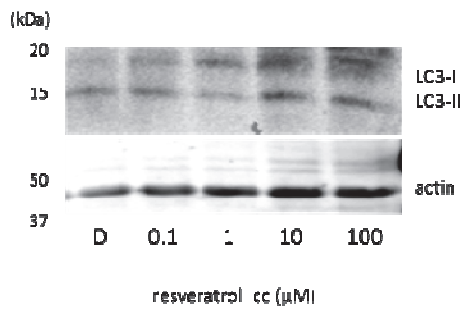
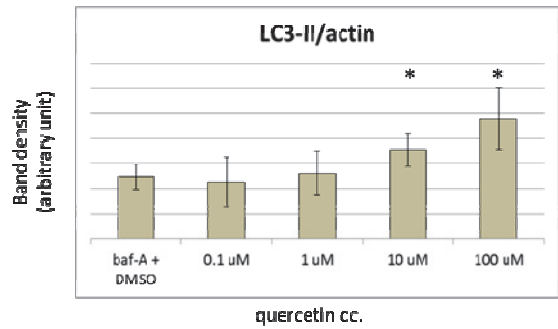
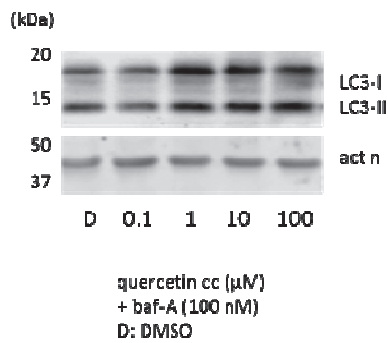
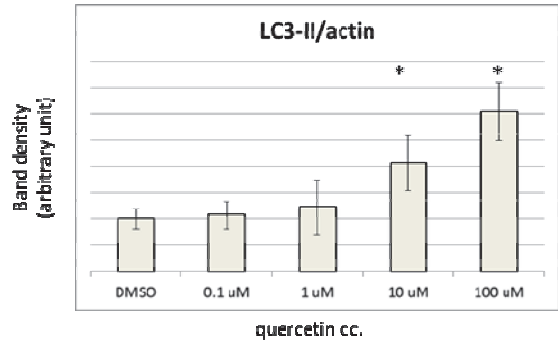
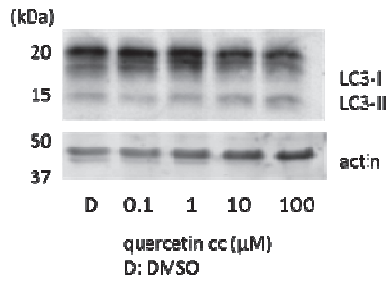


Fig. 3.10. a) No polyphenols in this study were cytotoxic at the highest concentration (100μM) tested. WST-1 assay in HEK-293 cultures, treated with RSV, QRC, EC, Cy3G, Pe3G, Ma3G or DMSO (control). OD values are represented graphically as mean \pm SD; means of polyphenol and DMSO treated samples were compared by Student's t-test *: $p < 0.05$ **b) c) High concentrations of RSV or QRC (from above 10 uM) induce formation of autophagosomes** (GFP puncta of 0.5-1.2 μ m diameter) HEK293::GFP-LC3 cells treated with increasing concentrations of RSV or QRC. Negative control: DMSO (0.1%) Hoechst nuclear staining (blue). Autophagosome content of cells is represented graphically as mean \pm SD; means compared by one-way ANOVA. Approx. 300 cells were counted from 5 fields for each condition tested. *: significant change ($p < 0.05$) compared to control (DMSO) sample **d) representative images.**

a



b



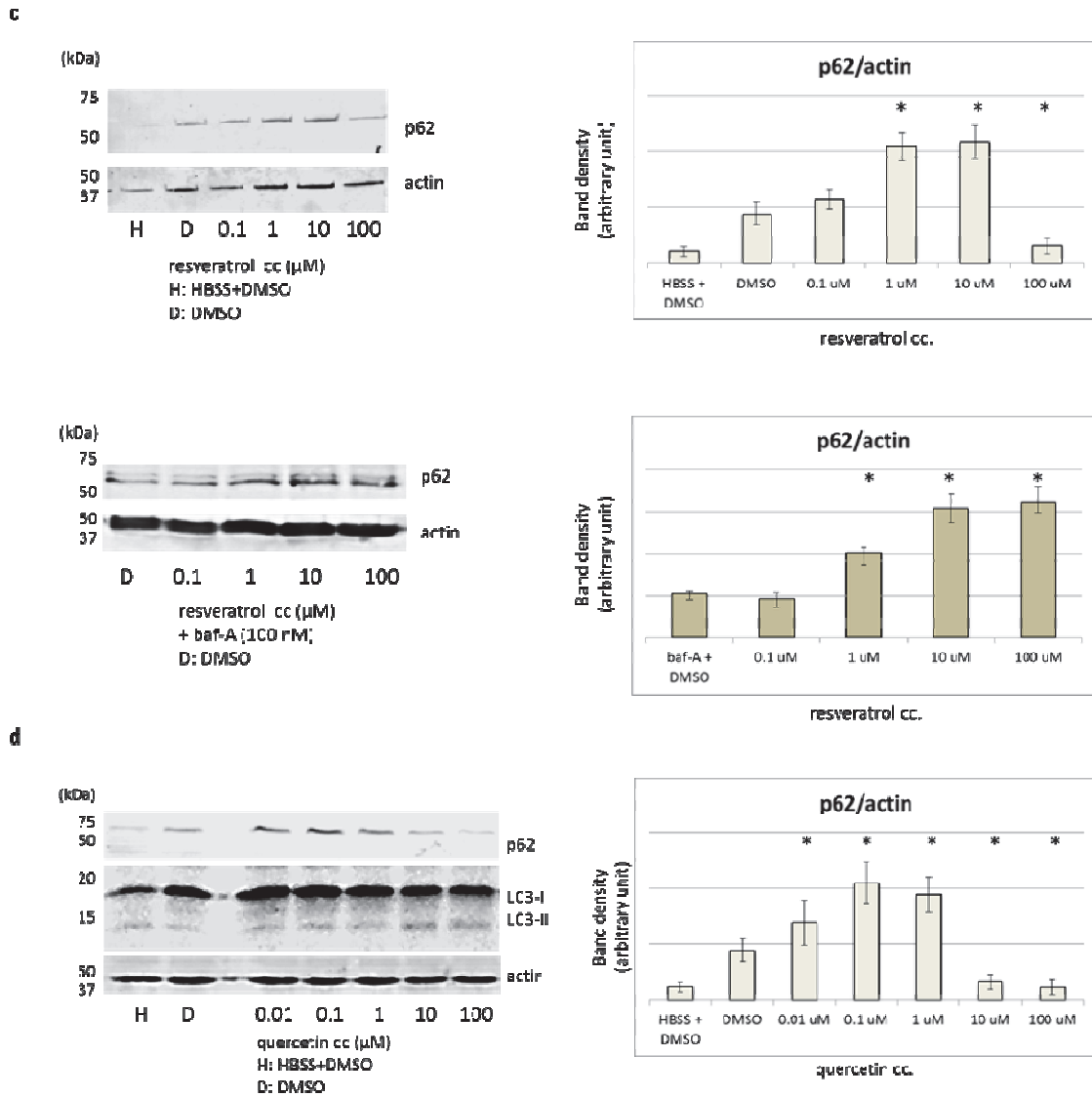
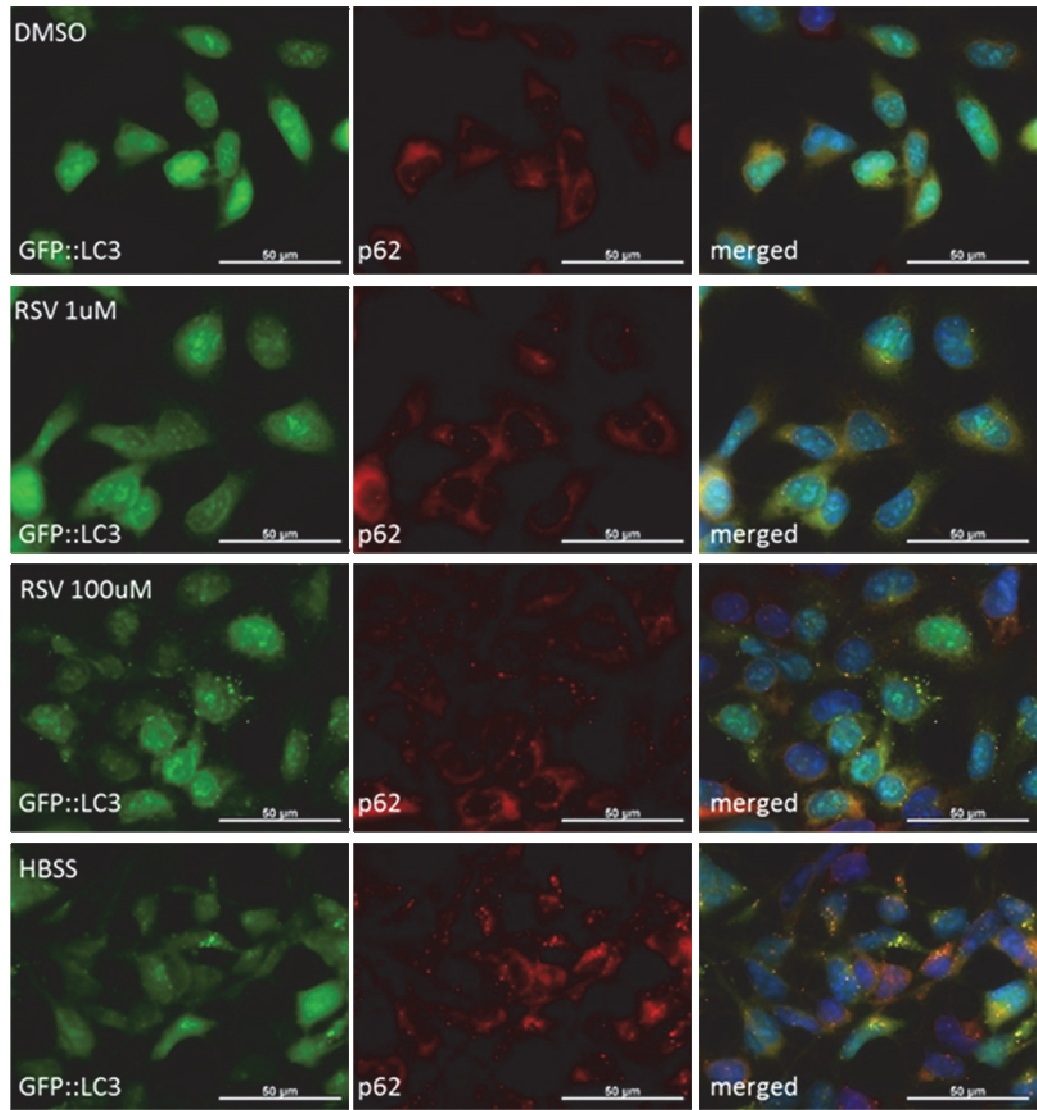


Fig. 3.11. a) b) LC3-western blots from RSV or QRC-treated HEK293 cultures show dose-dependent autophagy induction. 10 μM or higher concentration of a) RSV or b) QRC increased LC3-II accumulation compared to DMSO or baf-A + DMSO treated controls. Densitometric values are represented graphically as mean from 5 independent experiments \pm SD. Asterisk (*) indicates a significant difference between KO and WT samples; means of polyphenol and control (DMSO or baf-A + DMSO treated samples) **c) d) Western blots show a non-linear relationship between RSV or QRC concentration and p62 expression in SH-SY5Y cells.** p62 was increased at lower concentrations while decreased at high concentrations of c) RSV or d) QRC. c) p62 expression increased linearly in the presence of baf-A. HBSS (positive control) decreased p62-levels. Densitometric values are represented graphically as mean from 5 independent experiments \pm SD. Asterisk (*) indicates a significant difference between KO and WT samples; means of polyphenol and control (DMSO or baf-A + DMSO treated samples).

a



b

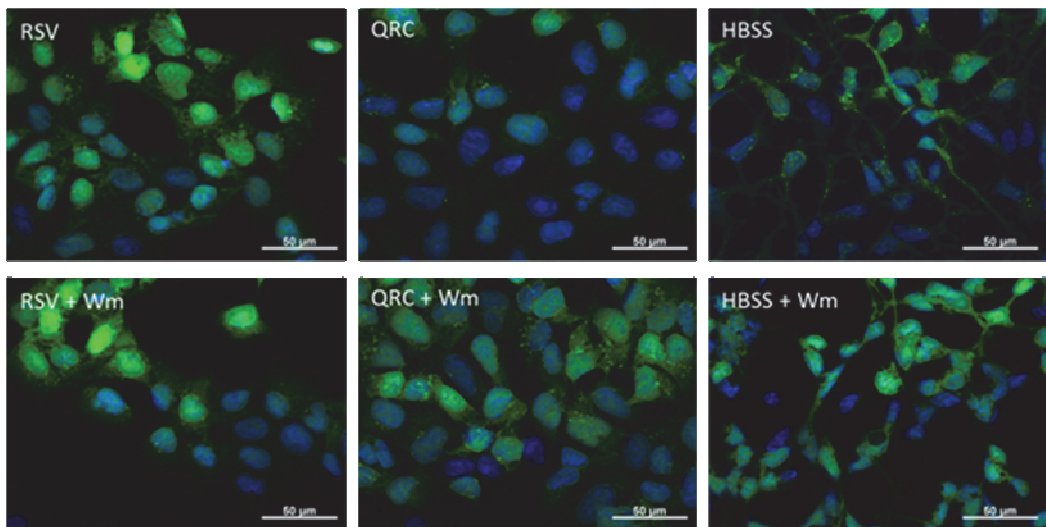
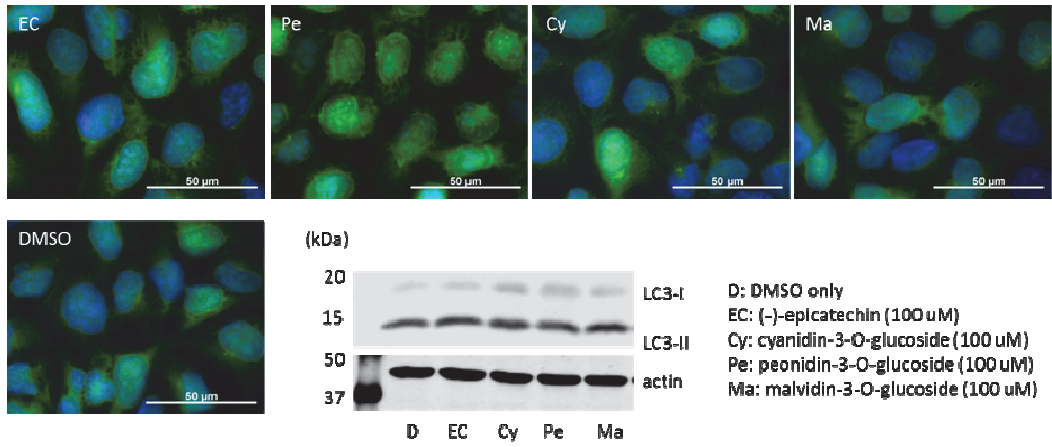


Fig. 3.12. a) p62-accumulation in RSV-treated cells below autophagy-inducing threshold concentration. Low-dose (1uM) RSV increased p62-puncta in the absence of autophagosomes, while high-dose (100 uM) RSV increased p62 redistribution to autophagosomes. HEK-293 GFP::LC3 cells, treated with RSV or with HBSS, as indicated. p62 immunostaining (red) + Hoechst nuclear staining (blue). **b) Wortmannin (40 nM) abolished autophagy induction by amino acid starvation (HBSS), but did not affect autophagy induction by RSV or QRC.** Autophagy was induced in HEK293::GFP-LC3 cells with RSV (100uM) or QRC (100uM) or with HBSS treatment. Autophagosomes are visible as GFP-LC3 puncta. Hoechst nuclear staining (blue).

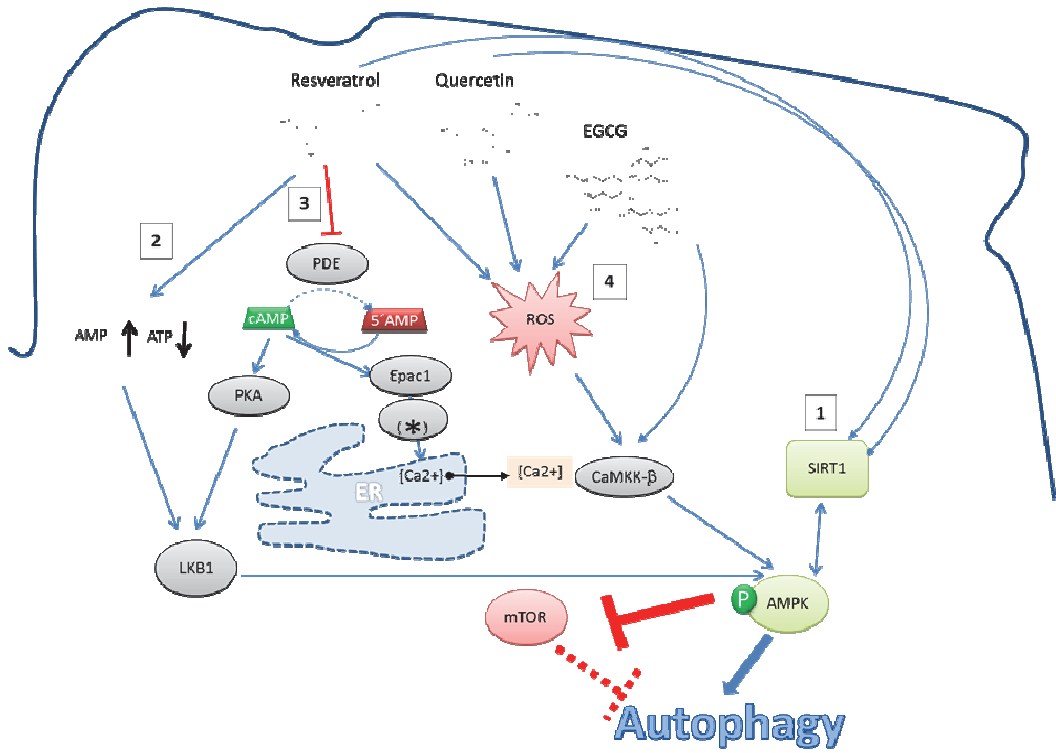
The same experiments were done with other red wine polyphenols as well: (-)-epicatechin, cyanidin-3-*O*-glucoside, peonidin-3-*O*-glucoside and malvidin-3-*O*-glucoside failed to induce autophagy (Fig.3.13.a).

Fig. 3.13. (see next page) a) EC, Cy3G, Pe3G and Ma3G do not activate autophagy in HEK-293 GFP::LC3 cells. No accumulation of autophagosomes (GFP-LC3 puncta) observed. Hoechst nuclear staining (blue). Densitometric values are represented graphically as mean from 5 independent experiments \pm SD; means of polyphenol and control samples compared by one-way ANOVA **b) A proposed mechanism of autophagy activation by polyphenols (see in detail in chapter 4.3.4.)** RSV and QRC are allosteric activators of SIRT1 (1), which in turn phosphorylates and activates AMPK. In addition, RSV reduces ATP production (2) and is a nonspecific inhibitor of phosphodiesterases (3), to activate AMPK via LKB1 and Ca²⁺-CaMKK β . The generation of free radicals (4), as potent activators of autophagy, plays a central role in polyphenol-mediated autophagy activation. (*): pathway components omitted for clarity.

a



b



3.3.3. Summary

Among the polyphenols tested, only resveratrol (RSV) and quercetin (QRC) activated autophagy *in vitro*. At the concentrations tested, polyphenols were not toxic to cells. Autophagy activation was detected by western blots from 10 μ M RSV or QRC concentrations in various monolayer cultures, while microscopic counting of autophagosomes showed a non-significant increase at similar concentrations. To avoid observer bias in microscopic counting and to differentiate increased autophagosome formation from an impaired degradation, the concentration threshold for autophagy activation was determined by western blot results. As the stilbene resveratrol and the flavonol quercetin activated autophagy, while other flavonoids failed to do so, the presence of specific polyphenol binding proteins can be hypothesised. An intriguing finding is the inverse U-shaped curve of concentration-dependent p62 expression; as low RSV or QRC concentrations increased, while high RSV or QRC concentrations strongly decreased p62 expression. Adding the lysosomal inhibitor baf-A has led to a linear relationship between RSV or QRC concentration and p62 expression; which implies the role of p62 in polyphenol-activated (autophagy-dependent and independent) signalling pathways.

4. DISCUSSION

4.1. Ubiquitinated protein aggregates in Atg16 KO mice

4.1.1. Why do Atg16 KO mice die?

These experiments confirm that loss of Atg16l1 results in a deficient autophagy pathway, not compensated by Atg16l2 (Ishibashi et al., 2011). Atg16 KO mice suffer early neonatal lethality in the absence of gross anatomical malformation similar to Atg5 and Atg7 KO mice (Komatsu et al., 2005, Kuma et al., 2004). The aforementioned studies suggested that neonatal lethality was a consequence of exhaustion of amino-acid supplies, especially those of branched-chain amino acids in newborn pups. Nevertheless, neonatal metabolism studies do not entirely support this hypothesis.

Maintenance of energy supply to meet increased expenditure is a major challenge during the transition period from *in utero* to postnatal life. While no literature data support a “physiological starvation period” of newborn mice; newborn rats are exposed to 1-2 hours of starvation after birth under laboratory conditions (Girard et al., 1992). Neonate rodents are sensitive to starvation, and develop hypoglycaemia in the absence of nutrient supplies. Glucose plays a critical role as a source of ATP, to which ketone bodies (lactate and b-hydroxybutyrate) contribute (Lanoue et al., 1999, Battaglia 1989, Girard et al., 1992). Rodents, like mice and rats build glycogen reserves, which is broken down as soon as placental supply ceases (Shelley, 1961).

Studies with newborn rats confirm that gluconeogenesis is essential to maintain blood euglycaemia in suckling neonates; as they are supplied with a high-fat, high-protein and low-carbohydrate diet by mother's milk (Girard et al., 1992). Autophagy contributes to the breakdown of proteins to amino acids; hence generating glucogenic amino acids (alanine and glutamate) which may be essential to avoid hypoglycaemia if breastfeeding is not readily available. Hepatic gluconeogenesis has been shown to commence within 4-6 h from birth with the onset of hepatic phosphoenolpyruvate carboxykinase (PEPCK) expression (Philippidis and Ballard, 1970). In the absence of PEPCK expression, loss of gluconeogenesis results in hypoglycaemia and mouse viability is reduced to 3 days (She et al., 2000; Girard et al., 1992). The short, but significantly prolonged life span of PEPCK KO mice compared to the early loss of Atg16 KO and other autophagy deficient (Atg5 KO and Atg7 KO) suggests that loss of liver gluconeogenesis is not the sole explanation for their early lethality.

Studies on Atg5 KO neonates found a significantly lower level of branched-chain amino acids (BCAA; leucine, isoleucine, and valine) upon experimental starvation (Kuma et al., 2004). BCAA are important regulators of autophagy, as they stimulate protein synthesis via mTOR activation (Kimball and Jefferson, 2006). Furthermore, high plasma levels of BCAA have an anorexygenic effect (Purpera et al., 2012), while low level of BCAA in autophagy KO mice would trigger hunger sensation and suckling on mother's teats. None of the BCAA per se is essential, however their metabolism is regulated together. Impaired catabolism leads to abnormally high plasma levels and maple syrup urine disease in humans (Strauss et al., 1993) and neurologic impairment in mice (Purpera et al., 2012); while unregulated oxidation - hence low BCAA levels - results in seizures and motor impairment (Joshi et al., 2006). The viability of mice in the relative absence of BCAA also underscores a hypothesis that a dysregulation of amino acid metabolism is not the primary reason for mortality of Atg16 KO neonates.

In the presence of lactating mothers, Atg16 KO neonates were distinguished from WT littermates by the absence of milk in their stomach. According to the above observations it can be concluded that Atg16 KO neonates survive a short postnatal starvation with their intrauterine carbohydrate reserves. This raises the question whether Atg16 is essential for the survival of neonatal starvation period in mice, or it is necessary for hunger sensation and proper suckling.

4.1.2. Neuronal pathology of autophagy KO mice - correlation and differences between human neurodegenerative disease

The importance of protein inclusions in Atg16 KO brain lies in the similarity with the intraneural inclusions, commonly found in human neurodegenerative diseases. Tauopathies (e.g. Alzheimer's disease, AD), synucleinopathies (e.g. Parkinson's disease, PD) and most variants of the frontotemporal lobar degeneration (FTLD) and amyotrophic lateral sclerosis (ALS) spectrum disorders are characterized by the accumulation of polyubiquitin- and p62-tagged protein aggregates. p62 has recently gained importance as a sensitive marker for the early phase detection of human neurodegenerative diseases (Kuusisto et al., 2008, Nakano et al., 2004).

Polyubiquitinated inclusions in Atg16 KO were not confined to the central nervous system: they were most prominent in size in the sensory ganglia (dorsal root ganglia and ganglia of cranial sensory nerves); smaller aggregates were also detectable in the liver and in smooth muscles of the small intestine. This indicates that loss of autophagy has a tissue-specific effect on the turnover rate of polyubiquitinated substrates. Inclusions were not detectable in the skin, skeletal muscle, vessel walls, bone and chondrocytes; also some areas of the CNS, e.g. Purkinje cells were free from inclusions (not shown in figures). There was no direct association with the ontogenetic age of brain structures and the size of aggregates in neuron populations (Finlay and Darlington, 1995).

The role of Atg16 in (auto-)immunity has been described in previous studies (Saitoh et al., 2008, Cadwell et al., 2008). This thesis is the first to describe its importance in ubiquitinated protein clearance; which underscores a common, polyubiquitination and autophagy-dependent removal of proteins, demonstrated in Atg4b KO, Atg5 KO and Atg7 KO mice (Komatsu et al., 2006, Read et al., 2011, Hara et al., 2006) as well as in Vps15 KO *Drosophila* (Lindmo et al., 2008). Nonetheless, the impact of autophagy genes may differ: while Atg5 KO and Atg7 KO completely disrupts autophagy in mice and results in a widespread accumulation of ubiquitinated protein aggregates, the effect of Atg4b or Atg4c mutations are relatively mild (Mariño et al., 2007, Read et al., 2011).

Biochemical properties of polyubiquitinated aggregates in Atg16 KO mice were characterized by solubilization studies. Aggregates remained in the solid phase in the presence of non-ionic detergents, like Triton-x100, and were retained on nitrocellulose filter. Ionic detergents, like 2% SDS, were able to completely dissolve these aggregates, and made them amenable for SDS-PAGE and subsequent western blots. Thus, nitrocellulose membrane filtering appears as a straightforward method to recover and further characterize aggregated proteins in autophagy-deficient models. This method was previously evaluated for the detection of protein inclusions in human proteinopathies (Kramer et al., 2008). These findings in an autophagy knockout brain correlate with the common feature of detergent-insoluble protein aggregates described for various human neurodegenerative diseases like huntingtin in HD (Kazantsev et al., 1999), amyloid- β protein in AD (Refolo et al., 1991), α -Synuclein PD or in DLB (Campbell et al., 2000, Campbell et al., 2001, Culvenor et al., 1999).

To find further correlates with human neurodegenerative diseases, of particular interest are the presence of aggregation-prone proteins or other pathognomonic features in Atg16 KO neuronal aggregates. The neurodegenerative disease marker proteins amyloid, α -Synuclein, TDP-43, GSK3 β or tau are all expressed in prenatal brain (Zhong et al., 2010, Salbaum and Ruddle, 1994, Drubin et al., 1984, Leroy and

Brion, 1999, Sephton et al., 2010, Kraemer et al., 2010, Yao et al., 2002). While autophagy has been implicated in their metabolism, amyloid, α -Synuclein, TDP-43, GSK3 β or tau proteins did not co-aggregate with CNS inclusions in Atg16 KO mice; furthermore, no Lewy-body-like, amyloid or argyrophilic deposits were observed in this model organism.

Accumulation of GSK3 β and hyperphosphorylated tau was previously found in a forebrain-specific conditional Atg7 KO mouse model (CamK^{Cre/+}Atg7^{flox/flox}), also characterized by ubiquitin/p62-positive inclusions in affected neurons (Inoue et al., 2012). Accumulation of tau-positive aggregates only appeared in adult mice, similar to age-dependent onset of human neurodegeneration. Concentrations of GSK3 β , tau and phosphorylated Tau were not elevated in Atg16 KO mice. Similarly, no accumulation of the AD marker β -Amyloid (1-42) or the ALS-associated protein TDP-43 (Wang et al., 2010) was observed. While special effort was put into identifying α -Synuclein expression and localization in Atg16KO brains, using different antibodies directed against the N-terminal or C-terminal peptide sequences, antibodies reacted in western blots equally with Atg16KO and WT brain homogenates, and no association to the polyubiquitinated aggregates in Atg16 KOs was detected. Loss of autophagy therefore did not lead to accumulation and aggregate formation of endogenous α -Synuclein in Atg16 KO mice.

It is intriguing to find out if dysfunctional autophagy in aged neurons would contribute to the pathological aggregation of potentially toxic proteins; as the role of autophagy as a causative or a secondary contributing factor remains elusive. The results presented here suggest that neurodegeneration may be initiated by pathogenic proteins; while dysfunctional autophagy potentially exacerbates the disease pathogenesis. α -Synuclein is a candidate culprit in neurodegenerative diseases as previous studies brought evidence for its autophagosomal-lysosomal degradation (Webb et al., 2003, Vogiatzi et al., 2008, Wang et al., 2012, Cuervo, 2004), while disease-associated forms disrupt the autophagy pathway by their increased affinity to lysosomes and impaired internalization (Cuervo et al., 2004).

4.1.3. Cell death in Atg16 KO tissues

Programmed cell death in various neuronal layers have been observed in autophagy-defective mouse models (Nestin^{Cre/+}Atg5^{flox/flox}, Nestin^{Cre/+}Atg7^{flox/flox} and CamK^{Cre/+}Atg7^{flox/flox}) (Hara et al. 2006; Komatsu et al. 2006; Inoue et al., 2012). TUNEL staining did not indicate an accelerated apoptosis in Atg16 KO brains as compared to WT littermates; and viability of cultured Atg16 KO tissues (MEFs and organotypic brain slices) were not different from WT counterparts. These observations imply that neurons are able to survive a long period with polyubiquitinated inclusion pathology. An age-dependent increase in neurotoxic factors (e.g. exposure to oxidative stress) or reduced activity of neuroprotective mechanisms can not be excluded; which eventually lead to neuronal damage and cell death.

It is demonstrated here that loss of autophagy results in abnormal cell death morphology in Atg16 KO MEFs, with persisting nuclear fragments. As autophagy has been implicated in the phagocytic clearance of apoptotic debris (Qu et al., 2007), abnormal nuclei may represent an impaired phagocytosis of dead cells by neighbouring fibroblasts. Autophagosome accumulation has been described in various human neurodegenerative conditions, like AD and DLBD (Higashi et al., 2011, Nixon et al., 2005). Various resident cell populations in brain are involved in phagocytic clearance of cellular debris, including microglia as well as astrocytes; yet their phagocytic activity in organotypic brain slices has not been extensively studied. Further studies are recommended to estimate the significance of the presented findings, if phagocytosis of dying neurons may proceed even in the absence of functional autophagy; alternatively, if cells undergo TUNEL-negative necrosis. Also noteworthy is that neurons tolerated large polyubiquitinated aggregates without aberrant morphology. This is consistent with studies describing aggregate accumulation as a cell protective rather than a cell damaging mechanism.

An increasing literature supports the hypothesis that the appearance of large deposits represents an epiphenomenon, while sub-microscopical amyloid oligomers are responsible for neurotoxicity (Lotharius and Brundin, 2002, Conway et al., 2000), (Stefani and Dobson, 2003)

Inducible-conditional KO models are optimal tools to study the role of genes if their expression is essential for embryonic or perinatal survival. A further aim of this study was switching off Atg16 expression at different stages of the neuronal development. To achieve this, mice expressing Cre recombinase (CRE) under the control of an estrogen-analog sensitive Nestin gene regulatory sequence (Nestin-Cre-ERT2) were interbred with Atg16 flox/flox mice. Unfortunately, Tamoxifen administration to pregnant or lactating females (either by subcutaneous or intraperitoneal injection or by subcutaneous pellet implantation) lead to a high mortality among injected females and their offspring, thus further breeding had to be interrupted.

4.2. Semliki Forest Virus infection in Atg16 KO mouse tissues

4.2.1. Atg16 KO does not impair SFV infection

The purpose of these studies has been to characterize the role of autophagy in Semliki Forest Virus (SFV) infection, *in vitro* in mouse embryonic fibroblast (MEF) cultures and *ex vivo* in mouse organotypic brain cultures (OBCs). SFV is extensively used in laboratories and propagation has been demonstrated in a wide range of cell cultures. While SFV is a neurotropic virus, no previous studies used neuronal cell lines or brain cultures to investigate autophagy in the context of virus infection or the effect of autophagy modulation on virus replication.

SFV proliferated rapidly in both in autophagy competent and -defective cell cultures until the lysis of host cells. There was an apparent discordance between rapid virus proliferation and the late appearance of SFV-infected apoptotic cells in MEF cultures. This phenomenon was even more pronounced in OBCs, where TUNEL-staining and SFV infection appeared mutually exclusive. Together with a number of disintegrating (probably necrotic) cells observed, it can be speculated that cells shut down SFV replication as soon as they are committed to apoptosis - or apoptotic cells may represent a different cell population, sensitized for apoptosis by cytokines released by other cells. SFV infection may induce cell death in a cell type-specific manner; apoptosis was observed in mixed glial cell cultures, while necrosis in primary neuronal culture (Glasgow et al., 1997).

WST-1 assay poorly correlated with SFV replication and concomitant cell death in cell cultures, while it demonstrated an increased optical density (OD) of OBC culture media. It can be hypothesised that elevated OD in WST-1 assay (which would

spuriously imply an increased viability of SFV infected samples) can be best explained by a NAD⁺-dependent formazan production. SFV infection interferes with host cell metabolism, leading to an increased generation of NAD⁺ to promote its own proliferation (Cassells and Burke, 1973a).

Induction of apoptosis by SFV has been associated with the mitochondrial-apoptosomal pathway by exporting cytochrome-c into the cytosol after 10 h post infection (Urban et al., 2008), while unfolded protein response (UPR) to ER stress is also activated from 7-9 h post infection (Barry et al., 2010a). For further consideration to quantify cell death upon SFV infection, Glasgow and colleagues describe [³H]-uridine incorporation as a viability assay that correlates to the microscopically observed cytopathy (Glasgow et al., 1997).

Recombinant (avirulent) SFV strains have been tested on organotypic brain cultures (Ehrensgruber et al., 1999), while ours is the first report on SFV4 infection of mouse brain slices to model encephalitogenic SFV infection. The results presented above demonstrated that virus production peaked on the first day after infection while diminishing number of infectious particles were recovered from OBC media on the following days. This phenomenon can not be explained by deleterious infection as demonstrated by the presence of viral dsRNA, non-structural and capsid proteins. Nevertheless, the results are strikingly different from previous *in vivo* SFV studies, which demonstrated productive infection of SFV in mouse brain, rapidly leading to panencephalitis and lethality (Balluz et al., 1993). This emphasises the necessity of further research, in order to elucidate the role of intrinsic or extrinsic factors (e.g. lymphocyte mediated apoptosis) in this model of viral encephalitis.

In agreement with a previous report on Atg5 KO (Eng et al., 2012), loss of Atg16 had no significant effect on infectious SFV titers produced in MEFs or OBCs. These results point toward a lack of interaction between SFV replication and the autophagy pathway. An intriguing observation is that loss of Atg16 altered the expression of viral proteins nsP1 and capsid, leaving virus production unaffected.

nsP1 is an mRNA-capping enzyme with guanine-7-methyltransferase and guanylyltransferase activities (Ahola and Kaariainen, 1995). Non-structural proteins are expressed during SFV infection at low levels, and, as they do not incorporate into virions, replication may tolerate abnormal stoichiometry. An exception to that is an excess dose of nsP1, found to inhibit SFV replication (Kiiver et al., 2008). Alphaviruses normally produce an excess of capsid protein during infection (Scheele and Pfefferkorn, 1969), which may explain why reduced capsid production does not inhibit viral replication rate (Orvedahl et al., 2010).

Taken in context with other studies, there is no evidence that autophagosomal membranes would serve for alphavirus replication sites (Eng et al., 2012, Zheng and Kielian, 2013, Orvedahl et al., 2010, Joubert et al., 2012). While autophagy has been cell-protective in the context of CHIKV and in SINV infection models by inhibiting apoptosis, and tissue-protective by reducing viral propagation; the studies presented here (together with that of Eng and colleagues (Eng et al., 2012)) demonstrate that autophagy is ineffective in the containment of SFV infection. SINV and CHIKV capsid proteins are successfully recognized by host p62 (without the need for polyubiquitination), these viruses are then effectively targeted to autophagosomes (Judith et al., 2013, Orvedahl et al., 2010). Different affinity of the autophagosome-ubiquitin adaptor p62 to virus capsid may explain the versatile role of autophagy in host cell reaction to alphavirus infection.

4.2.2. SFV infection impairs autophagy by protein synthesis dysregulation

Autophagy markers in OBCs were assayed by western blots 5 days *post inoculation*, by the time SFV infectious particle production has reached a steady state. Expression of autophagy markers LC3-I, LC3-II and p62 were decreased compared to mock-infected OBCs, independent from autophagy-competent or autophagy-

defective genotype. It can be hypothesised that protein levels changed secondary to SFV-dependent depletion of autophagy factors and independent from autophagosomal degradation. A confounding factor in the presented model is an antagonistic combination of SFV-dependent metabolic effects: SFV replication leads to a shutdown of protein transcription (incl. autophagy proteins) while cellular stress response may involve autophagy activation. In a previous study, Eng and colleagues described LC3-II accumulation in SFV-infected human osteosarcoma cells, due to an impaired autophagosome-lysosome fusion (Eng et al., 2012). Notably, Eng and colleagues monitored SFV infection in cell cultures over 48 h; while SFV induced cytolysis was complete by 24 h in the presented tissue-culture studies. It can be reasoned that SFV infection may trigger autophagy in the early phases of infection, impaired during the course of infection by the virus-mediated shutdown of protein synthesis and lack of availability of autophagosome components. Autophagy induction is marked by an inverse relationship between LC3-II and p62 protein levels: while LC3-II is generated p62 is degraded in the course of autophagy. However, these markers are validated in cell monolayers over a short period of time: while LC3-II accumulation is a typical marker for autophagy activation, LC3-II levels decrease over time; as autophagosomal content is degraded in lysosomes (Klionsky et al., 2012). A further confounding factor to consider is that cell lysis and western blot captures a snapshot from brain slices, with cells in different phases of viral infection (or re-infection).

In conclusion, the above studies on autophagy and SFV infection highlight the difference in host-pathogen interaction between phylogenetically closely related alphaviruses. Thus, a cautionary approach is advocated in extrapolating the results from non-pathogenic laboratory virus studies to clinically relevant alphaviruses.

4.3. Autophagy induction *in vitro* by red wine polyphenols

4.3.1. Dose-dependent induction of autophagy in vitro and in vivo – lessons from nutritional studies

The relevance of autophagy in polyphenol-dependent metabolic changes and health benefits remains largely unexplained. For the above studies a pool of polyphenols ingested in the form of grape, white wine or red wine was selected; with the aim of identifying autophagy inducing phenolic compounds (Perez-Jimenez et al., 2010, Ehala et al., 2005). In the presence of sufficient nutrients and growth factors, RSV and QRC activated autophagy *in vitro* from a threshold concentration of approx. 10uM. Being aware of previous studies, which demonstrated concentration-dependent autophagy activation by RSV from above 40 uM (Vingtdeux et al., 2010) or 100 uM (Morselli et al., 2010) *in vitro*; these results imply that a supraphysiological RSV dosage is necessitated to reach its autophagy inducing threshold. Free RSV can only be found at trace levels after 600 ml red wine (approx. 3 glasses) in serum (concentrations of approx. 20 nM), which together with its metabolites RSV 4-glucuronide and RSV 3-glucuronide add up to 2 uM (Vitaglione et al., 2005, Goldberg et al., 2003). This is also true for other autophagy inducing polyphenols: the concentration at which EGCG (10 uM) (Li et al., 2011), apigenin (20 uM) (Tong et al., 2011) or curcumin (50uM) (Xiao et al., 2013) induced autophagy *in vitro*, lies at least an order of magnitude higher than peak concentrations observed *in vivo*.

QRC stands out with a combination of high dietary intake, slow elimination and relatively high concentration after ingestion (Hertog et al., 1993, Egert et al., 2008,

Crozier et al., 1997). In contrast to RSV, only sparse literature has been published on pro-autophagic effects of QRC: autophagy, proteasome-inhibition and ER-stress was induced from 60 uM QRC in MCF7 breast cancer cells (Wang et al., 2011). The ease of access and the abundance of QRC in dietary fruits may justify the physiological relevance of the above studies.

Clearance of the ubiquitin-binding p62 from cells is a widely accepted method to monitor autophagy (Klionsky et al., 2012). A biphasic change of p62 upon polyphenol exposure was demonstrated, with lower (0.1-1 uM) concentration of RSV or QRC inducing p62 accumulation, while higher (10-100 uM) concentrations inducing autophagy-dependent p62 elimination. While the exact mechanism was beyond the scope of this study, autophagy-independent polyphenol effects, involving cellular antioxidant response appear plausible. A study on endotoxin-stimulated macrophages (Fujita et al., 2011) describe a Nrf2–Keap1 mediated and Wm-insensitive pathway of autophagy induction, with an upregulation of p62 transcription and formation of p62/LC3 double-positive puncta in the absence of increased LC3-I/II conversion. From the remarkable similarities to the *in vitro* effect of RSV and QRC, a hypothetical role of p62 accumulation in polyphenol mediated cellular antioxidant signalling may be inferred. Thus, the role of Nrf2 may be proposed for further investigation as an intracellular mediator of RSV and QRC.

4.3.2. Polyphenol effects in neural tissue in vivo and ex vivo

Wild-type organotypic brain slices (OBCs) (harvested from newborn or 14 day old C57/B6 mice) were also used for autophagy studies, where autophagy-inducing or lysosome-inhibiting drugs were applied. In agreement with the observations in *post mortem* fixed brains (Mizushima et al., 2004b), autophagosomes (identified as LC3-positive puncta) were scarcely present in brain tissue. As no convincing evidence of autophagy induction by amino acid starvation (HBSS), mTORc1 inhibition (Torin) or polyphenols (RSV or QRC) was obtained either by fluorescent microscopy or by western blots; these results are not presented in the Results 3.3. “Autophagy induction in vitro by red wine polyphenols” chapter.

It remains a long-standing question, how polyphenols interfere with the pathogenesis of chronic diseases, like the neurodegenerative diseases of the elderly. Most polyphenols (and all of the polyphenols included in this study) undergo rapid metabolism, yielding methylated, sulphated and glucuronidated conjugates (Manach et al., 2005). Conjugation allows for easier renal elimination due to their hydrophilic properties. Consequently, serum polyphenol concentrations peak rapidly after ingestion, followed by a decrease as they undergo glucuronidation and elimination. To assume a long-term effect, a frequent consumption is needed – or a penetrance of the blood-brain barrier (BBB) and persistence in the brain tissue.

Without known transporters, lipophilicity is essential for polyphenols to cross the blood-brain barrier. Glucuronidated and sulphated QRC and (and methyl-QRC, i.e. isorhamnetin) conjugates were recovered in tissues including the brain of rats fed on QRC-rich diet (Ishisaka et al., 2011). Traces of RSV aglycone were recovered from various rat tissues after a single dose of 50 mg/kg (Abd El-Mohsen et al., 2006), glucuronidated and sulphated metabolites were recovered after feeding rats with 30 mg/kg for 6 weeks (Andres-Lacueva et al., 2012). The dosis equivalent to this

amount is more than 350 mg in a 70 kg person, the RSV content of 100 liters of red wine (Crozier et al., 2009, Reagan-Shaw S., 2007). Hence, the observations in human follow-up dietary studies can not be explained by this mechanism. Tissue accumulation of metabolites in many animal studies are best explained by the saturation of phase-II biotransformation enzymes and the appearance of circulating hydrophobic compounds (Piskula and Terao, 1998). While the results presented here do not support a notion that their dietary consumption would induce autophagy, they also underscore the physiological feasibility of autophagy induction if large doses – e.g. in the form of food supplements – are ingested. Bulk RSV intake of 5g (71 mg/kg calculated for 70 kg) have been documented and peak concentrations of above 1 μ M tolerated in volunteers (Brown et al., 2010, Boocock et al., 2007). Similarly, high-dose QRC administration (114 mg QRC from 220 g cooked yellow onions for 7 consecutive days) was tolerated without significant adverse effect, while plasma concentrations of 1.5 μ M QRC were measured 90' after onion intake (Janssen et al., 1998). Nonetheless, further research is warranted before high-dose polyphenol supplements can be advocated.

4.3.3. Pharmacological targeting of the autophagy pathway

The growing awareness of autophagy sparked an intense search for autophagy modulating drug candidates (Fleming et al., 2011). A principal target of these chemicals is the mTOR complex (Sabatini et al., 1994, Brown et al., 1994). Given that mTOR is an important hub of signalling cascades, it is not surprising to find numerous chemicals to enhance or silence its activity to some extent. As the name “Target Of Rapamycin” implies, rapamycin, a macrolide antibiotic derived from *Streptomyces hygroscopicus*, has been the first described mTOR inhibitor, thus autophagy inducer. Rapamycin and its analogues (the so-called rapalogues) are now licensed for anticancer therapy (Law, 2005, Benjamin et al., 2011). Their therapeutic

applications, however, have not led to a major breakthrough. Undesirable effects of mTOR inhibition potentially outweigh the benefits of autophagy induction; which highlighted the alternative autophagy activation by trehalose or lithium in an mTOR independent manner (Sarkar et al., 2007, Sarkar et al., 2005) .

Perhaps the most often prescribed autophagy activator is metformin, a first-line drug for the treatment of type-II diabetes mellitus, activating mTOR via AMPK signalling. Other approved drugs acting on mTOR include perhexilene, niclosamide and amiodarone; however, they potently block Ca^{2+} channels at lower doses, which is probably more relevant for autophagy induction (Balgı et al., 2009, Fleming et al., 2011). Nevertheless, our understanding is far from complete, in particular how autophagy is regulated by cytoplasmic and ER Ca^{2+} -stores. Ca^{2+} mobilizing agents such as 1,25-dihydroxyvitamin D_3 and thapsigargin are potent inducers of autophagy via Ca^{2+} -activated kinase CaMKK- β signalling pathway, while Ca^{2+} chelators downregulate autophagy (Høyer-Hansen et al., 2007).

Downstream modulators of the autophagy pathway may offer novel therapeutic strategies in anticancer treatment. Malignant cells accelerate autophagy to support increased metabolism and utilize autophagy to fight back chemotherapy drugs. Hydroxychloroquine, a malaria drug that inhibits the fusion of autophagosomes with lysosomes are currently being tested in phase I clinical trials as an adjunct to treat myeloma and various solid tumors (Amaravadi et al., 2011). Other autophagy inhibiting drugs are currently more of experimental interest. Class III PI3K inhibitors, like 3-methyladenine (3-MA) and wortmannin (Wm) are commonly used to inhibit the synthesis of isolation membranes, thus autophagosome formation (Blommaert et al., 1997, Seglen and Gordon, 1982).

Caloric restriction, the first described autophagy inducer, has a multi-pronged effect: While mTOR activity is reduced in the absence of nutrients, the NAD^+ -dependent deacetylase sirtuin-1 (SIRT1) becomes activated, inducing autophagy in an mTOR-independent manner (Morselli et al., 2010, Blagosklonny, 2010).

4.3.4. Polyphenol signalling pathways in autophagy induction

Various pathways have been implicated in the mechanism of autophagy regulation by polyphenols (Fig.3.13.b). One of the most studied implies the induction of Sirtuin-1 (SIRT1) (Morselli et al., 2010), a chief regulator of a yet mysterious longevity pathway in various organisms (Rogina and Helfand, 2004, Tissenbaum and Guarente, 2001). SIRT1 activates autophagy proteins Atg5, Atg7 and LC3 (Lee et al., 2008), as well as the Forkhead box O3 (FOXO3) transcription factor that controls the expression of autophagy genes (Kume et al., 2010). RSV has also been shown to act via the Ca^{2+} /calmodulin-dependent protein kinase kinase β (CaMKK β) - 5' AMP-activated protein kinase (AMPK) pathway by increasing cytoplasmic Ca^{2+} concentration (Vingtdeux et al., 2010) or by acting as a non-specific inhibitor of phosphodiesterases (Park et al., 2012). These pathways may be linked together, as SIRT1 signalling appears to be dependent on a functional AMPK regulation (Cantó et al., 2010). An AMPK activating effect of curcumin has been described in lung adenocarcinoma cells (Xiao et al., 2013). Autophagy activation by QRC may be mediated by the upregulation of HIF-1 α , an upstream regulator of the mTOR signalling pathway (Wang et al., 2011). EGCG was found to upregulate CaMKK β - AMPK signaling pathway (Kim et al., 2013). Similar to RSV, this is most probably through a stimulation of Ca^{2+} -influx at *in vitro* concentrations of 10 μ M (Vingtdeux et al., 2010, Kim et al., 2013).

A hypothesis to explain their anti-tumor effect implies polyphenol cytotoxicity as a result of *pro-oxidant* effect from micromolar concentrations (Kim et al., 2014, Nakazato et al., 2005, Lee et al., 2011). Reactive oxygen species (ROS) were shown to activate autophagy and have been recognized as being an integral part of autophagy cascade (Scherz-Shouval and Elazar, 2007). Therefore, activation of autophagy in response to ROS-mediated polyphenol toxicity appears as a plausible cell-protective mechanism.

The nuclear factor erythroid 2-related factor 2 (Nrf2) is involved in cellular responses to chemical stressors, as Nrf2-activation by p62 has been demonstrated in previous studies (Komatsu et al., 2010). Nrf2 is a transcription factor when released from the interaction with Keap1, which binds an Antioxidant Response Element (ARE) on target gene promoters to induce phase-II detoxifying enzymes (Leiser and Miller, 2010, Itoh et al., 1997). Under basal conditions, Nrf2 is constantly degraded by the ubiquitin-proteasomal system. Nrf2 can be stabilized by free radicals which disrupt the Nrf2-Keap1 interaction. Autophagy plays an important role of Nrf2 regulation by sequestering Keap1 for degradation in a p62 dependent manner (Komatsu et al., 2010). Polyphenols have been implicated in Nrf2 induction by previous studies (Scapagnini et al., 2011, Hao et al., 2013); a non-canonical, Wm-insensitive autophagy induction by RSV and QRC may be mediated through this mechanism.

List of abbreviations

‘: minute(s)

”: second(s)

AA: amino acid

AD: Alzheimer’s disease

ALS: amyotrophic lateral sclerosis

AMPK: AMP-activated protein kinase

Atg: AuTophagy-related

Atg16l1: autophagy related 16-like 1, a mammalian homologue of the yeast Atg16

baf-A: bafilomycin A1

BCAA: branched-chain amino acid(s)

bp: base pair

CaMKK-β: Ca²⁺/calmodulin-dependent protein kinase kinase-beta

CCV: clathrin-coated vesicles

CD: Crohn's disease

CHIKV: Chikungunya virus

CHO: cell line derived from the ovary of the Chinese hamster

CMA: chaperone-mediated autophagy

Cy3G: cyanidin-3-O-glucoside

120

ddH₂O: double distilled water
DLBD: Dementia with Lewy bodies or Diffuse Lewy body disease
DNA: deoxyribonucleic acid
dsRNA: double-stranded RNA
EC: (-)-Epicatechin
EE: early endosome
EGCG: epigallocatechin-3-gallate
ER: endoplasmic reticulum
ERGIC: ER– Golgi intermediate compartment
FTLD: frontotemporal lobar degeneration
GFP: green fluorescent protein
GSK3 β : glycogen synthase kinase-3beta
HEK293: cell line derived from human embryonic kidney cells
HM: hypomorphic
h: hour(s)
kb: kilobase
kDa: kiloDalton
KFERQ: Lysine - Phenylalanine-Glutamic acid - Arginine-Glutamine pentapeptide sequence
KO: knockout
IM: isolation membrane
LC3: Microtubule-associated protein light chain 3
LE: late endosome
Ma3G: malvidin-3-O-glucoside
MAM: mitochondria-associated ER membrane
MEF: mouse embryonic fibroblast
miA: microautophagy
MOI: multiplicity of infection
mTORc1 and mTORc2: mammalian Target Of Rapamycin complex 1 and 2
MVB: multivesicular bodies
n.a.: not applicable
NAC: non-amyloid-beta component
NAD⁺: nicotinamide adenine dinucleotide
NBR1: neighbour of BRCA1 gene 1
NDS: normal donkey serum
NGS: normal goat serum
nsP: non-structural protein
OBC: organotypic brain slice culture
p.: page(s)
PAGE: Polyacrylamide gel electrophoresis
PBS: Phosphate buffered saline
Pe3G: peonidin-3-O-glucoside
PEPCK: phosphoenolpyruvate carboxykinase
QRC: quercetin
RSV: resveratrol

PC12: cell line derived from rat pheochromocytoma
p.c.: post coitum
PCR: Polymerase Chain Reaction
PD: Parkinson's disease
p.i.: post inoculationem
PI3P: phosphatidylinositol 3-phosphate
PM: plasma membrane
RE: recycling endosomes
RNA: ribonucleic acid
RPE: retinal pigment epithelium
RT: room temperature
SD: standard deviation
SDS: sodium dodecyl sulphate
SINV: Sindbis Virus
SIRT1: sirtuin-1
SFV: Semliki Forest Virus
TBS: Tris-buffered saline
TBS-T0.1 or TBS-T0.5: Tris-buffered saline + 0.1 or 0.5 w/V % Tween
TDP-43: TAR DNA-binding protein 43
TOR: Target Of Rapamycin
Trans-Golgi-network (TGN)
TUNEL: Terminal deoxynucleotidyl transferase dUTP nick end labelling
Wm: wortmannin
WT: wild type

List of references

- ABD EL-MOHSEN, M., BAYELE, H., KUHNLE, G., GIBSON, G., DEBNAM, E., KAILA SRAI, S., RICE-EVANS, C. & SPENCER, J. P. 2006. Distribution of [3H]trans-resveratrol in rat tissues following oral administration. *British Journal of Nutrition*, 96, 62-70.
- AHOLA, T. & KAARIAINEN, L. 1995. Reaction in alphavirus mRNA capping: formation of a covalent complex of nonstructural protein nsP1 with 7-methyl-GMP. *Proceedings of the National Academy of Sciences USA*, 92, 507-11.
- AMARAVADI, R. K., LIPPINCOTT-SCHWARTZ, J., YIN, X.-M., WEISS, W. A., TAKEBE, N., TIMMER, W., DIPAOLA, R. S., LOTZE, M. T. & WHITE, E. 2011. Principles and Current Strategies for Targeting Autophagy for Cancer Treatment. *Clinical Cancer Research*, 17, 654-666.
- ANDRES-LACUEVA, C., MACARULLA, M. T., ROTCHES-RIBALTA, M., BOTO-ORDÓÑEZ, M., URPI-SARDA, M., RODRÍGUEZ, V. M. & PORTILLO, M. P. 2012. Distribution of Resveratrol Metabolites in Liver, Adipose Tissue, and Skeletal Muscle in Rats Fed Different Doses of This Polyphenol. *Journal of Agricultural and Food Chemistry*, 60, 4833-4840.
- AOKI, H., TAKADA, Y., KONDO, S., SAWAYA, R., AGGARWAL, B. B. & KONDO, Y. 2007. Evidence That Curcumin Suppresses the Growth of Malignant Gliomas in Vitro and in Vivo through Induction of Autophagy: Role of Akt and Extracellular Signal-Regulated Kinase Signaling Pathways. *Molecular Pharmacology*, 72, 29-39.
- ARASTEH, J. M. 2012. Generation of mouse models to study the role of Atg16L1 in Inflammatory Bowel Disease (IBD).
- ATKINS, G. J. 2013. The Pathogenesis of Alphaviruses. *ISRN Virology*, 2013, 22.
- AXE, E. L., WALKER, S. A., MANIFAVA, M., CHANDRA, P., RODERICK, H. L., HABERMANN, A., GRIFFITHS, G. & KTISTAKIS, N. T. 2008. Autophagosome formation from membrane compartments enriched in phosphatidylinositol 3-phosphate and dynamically connected to the endoplasmic reticulum. *The Journal of Cell Biology*, 182, 685-701.
- BABA, S., OSAKABE, N., YASUDA, A., NATSUME, M., TAKIZAWA, T., NAKAMURA, T. & TERAQ, J. 2000. Bioavailability of (-)-epicatechin upon intake of chocolate and cocoa in human volunteers. *Free Radical Research*, 33, 635-641.
- BALGI, A. D., FONSECA, B. D., DONOHUE, E., TSANG, T. C. F., LAJOIE, P., PROUD, C. G., NABI, I. R. & ROBERGE, M. 2009. Screen for Chemical Modulators of Autophagy Reveals Novel Therapeutic Inhibitors of mTORC1 Signaling. *PLoS ONE*, 4, e7124.
- BALLUZ, I. M., GLASGOW, G. M., KILLEN, H. M., MABRUK, M. J., SHEAHAN, B. J. & ATKINS, G. J. 1993. Virulent and avirulent strains of Semliki Forest virus show similar cell tropism for the murine central nervous system but differ in the severity and rate of induction of cytolytic damage. *Neuropathology and applied neurobiology*, 19, 233-239.

- BANCROFT, M. G. A. J. D. (ed.) 2001. *Theory and Practice of Histological Techniques*: Churchill Livingstone.
- BARRY, G., FRAGKOUDIS, R., FERGUSON, M. C., LULLA, A., MERITS, A., KOHL, A. & FAZAKERLEY, J. K. 2010a. Semliki Forest Virus-Induced Endoplasmic Reticulum Stress Accelerates Apoptotic Death of Mammalian Cells. *Journal of Virology*, 84, 7369-7377.
- BARRY, G., FRAGKOUDIS, R., FERGUSON, M. C., LULLA, A., MERITS, A., KOHL, A. & FAZAKERLEY, J. K. 2010b. Semliki forest virus-induced endoplasmic reticulum stress accelerates apoptotic death of mammalian cells. *Journal of Virology*, 84, 7369-77.
- BAUR, J. A. & SINCLAIR, D. A. 2006. Therapeutic potential of resveratrol: the in vivo evidence. *Nature Reviews Drug Discovery*, 5, 493-506.
- BENJAMIN, D., COLOMBI, M., MORONI, C. & HALL, M. N. 2011. Rapamycin passes the torch: a new generation of mTOR inhibitors. *Nature reviews Drug discovery*, 10, 868-880.
- BERNDSSEN, C. E. & WOLBERGER, C. 2014. New insights into ubiquitin E3 ligase mechanism. *Nature Structural & Molecular Biology*, 21, 301-7.
- BJØRKØY, G., LAMARK, T., BRECH, A., OUTZEN, H., PERANDER, M., OVERVATN, A., STENMARK, H. & JOHANSEN, T. 2005. p62/SQSTM1 forms protein aggregates degraded by autophagy and has a protective effect on huntingtin-induced cell death. *Journal of Cell Biology*, 171, 603-614.
- BLAGOSKLONNY, M. V. 2010. Linking calorie restriction to longevity through sirtuins and autophagy: any role for TOR. *Cell death & disease*, 1, e12.
- BLOMMAART, E. F. C., KRAUSE, U., SCHELLENS, J. P. M., VREELING-SINDELÁROVÁ, H. & MEIJER, A. J. 1997. The Phosphatidylinositol 3-Kinase Inhibitors Wortmannin and LY294002 Inhibit Autophagy in Isolated Rat Hepatocytes. *European Journal of Biochemistry*, 243, 240-246.
- BOADA-ROMERO, E., LETEK, M., FLEISCHER, A., PALLAUF, K., RAMON-BARROS, C. & PIMENTEL-MUINOS, F. X. 2013. TMEM59 defines a novel ATG16L1-binding motif that promotes local activation of LC3. *EMBO J*, 32, 566-582.
- BOOCOCK, D. J., FAUST, G. E. S., PATEL, K. R., SCHINAS, A. M., BROWN, V. A., DUCHARME, M. P., BOOTH, T. D., CROWELL, J. A., PERLOFF, M., GESCHER, A. J., STEWARD, W. P. & BRENNER, D. E. 2007. Phase I Dose Escalation Pharmacokinetic Study in Healthy Volunteers of Resveratrol, a Potential Cancer Chemopreventive Agent. *Cancer Epidemiology Biomarkers & Prevention*, 16, 1246-1252.
- BOSETTI, C., SPERTINI, L., PARPINEL, M., GNAGNARELLA, P., LAGIOU, P., NEGRI, E., FRANCESCHI, S., MONTELLA, M., PETERSON, J., DWYER, J., GIACOSA, A. & LA VECCHIA, C. 2005. Flavonoids and Breast Cancer Risk in Italy. *Cancer Epidemiology Biomarkers & Prevention*, 14, 805-808.
- BROWN, E. J., ALBERS, M. W., BUM SHIN, T., ICHIKAWA, K., KEITH, C. T., LANE, W. S. & SCHREIBER, S. L. 1994. A mammalian protein targeted by G1-arresting rapamycin-receptor complex. *Nature*, 369, 756-758.
- BROWN, V. A., PATEL, K. R., VISKADURAKI, M., CROWELL, J. A., PERLOFF, M., BOOTH, T. D., VASILININ, G., SEN, A., SCHINAS, A. M., PICCIRILLI, G., BROWN,

- K., STEWARD, W. P., GESCHER, A. J. & BRENNER, D. E. 2010. Repeat Dose Study of the Cancer Chemopreventive Agent Resveratrol in Healthy Volunteers: Safety, Pharmacokinetics, and Effect on the Insulin-like Growth Factor Axis. *Cancer Research*, 70, 9003-9011.
- CADWELL, K., LIU, J. Y., BROWN, S. L., MIYOSHI, H., LOH, J., LENNERZ, J. K., KISHI, C., KC, W., CARRERO, J. A., HUNT, S., STONE, C. D., BRUNT, E. M., XAVIER, R. J., SLECKMAN, B. P., LI, E., MIZUSHIMA, N., STAPPENBECK, T. S. & VIRGIN IV, H. W. 2008. A key role for autophagy and the autophagy gene Atg16l1 in mouse and human intestinal Paneth cells. *Nature*, 456, 259-263.
- CADWELL, K., PATEL, K. K., MALONEY, N. S., LIU, T.-C., NG, A. C. Y., STORER, C. E., HEAD, R. D., XAVIER, R., STAPPENBECK, T. S. & VIRGIN, H. W. 2010. Virus-Plus-Susceptibility Gene Interaction Determines Crohn's Disease Gene Atg16L1 Phenotypes in Intestine. *Cell*, 141, 1135-1145.
- CAMPBELL, B. C., MCLEAN, C. A., CULVENOR, J. G., GAI, W. P., BLUMBERGS, P. C., JAKALA, P., BEYREUTHER, K., MASTERS, C. L. & LI, Q. X. 2001. The solubility of alpha-synuclein in multiple system atrophy differs from that of dementia with Lewy bodies and Parkinson's disease. *Journal of Neurochemistry*, 76, 87-96.
- CAMPBELL, B. C. V., LI, Q.-X., CULVENOR, J. G., JÄKÄLÄ, P., CAPPAL, R., BEYREUTHER, K., MASTERS, C. L. & MCLEAN, C. A. 2000. Accumulation of Insoluble α -Synuclein in Dementia with Lewy Bodies. *Neurobiology of Disease*, 7, 192-200.
- CANN, G. M., GUIGNABERT, C., YING, L., DESHPANDE, N., BEKKER, J. M., WANG, L., ZHOU, B. & RABINOVITCH, M. 2008. Developmental expression of LC3alpha and beta: absence of fibronectin or autophagy phenotype in LC3beta knockout mice. *Developmental Dynamics*, 237, 187-95.
- CANTÓ, C., JIANG, L. Q., DESHMUKH, A. S., MATAKI, C., COSTE, A., LAGOUGE, M., ZIERATH, J. R. & AUWERX, J. 2010. Interdependence of AMPK and SIRT1 for metabolic adaptation to fasting and exercise in skeletal muscle. *Cell Metabolism*, 11, 213-219.
- CASSELLS, A. C. & BURKE, D. C. 1973a. Changes in the Constitutive Enzymes of Chick Cells Following Infection with Semliki Forest Virus. *Journal of General Virology*, 18, 135-141.
- CASSELLS, A. C. & BURKE, D. C. 1973b. Changes in the constitutive enzymes of chick cells following infection with Semliki Forest virus. *Journal of General Virology*, 18, 135-141.
- CEBOLLERO, E., VAN DER VAART, A. & REGGIORI, F. 2012. Understanding phosphatidylinositol-3-phosphate dynamics during autophagosome biogenesis. *Autophagy*, 8, 1868-1870.
- CHAU, V., TOBIAS, J. W., BACHMAIR, A., MARRIOTT, D., ECKER, D. J., GONDA, D. K. & VARSHAVSKY, A. 1989. A multiubiquitin chain is confined to specific lysine in a targeted short-lived protein. *Science*, 243, 1576-83.
- CHEN, N. & KARANTZA-WADSWORTH, V. 2009. Role and regulation of autophagy in cancer. *Biochimica et Biophysica Acta (BBA) - Molecular Cell Research*, 1793, 1516-1523.

- CHEONG, H., LINDSTEN, T., WU, J., LU, C. & THOMPSON, C. B. 2011. Ammonia-induced autophagy is independent of ULK1/ULK2 kinases. *Proceedings of the National Academy of Sciences of the United States of America*, 108, 11121-11126.
- CONWAY, K. A., LEE, S. J., ROCHET, J. C., DING, T. T., WILLIAMSON, R. E. & LANSBURY, P. T., JR. 2000. Acceleration of oligomerization, not fibrillization, is a shared property of both alpha-synuclein mutations linked to early-onset Parkinson's disease: implications for pathogenesis and therapy. *Proceedings of the National Academy of Sciences USA*, 97, 571-6.
- CROZIER, A., JAGANATH, I. B. & CLIFFORD, M. N. 2009. Dietary phenolics: chemistry, bioavailability and effects on health. *Natural Product Reports*, 26, 1001-1043.
- CROZIER, A., LEAN, M. E. J., MCDONALD, M. S. & BLACK, C. 1997. Quantitative analysis of the flavonoid content of commercial tomatoes, onions, lettuce, and celery. *Journal of Agricultural and Food Chemistry*, 45, 590-595.
- CUERVO, A. M. 2004. Autophagy: in sickness and in health. *Trends in Cell Biology*, 14, 70-7.
- CUERVO, A. M., STEFANIS, L., FREDENBURG, R., LANSBURY, P. T. & SULZER, D. 2004. Impaired degradation of mutant alpha-synuclein by chaperone-mediated autophagy. *Science*, 305, 1292-5.
- CULVENOR, J. G., MCLEAN, C. A., CUTT, S., CAMPBELL, B. C., MAHER, F., JAKALA, P., HARTMANN, T., BEYREUTHER, K., MASTERS, C. L. & LI, Q. X. 1999. Non-Abeta component of Alzheimer's disease amyloid (NAC) revisited. NAC and alpha-synuclein are not associated with Abeta amyloid. *American Journal of Pathology*, 155, 1173-81.
- DAY, A. J., MELLON, F., BARRON, D., SARRAZIN, G., MORGAN, M. R. & WILLIAMSON, G. 2001. Human metabolism of dietary flavonoids: identification of plasma metabolites of quercetin. *Free radical research*, 35, 941-952.
- DEL RIO, D., BORGES, G. & CROZIER, A. 2010. Berry flavonoids and phenolics: bioavailability and evidence of protective effects. *British Journal of Nutrition*, 104 Suppl 3, S67-90.
- DERETIC, V. & LEVINE, B. 2009. Autophagy, Immunity, and Microbial Adaptations. *Cell host & microbe*, 5, 527-549.
- DICKSON, D. W., BRAAK, H., DUDA, J. E., DUYCKAERTS, C., GASSER, T., HALLIDAY, G. M., HARDY, J., LEVERENZ, J. B., DEL TREDICI, K., WSZOLEK, Z. K. & LITVAN, I. 2009. Neuropathological assessment of Parkinson's disease: refining the diagnostic criteria. *Lancet Neurology*, 8, 1150-1157.
- DOHERTY, M. K., HAMMOND, D. E., CLAGUE, M. J., GASKELL, S. J. & BEYNON, R. J. 2009. Turnover of the human proteome: determination of protein intracellular stability by dynamic SILAC. *Journal of Proteome Research*, 8, 104-12.
- DOOLEY, H. C., RAZI, M., POLSON, H. E. J., GIRARDIN, S. E., WILSON, M. I. & TOOZE, S. A. 2014. WIPI2 links LC3 conjugation with PI3P, autophagosome formation, and pathogen clearance by recruiting Atg12-5-16L1. *Molecular cell*, 55, 238-252.

- DRUBIN, D. G., CAPUT, D. & KIRSCHNER, M. W. 1984. Studies on the expression of the microtubule-associated protein, tau, during mouse brain development, with newly isolated complementary DNA probes. *The Journal of Cell Biology*, 98, 1090-7.
- DUVE, C. D. 1963. The lysosome. *Scientific American*, 208, 64-72.
- EGAN, D. F., SHACKELFORD, D. B., MIHAYLOVA, M. M., GELINO, S., KOHNZ, R. A., MAIR, W., VASQUEZ, D. S., JOSHI, A., GWINN, D. M., TAYLOR, R., ASARA, J. M., FITZPATRICK, J., DILLIN, A., VIOLLET, B., KUNDU, M., HANSEN, M. & SHAW, R. J. 2011. Phosphorylation of ULK1 (hATG1) by AMP-activated protein kinase connects energy sensing to mitophagy. *Science*, 331, 456-461.
- EGERT, S., WOLFFRAM, S., BOSY-WESTPHAL, A., BOESCH-SAADATMANDI, C., WAGNER, A. E., FRANK, J., RIMBACH, G. & MUELLER, M. J. 2008. Daily Quercetin Supplementation Dose-Dependently Increases Plasma Quercetin Concentrations in Healthy Humans. *The Journal of Nutrition*, 138, 1615-1621.
- EHALA, S., VAHER, M. & KALJURAND, M. 2005. Characterization of phenolic profiles of Northern European berries by capillary electrophoresis and determination of their antioxidant activity. *Journal of Agricultural and Food Chemistry*, 53, 6484-90.
- EHRENGRUBER, M. U., LUNDSTROM, K., SCHWEITZER, C., HEUSS, C., SCHLESINGER, S. & GÄHWILER, B. H. 1999. Recombinant Semliki Forest virus and Sindbis virus efficiently infect neurons in hippocampal slice cultures. *Proceedings of the National Academy of Sciences*, 96, 7041-7046.
- ENG, K. E., PANAS, M. D., MURPHY, D., KARLSSON HEDESTAM, G. B. & MCINERNEY, G. M. 2012. Accumulation of autophagosomes in Semliki Forest virus-infected cells is dependent on expression of the viral glycoproteins. *Journal of Virology*, 86, 5674-5685.
- FIELDS, B. N., KNIPE, D. M. & HOWLEY, P. M. 2007. *Fields' virology [electronic book] / editors-in-chief, David M. Knipe, Peter M. Howley ; associate editors, Diane E. Griffin ... [et al.]*, Philadelphia : Wolters kluwer/Lippincott Williams & Wilkins, 2007. 5th ed.
- FIMIA, G. M., STOYKOVA, A., ROMAGNOLI, A., GIUNTA, L., DI BARTOLOMEO, S., NARDACCI, R., CORAZZARI, M., FUOCO, C., UCAR, A., SCHWARTZ, P., GRUSS, P., PIACENTINI, M., CHOWDHURY, K. & CECCONI, F. 2007. Ambra1 regulates autophagy and development of the nervous system. *Nature*, 447, 1121-5.
- FINDLAY, G. M., HARRINGTON, L. S. & LAMB, R. F. 2005. TSC1-2 tumour suppressor and regulation of mTOR signalling: linking cell growth and proliferation? *Current Opinion in Genetics and Development*, 15, 69-76.
- FINLAY, B. L. & DARLINGTON, R. B. 1995. Linked regularities in the development and evolution of mammalian brains. *Science*, 268, 1578-84.
- FLEMING, A., NODA, T., YOSHIMORI, T. & RUBINSZTEIN, D. C. 2011. Chemical modulators of autophagy as biological probes and potential therapeutics. *Nature Chemical Biology*, 7, 9-17.

- FROSHAUER, S., KARTENBECK, J. & HELENIUS, A. 1988. Alphavirus RNA replicase is located on the cytoplasmic surface of endosomes and lysosomes. *The Journal of Cell Biology*, 107, 2075-2086.
- FUJITA, K., MAEDA, D., XIAO, Q. & SRINIVASULA, S. M. 2011. Nrf2-mediated induction of p62 controls Toll-like receptor-4-driven aggresome-like induced structure formation and autophagic degradation. *Proceedings of the National Academy of Sciences USA*, 108, 1427-32.
- FUJITA, N., ITOH, T., OMORI, H., FUKUDA, M., NODA, T. & YOSHIMORI, T. 2008. The Atg16L Complex Specifies the Site of LC3 Lipidation for Membrane Biogenesis in Autophagy. *Molecular Biology of the Cell*, 19, 2092-2100.
- FUJITA, N., SAITOH, T., KAGEYAMA, S., AKIRA, S., NODA, T. & YOSHIMORI, T. 2009. Differential Involvement of Atg16L1 in Crohn Disease and Canonical Autophagy: ANALYSIS OF THE ORGANIZATION OF THE Atg16L1 COMPLEX IN FIBROBLASTS. *Journal of Biological Chemistry*, 284, 32602-32609.
- GAMMOH, N., FLOREY, O., OVERHOLTZER, M. & JIANG, X. 2013a. Interaction between FIP200 and ATG16L1 distinguishes ULK1 complex-dependent and -independent autophagy. *Nature Structural & Molecular Biology*, 20, 144-149.
- GAN, B., PENG, X., NAGY, T., ALCARAZ, A., GU, H. & GUAN, J. L. 2006. Role of FIP200 in cardiac and liver development and its regulation of TNFalpha and TSC-mTOR signaling pathways. *The Journal of Cell Biology*, 175, 121-33.
- GANLEY, I. G., LAM, D. H., WANG, J., DING, X., CHEN, S. & JIANG, X. 2009. ULK1·ATG13·FIP200 Complex Mediates mTOR Signaling and Is Essential for Autophagy. *Journal of Biological Chemistry*, 284, 12297-12305.
- GAO, L. & MAZZA, G. 1994. Quantitation and Distribution of Simple and Acylated Anthocyanins and Other Phenolics in Blueberries. *Journal of Food Science*, 59, 1057-1059.
- GARMASHOVA, N., GORCHAKOV, R., VOLKOVA, E., PAESSLER, S., FROLOVA, E. & FROLOV, I. 2007. The Old World and New World Alphaviruses Use Different Virus-Specific Proteins for Induction of Transcriptional Shutoff. *Journal of Virology*, 81, 2472-2484.
- GAROFF, H., SIMONS, K. & RENKONEN, O. 1974. Isolation and characterization of the membrane proteins of Semliki Forest virus. *Virology*, 61, 493-504.
- GHASEMI, A. & ZAHEDIASL, S. 2012. Normality tests for statistical analysis: a guide for non-statisticians. *International Journal of Endocrinology and Metabolism*, 10, 486-489.
- GIRARD, J., FERRE, P., PEGORIER, J. P. & DUEE, P. H. 1992. Adaptations of glucose and fatty acid metabolism during perinatal period and suckling-weaning transition. *Physiology Review*, 72, 507-62.
- GLASGOW, G. M., MCGEE, M. M., SHEAHAN, B. J. & ATKINS, G. J. 1997. Death mechanisms in cultured cells infected by Semliki Forest virus. *Journal of General Virology*, 78 (Pt 7), 1559-63.
- GOLDBERG, D. M., YAN, J. & SOLEAS, G. J. 2003. Absorption of three wine-related polyphenols in three different matrices by healthy subjects. *Clinical Biochemistry*, 36, 79-87.

- GURUSAMY, N., LEKLI, I., MUKHERJEE, S., RAY, D., AHSAN, M. K., GHERGHICEANU, M., POPESCU, L. M. & DAS, D. K. 2010. Cardioprotection by resveratrol: a novel mechanism via autophagy involving the mTORC2 pathway. *Cardiovascular Research*, 86, 103-112.
- GWINN, D. M., SHACKELFORD, D. B., EGAN, D. F., MIHAYLOVA, M. M., MERY, A., VASQUEZ, D. S., TURK, B. E. & SHAW, R. J. 2008. AMPK Phosphorylation of Raptor Mediates a Metabolic Checkpoint. *Molecular cell*, 30, 214-226.
- HAGLUND, K., DI FIORE, P. P. & DIKIC, I. 2003a. Distinct monoubiquitin signals in receptor endocytosis. *Trends in Biochemical Sciences*, 28, 598-603.
- HAGLUND, K., SIGISMUND, S., POLO, S., SZYMKIEWICZ, I., DI FIORE, P. P. & DIKIC, I. 2003b. Multiple monoubiquitination of RTKs is sufficient for their endocytosis and degradation. *Nature Cell Biology*, 5, 461-466.
- HAILEY, D. W., RAMBOLD, A. S., SATPUTE-KRISHNAN, P., MITRA, K., SOUGRAT, R., KIM, P. K. & LIPPINCOTT-SCHWARTZ, J. 2010. Mitochondria Supply Membranes for Autophagosome Biogenesis during Starvation. *Cell*, 141, 656-667.
- HAMPE, J., FRANKE, A., ROSENSTIEL, P., TILL, A., TEUBER, M., HUSE, K., ALBRECHT, M., MAYR, G., DE LA VEGA, F. M., BRIGGS, J., GUNTHER, S., PRESCOTT, N. J., ONNIE, C. M., HASLER, R., SIPOS, B., FOLSCH, U. R., LENGAUER, T., PLATZER, M., MATHEW, C. G., KRAWCZAK, M. & SCHREIBER, S. 2007. A genome-wide association scan of nonsynonymous SNPs identifies a susceptibility variant for Crohn disease in ATG16L1. *Nature Genetics*, 39, 207-211.
- HANADA, T., NODA, N. N., SATOMI, Y., ICHIMURA, Y., FUJIOKA, Y., TAKAO, T., INAGAKI, F. & OHSUMI, Y. 2007. The Atg12-Atg5 Conjugate Has a Novel E3-like Activity for Protein Lipidation in Autophagy. *Journal of Biological Chemistry*, 282, 37298-37302.
- HAO, E., LANG, F., CHEN, Y., ZHANG, H., CONG, X., SHEN, X. & SU, G. 2013. Resveratrol alleviates endotoxin-induced myocardial toxicity via the Nrf2 transcription factor. *PLoS ONE*, 8, e69452.
- HARA, T., NAKAMURA, K., MATSUI, M., YAMAMOTO, A., NAKAHARA, Y., SUZUKI-MIGISHIMA, R., YOKOYAMA, M., MISHIMA, K., SAITO, I., OKANO, H. & MIZUSHIMA, N. 2006. Suppression of basal autophagy in neural cells causes neurodegenerative disease in mice. *Nature*, 441, 885.
- HARRIS, J., HARTMAN, M., ROCHE, C., ZENG, S. G., O'SHEA, A., SHARP, F. A., LAMBE, E. M., CREAGH, E. M., GOLENBOCK, D. T., TSCHOPP, J., KORNFELD, H., FITZGERALD, K. A. & LAVELLE, E. C. 2011. Autophagy Controls IL-1 β Secretion by Targeting Pro-IL-1 β for Degradation. *Journal of Biological Chemistry*, 286, 9587-9597.
- HAYASHI-NISHINO, M., FUJITA, N., NODA, T., YAMAGUCHI, A., YOSHIMORI, T. & YAMAMOTO, A. 2009. A subdomain of the endoplasmic reticulum forms a cradle for autophagosome formation. *Nature Cell Biology*, 11, 1433-1437.
- HELENIUS, A., KARTENBECK, J., SIMONS, K. & FRIES, E. 1980. On the entry of semliki forest virus into BHK-21 cells. *The Journal of Cell Biology*, 84, 404-420.
- HELENIUS, A., MOREIN, B., FRIES, E., SIMONS, K., ROBINSON, P., SCHIRRMACHER, V., TERHORST, C. & STROMINGER, J. L. 1978. Human (HLA-A and HLA-B) and

- murine (H-2K and H-2D) histocompatibility antigens are cell surface receptors for Semliki Forest virus. *Proceedings of the National Academy of Sciences USA*, 75, 3846-3850.
- HERMAN, P. K. & EMR, S. D. 1990. Characterization of VPS34, a gene required for vacuolar protein sorting and vacuole segregation in *Saccharomyces cerevisiae*. *Molecular and Cellular Biology*, 10, 6742-6754.
- HERTOG, M. G., HOLLMAN, P. C., KATAN, M. B. & KROMHOUT, D. 1993. Intake of potentially anticarcinogenic flavonoids and their determinants in adults in The Netherlands. *Nutrition and cancer*, 20, 21-29.
- HIGASHI, S., MOORE, D. J., MINEGISHI, M., KASANUKI, K., FUJISHIRO, H., KABUTA, T., TOGO, T., KATSUSE, O., UCHIKADO, H., FURUKAWA, Y., HINO, H., KOSAKA, K., SATO, K., ARAI, H., WADA, K. & ISEKI, E. 2011. Localization of MAP1-LC3 in Vulnerable Neurons and Lewy Bodies in Brains of Patients With Dementia With Lewy Bodies. *Journal of Neuropathology & Experimental Neurology*, 70, 264-280 10.1097/NEN.0b013e318211c86a.
- HOLLMAN, P. C. H., CASSIDY, A., COMTE, B., HEINONEN, M., RICHELLE, M., RICHLING, E., SERAFINI, M., SCALBERT, A., SIES, H. & VIDRY, S. P. The Biological Relevance of Direct Antioxidant Effects of Polyphenols for Cardiovascular Health in Humans Is Not Established. *The Journal of Nutrition*, 141, 989S-1009S.
- HOOZEMANS, J. J. M., VAN HAASTERT, E. S., NIJHOLT, D. A. T., ROZEMULLER, A. J. M., EIKELBOOM, P. & SCHEPER, W. 2009. The Unfolded Protein Response Is Activated in Pretangle Neurons in Alzheimer's Disease Hippocampus. *The American Journal of Pathology*, 174, 1241-1251.
- HOSOKAWA, N., HARA, T., KAIZUKA, T., KISHI, C., TAKAMURA, A., MIURA, Y., IEMURA, S.-I., NATSUME, T., TAKEHANA, K., YAMADA, N., GUAN, J.-L., OSHIRO, N. & MIZUSHIMA, N. 2009. Nutrient-dependent mTORC1 Association with the ULK1-Atg13-FIP200 Complex Required for Autophagy. *Molecular Biology of the Cell*, 20, 1981-1991.
- HUANG WW, T. S., PENG SF, LIN MW, CHIANG JH, CHIU YJ, FUSHIYA S, TSENG MT, YANG JS 2013. Kaempferol induces autophagy through AMPK and AKT signaling molecules and causes G2/M arrest via downregulation of CDK1/cyclin B in SK-HEP-1 human hepatic cancer cells. *International Journal of Oncology*, 42, 2069-77.
- HØYER-HANSEN, M., BASTHOLM, L., SZYNIAROWSKI, P., CAMPANELLA, M., SZABADKAI, G., FARKAS, T., BIANCHI, K., FEHRENBACHER, N., ELLING, F., RIZZUTO, R., MATHIASSEN, I. S. & JÄÄTTELÄ, M. 2007. Control of Macroautophagy by Calcium, Calmodulin-Dependent Kinase Kinase- β , and Bcl-2. *Molecular cell*, 25, 193-205.
- INOKI, K., ZHU, T. & GUAN, K.-L. 2003. TSC2 Mediates Cellular Energy Response to Control Cell Growth and Survival. *Cell*, 115, 577-590.
- INOUE, K., RISPOLI, J., KAPHZAN, H., KLANN, E., CHEN, E., KIM, J., KOMATSU, M. & ABELIOVICH, A. 2012. Macroautophagy deficiency mediates age-dependent neurodegeneration through a phospho-tau pathway. *Molecular Neurodegeneration*, 7, 48.

- ISHIBASHI, K., FUJITA, N., KANNO, E., OMORI, H., YOSHIMORI, T., ITOH, T. & FUKUDA, M. 2011. Atg16L2, a novel isoform of mammalian Atg16L that is not essential for canonical autophagy despite forming an Atg12–5-16L2 complex. *Autophagy*, 7, 1500-1513.
- ISHIBASHI, K., UEMURA, T., WAGURI, S. & FUKUDA, M. 2012. Atg16L1, an essential factor for canonical autophagy, participates in hormone secretion from PC12 cells independently of autophagic activity. *Molecular Biology of the Cell*, 23, 3193-3202.
- ISHISAKA, A., ICHIKAWA, S., SAKAKIBARA, H., PISKULA, M. K., NAKAMURA, T., KATO, Y., ITO, M., MIYAMOTO, K.-I., TSUJI, A., KAWAI, Y. & TERAO, J. 2011. Accumulation of orally administered quercetin in brain tissue and its antioxidative effects in rats. *Free Radical Biology and Medicine*, 51, 1329-1336.
- ITAKURA, E., KISHI-ITAKURA, C. & MIZUSHIMA, N. 2012. The Hairpin-type Tail-Anchored SNARE Syntaxin 17 Targets to Autophagosomes for Fusion with Endosomes/Lysosomes. *Cell*, 151, 1256-1269.
- ITOH, K., CHIBA, T., TAKAHASHI, S., ISHII, T., IGARASHI, K., KATOH, Y., OYAKE, T., HAYASHI, N., SATOH, K., HATAYAMA, I., YAMAMOTO, M. & NABESHIMA, Y. 1997. An Nrf2/small Maf heterodimer mediates the induction of phase II detoxifying enzyme genes through antioxidant response elements. *Biochemical and Biophysical Research Communications*, 236, 313-22.
- ITOH, T., FUJITA, N., KANNO, E., YAMAMOTO, A., YOSHIMORI, T. & FUKUDA, M. 2008. Golgi-resident Small GTPase Rab33B Interacts with Atg16L and Modulates Autophagosome Formation. *Molecular Biology of the Cell*, 19, 2916-2925.
- JABER, N., DOU, Z., CHEN, J. S., CATANZARO, J., JIANG, Y. P., BALLOU, L. M., SELINGER, E., OUYANG, X., LIN, R. Z., ZHANG, J. & ZONG, W. X. 2012. Class III PI3K Vps34 plays an essential role in autophagy and in heart and liver function. *Proceedings of the National Academy of Sciences USA*, 109, 2003-2008.
- JACKSON, STEPHEN P. & DUROCHER, D. 2013. Regulation of DNA Damage Responses by Ubiquitin and SUMO. *Molecular Cell*, 49, 795-807.
- JANSSEN, K., MENSINK, R. P., COX, F. J., HARRYVAN, J. L., HOVENIER, R., HOLLMAN, P. C. & KATAN, M. B. 1998. Effects of the flavonoids quercetin and apigenin on hemostasis in healthy volunteers: results from an in vitro and a dietary supplement study. *The American Journal of Clinical Nutrition*, 67, 255-62.
- JOSHI, M., JEOUNG, N., OBAYASHI, M., HATTAB, E., BROCKEN, E., LIECHTY, E., KUBEK, M., VATTEM, K., WEK, R. & HARRIS, R. 2006. Impaired growth and neurological abnormalities in branched-chain α -keto acid dehydrogenase kinase-deficient mice. *Biochemical Journal*
- JOUBERT, P.-E., WERNEKE, S. W., DE LA CALLE, C., GUIVEL-BENHASSINE, F., GIODINI, A., PEDUTO, L., LEVINE, B., SCHWARTZ, O., LENSCHOW, D. J. & ALBERT, M. L. 2012. Chikungunya virus-induced autophagy delays caspase-dependent cell death. *The Journal of Experimental Medicine*, 209, 1029-1047.

- JUDITH, D., MOSTOWY, S., BOURAI, M., GANGNEUX, N., LELEK, M., LUCAS-HOURANI, M., CAYET, N., JACOB, Y., PREVOST, M. C., PIERRE, P., TANGY, F., ZIMMER, C., VIDALAIN, P. O., COUDERC, T. & LECUIT, M. 2013. Species-specific impact of the autophagy machinery on Chikungunya virus infection. *EMBO Reports*, 14, 534-44.
- JUNG, C. H., JUN, C. B., RO, S.-H., KIM, Y.-M., OTTO, N. M., CAO, J., KUNDU, M. & KIM, D.-H. 2009. ULK-Atg13-FIP200 Complexes Mediate mTOR Signaling to the Autophagy Machinery. *Molecular Biology of the Cell*, 20, 1992-2003.
- KAY, C. D., MAZZA, G., HOLUB, B. J. & WANG, J. 2004. Anthocyanin metabolites in human urine and serum. *The British Journal of Nutrition*, 91, 933-42.
- KAY, C. D., MAZZA, G. J. & HOLUB, B. J. 2005. Anthocyanins exist in the circulation primarily as metabolites in adult men. *The Journal of Nutrition*, 135, 2582-8.
- KAZANTSEV, A., PREISINGER, E., DRANOVSKY, A., GOLDGABER, D. & HOUSMAN, D. 1999. Insoluble detergent-resistant aggregates form between pathological and nonpathological lengths of polyglutamine in mammalian cells. *Proceedings of the National Academy of Sciences USA*, 96, 11404-11409.
- KIELIAN, M., CHANEL-VOS, C. & LIAO, M. 2010. Alphavirus Entry and Membrane Fusion. *Viruses*, 2, 796-825.
- KIHARA, A., NODA, T., ISHIHARA, N. & OHSUMI, Y. 2001. Two Distinct Vps34 Phosphatidylinositol 3-Kinase Complexes Function in Autophagy and Carboxypeptidase Y Sorting in *Saccharomyces cerevisiae*. *The Journal of Cell Biology*, 152, 519-530.
- KIIVER, K., TAGEN, I., ZUSINAITE, E., TAMBERG, N., FAZAKERLEY, J. K. & MERITS, A. 2008. Properties of non-structural protein 1 of Semliki Forest virus and its interference with virus replication. *Journal of General Virology*, 89, 1457-66.
- KIM, H.-S., QUON, M. J. & KIM, J.-A. 2014. New insights into the mechanisms of polyphenols beyond antioxidant properties; lessons from the green tea polyphenol, epigallocatechin 3-gallate. *Redox Biology*, 2, 187-195.
- KIM, H. S., MONTANA, V., JANG, H. J., PARPURA, V. & KIM, J. A. 2013. Epigallocatechin gallate (EGCG) stimulates autophagy in vascular endothelial cells: a potential role for reducing lipid accumulation. *The Journal of Biological Chemistry*, 288, 22693-22705.
- KIM, J., KUNDU, M., VIOLLET, B. & GUAN, K. L. 2011. AMPK and mTOR regulate autophagy through direct phosphorylation of Ulk1. *Nature Cell Biology*, 13, 132-141.
- KIMBALL, S. R. & JEFFERSON, L. S. 2006. Signaling pathways and molecular mechanisms through which branched-chain amino acids mediate translational control of protein synthesis. *The Journal of Nutrition*, 136, 227s-31s.
- KIRISAKO, T., BABA, M., ISHIHARA, N., MIYAZAWA, K., OHSUMI, M., YOSHIMORI, T., NODA, T. & OHSUMI, Y. 1999. Formation Process of Autophagosome Is Traced with Apg8/Aut7p in Yeast. *The Journal of Cell Biology*, 147, 435-446.
- KIRKIN, V., LAMARK, T., SOU, Y. S., BJØRKØY, G., NUNN, J. L., BRUUN, J. A., SHVETS, E., MCEWAN, D. G., CLAUSEN, T. H., WILD, P., BILUSIC, I., THEURILLAT, J. P., ØVERVATN, A., ISHII, T., ELAZAR, Z., KOMATSU, M., DIKIC, I. & JOHANSEN, T.

- 2009a. A role for NBR1 in autophagosomal degradation of ubiquitinated substrates. *Molecular cell*, 33, 505-516.
- KIRKIN, V., MCEWAN, D. G., NOVAK, I. & DIKIC, I. 2009b. A Role for Ubiquitin in Selective Autophagy. *Molecular cell*, 34, 259-269.
- KLIONSKY, D. J., ABDALLA, F. C., ABELIOVICH, H., ABRAHAM, R. T., ACEVEDO-AROEZENA, A., ADELI, K., AGHOLME, L., AGNELLO, M., AGOSTINIS, P., AGUIRRE-GHISO, J. A., AHN, H. J., AIT-MOHAMED, O., AIT-SI-ALI, S., AKEMATSU, T., AKIRA, S., AL-YOUNES, H. M., AL-ZEER, M. A., ALBERT, M. L., ALBIN, R. L., ALEGRE-ABARRATEGUI, J., ALEO, M. F., ALIREZAEI, M., ALMASAN, A., ALMONTE-BECERRIL, M., AMANO, A., AMARAVADI, R. K., AMARNATH, S., AMER, A. O., ANDRIEU-ABADIE, N., ANANTHARAM, V., ANN, D. K., ANOOPKUMAR-DUKIE, S., AOKI, H., APOSTOLOVA, N., ARANCIA, G., ARIS, J. P., ASANUMA, K., ASARE, N. Y. O., ASHIDA, H., ASKANAS, V., ASKEW, D. S., AUBERGER, P., BABA, M., BACKUES, S. K., BAEHRECKE, E. H., BAHR, B. A., BAI, X.-Y., BAILLY, Y., BAIOCCHI, R., BALDINI, G., BALDUINI, W., BALLABIO, A., BAMBER, B. A., BAMPTON, E. T. W., JUHÁSZ, G., BARTHOLOMEW, C. R., BASSHAM, D. C., BAST, R. C., BATOKO, H., BAY, B.-H., BEAU, I., BÉCHET, D. M., BEGLEY, T. J., BEHL, C., BEHREND, C., BEKRI, S., BELLAIRE, B., BENDALL, L. J., BENETTI, L., BERLIOCCHI, L., BERNARDI, H., BERNASSOLA, F., BESTEIRO, S., BHATIA-KIŠŠOVÁ, I., BI, X., BIARD-PIECHACZYK, M., BLUM, J. S., BOISE, L. H., BONALDO, P., BOONE, D. L., BORNHAUSER, B. C., BORTOLUCI, K. R., BOSSIS, I., BOST, F., BOURQUIN, J.-P., BOYA, P., BOYER-GUITTAUT, M., BOZHKO, P. V., BRADY, N. R., BRANCOLINI, C., BRECH, A., BRENMAN, J. E., BRENNAND, A., BRESNICK, E. H., BREST, P., BRIDGES, D., BRISTOL, M. L., BROOKES, P. S., BROWN, E. J., BRUMELL, J. H., et al. 2012. Guidelines for the use and interpretation of assays for monitoring autophagy. *Autophagy*, 8, 445-544.
- KLIONSKY, D. J., ELAZAR, Z., SEGLEN, P. O. & RUBINSZTEIN, D. C. 2008. Does bafilomycin-A block the fusion of autophagosomes with lysosomes? *Autophagy*, 4, 849-850.
- KOJIMA, T., YAMADA, T., AKAISHI, R., FURUTA, I., SAITOH, T., NAKABAYASHI, K., NAKAYAMA, K. I., NAKAYAMA, K., AKIRA, S. & MINAKAMI, H. 2015. Role of the Atg9a gene in intrauterine growth and survival of fetal mice. *Reproductive Biology*, 15, 131-8.
- KOMANDER, D. & RAPE, M. 2012. The ubiquitin code. *Annual Review of Biochemistry*, 81, 203-29.
- KOMATSU, M., KUROKAWA, H., WAGURI, S., TAGUCHI, K., KOBAYASHI, A., ICHIMURA, Y., SOU, Y. S., UENO, I., SAKAMOTO, A., TONG, K. I., KIM, M., NISHITO, Y., IEMURA, S., NATSUME, T., UENO, T., KOMINAMI, E., MOTOHASHI, H., TANAKA, K. & YAMAMOTO, M. 2010. The selective autophagy substrate p62 activates the stress responsive transcription factor Nrf2 through inactivation of Keap1. *Nature Cell Biology*, 12, 213-23.
- KOMATSU, M., WAGURI, S., CHIBA, T., MURATA, S., IWATA, J., TANIDA, I., UENO, T., KOIKE, M., UCHIYAMA, Y., KOMINAMI, E. & TANAKA, K. 2006. Loss of

- autophagy in the central nervous system causes neurodegeneration in mice. *Nature*, 441, 880.
- KOMATSU, M., WAGURI, S., KOIKE, M., SOU, Y.-S., UENO, T., HARA, T., MIZUSHIMA, N., IWATA, J.-I., EZAKI, J., MURATA, S., HAMAZAKI, J., NISHITO, Y., IEMURA, S.-I., NATSUME, T., YANAGAWA, T., UWAYAMA, J., WARABI, E., YOSHIDA, H., ISHII, T., KOBAYASHI, A., YAMAMOTO, M., YUE, Z., UCHIYAMA, Y., KOMINAMI, E. & TANAKA, K. 2007. Homeostatic Levels of p62 Control Cytoplasmic Inclusion Body Formation in Autophagy-Deficient Mice. *Cell*, 131, 1149-1163.
- KOMATSU, M., WAGURI, S., UENO, T., IWATA, J., MURATA, S., TANIDA, I., EZAKI, J., MIZUSHIMA, N., OHSUMI, Y., UCHIYAMA, Y., KOMINAMI, E., TANAKA, K. & CHIBA, T. 2005. Impairment of starvation-induced and constitutive autophagy in Atg7-deficient mice. *The Journal of Cell Biology*, 169, 425-434.
- KOTOULAS, O. B., KALAMIDAS, S. A. & KONDOMERKOS, D. J. 2006. Glycogen autophagy in glucose homeostasis. *Pathology - Research and Practice*, 202, 631-638.
- KRAEMER, B. C., SCHUCK, T., WHEELER, J. M., ROBINSON, L. C., TROJANOWSKI, J. Q., LEE, V. M. & SCHELLENBERG, G. D. 2010. Loss of murine TDP-43 disrupts motor function and plays an essential role in embryogenesis. *Acta Neuropathologica*, 119, 409-19.
- KRAMER, M. L., BEHRENS, C. & SCHULZ-SCHAEFFER, W. J. 2008. Selective detection, quantification, and subcellular location of alpha-synuclein aggregates with a protein aggregate filtration assay. *BioTechniques*, 44, 403-411.
- KROON, P. A., CLIFFORD, M. N., CROZIER, A., DAY, A. J., DONOVAN, J. L., MANACH, C. & WILLIAMSON, G. 2004. How should we assess the effects of exposure to dietary polyphenols in vitro? *The American Journal of Clinical Nutrition*, 80, 15-21.
- KUBALLA, P., HUETT, A., RIOUX, J. D., DALY, M. J. & XAVIER, R. J. 2008. Impaired Autophagy of an Intracellular Pathogen Induced by a Crohn's Disease Associated ATG16L1 Variant. *PLoS ONE*, 3, e3391.
- KUJALA, P., IKÄHEIMONEN, A., EHSANI, N., VIHINEN, H., AUVINEN, P. & KÄÄRIÄINEN, L. 2001. Biogenesis of the Semliki Forest Virus RNA Replication Complex. *Journal of Virology*, 75, 3873-3884.
- KUMA, A., HATANO, M., MATSUI, M., YAMAMOTO, A., NAKAYA, H., YOSHIMORI, T., OHSUMI, Y., TOKUHISA, T. & MIZUSHIMA, N. 2004. The role of autophagy during the early neonatal starvation period. *Nature*, 432, 1032-6.
- KUME, S., UZU, T., HORIIKE, K., CHIN-KANASAKI, M., ISSHIKI, K., ARAKI, S.-I., SUGIMOTO, T., HANEDA, M., KASHIWAGI, A. & KOYA, D. 2010. Calorie restriction enhances cell adaptation to hypoxia through Sirt1-dependent mitochondrial autophagy in mouse aged kidney. *The Journal of Clinical Investigation*, 120, 1043-1055.
- KUNDU, M., LINDSTEN, T., YANG, C. Y., WU, J., ZHAO, F., ZHANG, J., SELAK, M. A., NEY, P. A. & THOMPSON, C. B. 2008. Ulk1 plays a critical role in the autophagic clearance of mitochondria and ribosomes during reticulocyte maturation. *Blood*, 112, 1493-502.

- KUUSISTO, E., KAUPPINEN, T. & ALAFUZOFF, I. 2008. Use of p62/SQSTM1 antibodies for neuropathological diagnosis. *Neuropathology and applied neurobiology*, 34, 169-180.
- KÄÄRIÄINEN, L. & AHOLA, T. 2002. Functions of alphavirus nonstructural proteins in RNA replication. *Progress in nucleic acid research and molecular biology*, 71, 187-222.
- LAEMMLI, U. K. 1970. Cleavage of Structural Proteins during the Assembly of the Head of Bacteriophage T4. *Nature*, 227, 680-685.
- LAINNE, M., LUUKKAINEN, R. & TOIVANEN, A. 2004. Sindbis viruses and other alphaviruses as cause of human arthritic disease. *Journal of Internal Medicine*, 256, 457-71.
- LAMB, C. A., YOSHIMORI, T. & TOOZE, S. A. 2013. The autophagosome: origins unknown, biogenesis complex. *Nature Reviews Molecular Cell Biology*, 14, 759-774.
- LASSEN, K. G., KUBALLA, P., CONWAY, K. L., PATEL, K. K., BECKER, C. E., PELOQUIN, J. M., VILLABLANCA, E. J., NORMAN, J. M., LIU, T.-C., HEATH, R. J., BECKER, M. L., FAGBAMI, L., HORN, H., MERCER, J., YILMAZ, O. H., JAFFE, J. D., SHAMJI, A. F., BHAN, A. K., CARR, S. A., DALY, M. J., VIRGIN, H. W., SCHREIBER, S. L., STAPPENBECK, T. S. & XAVIER, R. J. 2014. Atg16L1 T300A variant decreases selective autophagy resulting in altered cytokine signaling and decreased antibacterial defense. *Proceedings of the National Academy of Sciences USA*, 111, 7741-7746.
- LAW, B. K. 2005. Rapamycin: An anti-cancer immunosuppressant? *Critical Reviews in Oncology/Hematology*, 56, 47-60.
- LEE, I. H., CAO, L., MOSTOSLAVSKY, R., LOMBARD, D. B., LIU, J., BRUNS, N. E., TSOKOS, M., ALT, F. W. & FINKEL, T. 2008. A role for the NAD-dependent deacetylase Sirt1 in the regulation of autophagy. *Proceedings of the National Academy of Sciences USA*, 105, 3374-3379.
- LEE, Y. J., KIM, N.-Y., SUH, Y.-A. & LEE, C. 2011. Involvement of ROS in Curcumin-induced Autophagic Cell Death. *Korean J Physiol Pharmacol*, 15, 1-7.
- LEISER, S. F. & MILLER, R. A. 2010. Nrf2 signaling, a mechanism for cellular stress resistance in long-lived mice. *Molecular Cell Biology*, 30, 871-84.
- LEROY, K. & BRION, J. P. 1999. Developmental expression and localization of glycogen synthase kinase-3beta in rat brain. *Journal of Chemical Neuroanatomy*, 16, 279-93.
- LEUNG, J. Y., NG, M. M. & CHU, J. J. 2011. Replication of alphaviruses: a review on the entry process of alphaviruses into cells. *Advances in virology*, 2011, 249640.
- LEVI, F., PASCHE, C., LUCCHINI, F., GHIDONI, R., FERRARONI, M. & LA VECCHIA, C. 2005. Resveratrol and breast cancer risk. *European Journal of Cancer Prevention*, 14, 139-42.
- LI, W., ZHU, S., LI, J., ASSA, A., JUNDORIA, A., XU, J., FAN, S., EISSA, N. T., TRACEY, K. J., SAMA, A. E. & WANG, H. 2011. EGCG stimulates autophagy and reduces cytoplasmic HMGB1 levels in endotoxin-stimulated macrophages. *Biochemical Pharmacology*, 81, 1152-1163.

- LILJESTRÖM, P., LUSA, S., HUYLEBROECK, D. & GAROFF, H. 1991. In vitro mutagenesis of a full-length cDNA clone of Semliki Forest virus: the small 6,000-molecular-weight membrane protein modulates virus release. *Journal of Virology*, 65, 4107-4113.
- LINDMO, K., BRECH, A., FINLEY, K. D., GAUMER, S., CONTAMINE, D., RUSTEN, T. E. & STENMARK, H. 2008. The PI 3-kinase regulator Vps15 is required for autophagic clearance of protein aggregates. *Autophagy*, 4, 500-506.
- LINDSAY, J., LAURIN, D., VERREAU, R., HÉBERT, R., HELLIWELL, B., HILL, G. B. & MCDOWELL, I. 2002. Risk Factors for Alzheimer's Disease: A Prospective Analysis from the Canadian Study of Health and Aging. *American Journal of Epidemiology*, 156, 445-453.
- LITCHFIELD, S. & NAGY, Z. 2001. New temperature modification makes the Bielschowsky silver stain reproducible. *Acta Neuropathologica*, 101, 17-21.
- LOTHARIUS, J. & BRUNDIN, P. 2002. Pathogenesis of Parkinson's disease: dopamine, vesicles and alpha-synuclein. *Nature Reviews Neuroscience*, 3, 932-42.
- LYONS, M. M., YU, C., TOMA, R. B., CHO, S. Y., REIBOLDT, W., LEE, J. & VAN BREEMEN, R. B. 2003. Resveratrol in Raw and Baked Blueberries and Bilberries. *Journal of Agricultural and Food Chemistry*, 51, 5867-5870.
- MACHEIX, J.-J., FLEURIET, A. & BILLOT, J. 1990. *Fruit Phenolics*, Boca Raton, Fla., CRC Press.
- MANACH, C., SCALBERT, A., MORAND, C., RÉMÉSY, C. & JIMÉNEZ, L. 2004. Polyphenols: food sources and bioavailability. *The American Journal of Clinical Nutrition*, 79, 727-747.
- MANACH, C., WILLIAMSON, G., MORAND, C., SCALBERT, A. & RÉMÉSY, C. 2005. Bioavailability and bioefficacy of polyphenols in humans. I. Review of 97 bioavailability studies. *The American Journal of Clinical Nutrition*, 81, 230S-242S.
- MARIÑO, G., SALVADOR-MONTOLIU, N., FUEYO, A., KNECHT, E., MIZUSHIMA, N. & LÓPEZ-OTÍN, C. 2007. Tissue-specific Autophagy Alterations and Increased Tumorigenesis in Mice Deficient in Atg4C/Autophagin-3. *Journal of Biological Chemistry*, 282, 18573-18583.
- MATHIOT, C. C., GRIMAUD, G., GARRY, P., BOUQUETY, J. C., MADA, A., DAGUISY, A. M. & GEORGES, A. J. 1990. An outbreak of human Semliki Forest virus infections in Central African Republic. *The American Journal of Tropical Medicine and Hygiene*, 42, 386-393.
- MCINTOSH, B. M., WORTH, C. B. & KOKERNOT, R. H. 1961. Isolation of semliki forest virus from *Aedes (Aedimorphus) argenteopunctatus* (theobald) collected in Portuguese East Africa. *Transactions of The Royal Society of Tropical Medicine and Hygiene*, 55, 192-198.
- MILBURY, P. E., VITA, J. A. & BLUMBERG, J. B. 2010. Anthocyanins are Bioavailable in Humans following an Acute Dose of Cranberry Juice. *The Journal of Nutrition*, 140, 1099-1104.
- MIZUSHIMA, N. 2007. Autophagy: process and function. *Genes & Development*, 21, 2861-2873.

- MIZUSHIMA, N., KUMA, A., KOBAYASHI, Y., YAMAMOTO, A., MATSUBAE, M., TAKAO, T., NATSUME, T., OHSUMI, Y. & YOSHIMORI, T. 2003. Mouse Apg16L, a novel WD-repeat protein, targets to the autophagic isolation membrane with the Apg12-Apg5 conjugate. *Journal of Cell Science*, 116, 1679-1688.
- MIZUSHIMA, N., NODA, T., YOSHIMORI, T., TANAKA, Y., ISHII, T., GEORGE, M. D., KLIONSKY, D. J., OHSUMI, M. & OHSUMI, Y. 1998. A protein conjugation system essential for autophagy. *Nature*, 395, 395-398.
- MIZUSHIMA, N., OHSUMI, Y. & YOSHIMORI, T. 2002. Autophagosome Formation in Mammalian Cells. *Cell Structure and Function*, 27, 421-429.
- MIZUSHIMA, N., YAMAMOTO, A., MATSUI, M., YOSHIMORI, T. & OHSUMI, Y. 2004b. In Vivo Analysis of Autophagy in Response to Nutrient Starvation Using Transgenic Mice Expressing a Fluorescent Autophagosome Marker. *Molecular Biology of the Cell*, 15, 1101-1111.
- MOREAU, K., RAVIKUMAR, B., RENNA, M., PURI, C. & RUBINSZTEIN, DAVID C. 2011. Autophagosome Precursor Maturation Requires Homotypic Fusion. *Cell*, 146, 303-317.
- MORSELLI, E., MAIURI, M. C., MARKAKI, M., MEGALOU, E., PASPARAKI, A., PALIKARAS, K., CRIOLLO, A., GALLUZZI, L., MALIK, S. A., VITALE, I., MICHAUD, M., MADEO, F., TAVERNARAKIS, N. & KROEMER, G. 2010. Caloric restriction and resveratrol promote longevity through the Sirtuin-1-dependent induction of autophagy. *Cell Death and Disease*, 1, e10.
- MORSELLI, E., MARIÑO, G., BENNETZEN, M. V., EISENBERG, T., MEGALOU, E., SCHROEDER, S., CABRERA, S., BÉNIT, P., RUSTIN, P., CRIOLLO, A., KEPP, O., GALLUZZI, L., SHEN, S., MALIK, S. A., MAIURI, M. C., HORIO, Y., LÓPEZ-OTÍN, C., ANDERSEN, J. S., TAVERNARAKIS, N., MADEO, F. & KROEMER, G. 2011. Spermidine and resveratrol induce autophagy by distinct pathways converging on the acetylproteome. *The Journal of Cell Biology*, 192, 615-629.
- MURTHY, A., LI, Y., PENG, I., REICHEL, M., KATAKAM, A. K., NOUBADE, R., ROOSE-GIRMA, M., DEVOSS, J., DIEHL, L., GRAHAM, R. R. & VAN LOOKEREN CAMPAGNE, M. 2014. A Crohn's disease variant in Atg16l1 enhances its degradation by caspase 3. *Nature*, 506, 456-62.
- NAKANO, T., NAKASO, K., NAKASHIMA, K. & OHAMA, E. 2004. Expression of ubiquitin-binding protein p62 in ubiquitin-immunoreactive intraneuronal inclusions in amyotrophic lateral sclerosis with dementia: analysis of five autopsy cases with broad clinicopathological spectrum. *Acta Neuropathologica*, 107, 359-364.
- NAKAZATO, T., ITO, K., IKEDA, Y. & KIZAKI, M. 2005. Green Tea Component, Catechin, Induces Apoptosis of Human Malignant B Cells via Production of Reactive Oxygen Species. *Clinical Cancer Research*, 11, 6040-6049.
- NEER, E. J., SCHMIDT, C. J., NAMBU DRIPAD, R. & SMITH, T. F. 1994. The ancient regulatory-protein family of WD-repeat proteins. *Nature*, 371, 297-300.
- NEMAZANY, I., BLAAUW, B., PAOLINI, C., CAILLAUD, C., PROTASI, F., MUELLER, A., PROIKAS-CEZANNE, T., RUSSELL, R. C., GUAN, K. L., NISHINO, I., SANDRI, M.,

- PENDE, M. & PANASYUK, G. 2013. Defects of Vps15 in skeletal muscles lead to autophagic vacuolar myopathy and lysosomal disease. *EMBO Molecular Medicine*, 5, 870-90.
- NEUMANN, M., SAMPATHU, D. M., KWONG, L. K., TRUAX, A. C., MICSENYI, M. C., CHOU, T. T., BRUCE, J., SCHUCK, T., GROSSMAN, M., CLARK, C. M., MCCLUSKEY, L. F., MILLER, B. L., MASLIAH, E., MACKENZIE, I. R., FELDMAN, H., FEIDEN, W., KRETZSCHMAR, H. A., TROJANOWSKI, J. Q. & LEE, V. M.-Y. 2006. Ubiquitinated TDP-43 in Frontotemporal Lobar Degeneration and Amyotrophic Lateral Sclerosis. *Science*, 314, 130-133.
- NEVEU, V., PEREZ-JIMÉNEZ, J., VOS, F., CRESPIY, V., DU CHAFFAUT, L., MENNEN, L., KNOX, C., EISNER, R., CRUZ, J., WISHART, D. & SCALBERT, A. 2010. Phenol-Explorer: an online comprehensive database on polyphenol contents in foods. *Database*, 2010.
- NISHIDA, Y., S, A., K, F., H, Y., T, M., T, K., M, K., K, O., Y, T. & S., S. 2009. Discovery of Atg5/Atg7-independent alternative macroautophagy. *Nature*.
- NIXON, R. A., WEGIEL, J., KUMAR, A., YU, W. H., PETERHOFF, C., CATALDO, A. & CUERVO, A. M. 2005. Extensive Involvement of Autophagy in Alzheimer Disease: An Immuno-Electron Microscopy Study. *Journal of Neuropathology & Experimental Neurology* 64, 113-122.
- NOOYENS, A. C. J., BUENO-DE-MESQUITA, H. B., VAN GELDER, B. M., VAN BOXTEL, M. P. J. & VERSCHUREN, W. M. M. 2013. Consumption of alcoholic beverages and cognitive decline at middle age: the Doetinchem Cohort Study. *British Journal of Nutrition*, FirstView, 1-9.
- O'SULLIVAN-COYNE, G., O'SULLIVAN, G. C., O'DONOVAN, T. R., PIWOCKA, K. & MCKENNA, S. L. 2009. Curcumin induces apoptosis-independent death in oesophageal cancer cells. *British Journal of Cancer*, 101, 1585-1595.
- ORGOGOZO JM, D. J., LAFONT S, LETENNEUR L, COMMENGES D, SALAMON R, RENAUD S, BRETELER MB. 1997. Wine consumption and dementia in the elderly: a prospective community study in the Bordeaux area. *Revue Neurologique*. 153, 185-92.
- ORVEDAHL, A., MACPHERSON, S., SUMPTER, R., TALLÓCZY, Z., ZOU, Z. & LEVINE, B. 2010. Autophagy Protects against Sindbis Virus Infection of the Central Nervous System. *Cell Host & Microbe*, 7, 115-127.
- OSOEGAWA, K., TATENO, M., WOON, P. Y., FRENGEN, E., MAMMOSER, A. G., CATANESE, J. J., HAYASHIZAKI, Y. & DE JONG, P. J. 2000. Bacterial artificial chromosome libraries for mouse sequencing and functional analysis. *Genome Research*, 10, 116-28.
- PARK, S.-J., AHMAD, F., PHILP, A., BAAR, K., WILLIAMS, T., LUO, H., KE, H., REHMANN, H., TAUSSIG, R., BROWN, ALEXANDRA L., KIM, MYUNG K., BEAVEN, MICHAEL A., BURGIN, ALEX B., MANGANIELLO, V. & CHUNG, JAY H. 2012. Resveratrol Ameliorates Aging-Related Metabolic Phenotypes by Inhibiting cAMP Phosphodiesterases. *Cell*, 148, 421-433.
- PEREZ-JIMENEZ, J., NEVEU, V., VOS, F. & SCALBERT, A. 2010. Systematic analysis of the content of 502 polyphenols in 452 foods and beverages: an application

- of the phenol-explorer database. *Journal of Agricultural and Food Chemistry*, 58, 4959-69.
- PERÄNEN, J., LAAKKONEN, P., HYVÖNEN, M. & KÄÄRIÄINEN, L. 1995. The Alphavirus Replicase Protein nsP1 Is Membrane-Associated and Has Affinity to Endocytic Organelles. *Virology*, 208, 610-620.
- PETIOT, A., OGIER-DENIS, E., BLOMMAART, E. F. C., MEIJER, A. J. & CODOGNO, P. 2000. Distinct Classes of Phosphatidylinositol 3'-Kinases Are Involved in Signaling Pathways That Control Macroautophagy in HT-29 Cells. *Journal of Biological Chemistry*, 275, 992-998.
- PHILIPPIDIS, H. & BALLARD, F. J. 1970. The development of gluconeogenesis in rat liver. Effects of glucagon and ether. *Biochem J*, 120, 385-92.
- PISKULA, M. K. & TERAQ, J. 1998. Accumulation of (-)-epicatechin metabolites in rat plasma after oral administration and distribution of conjugation enzymes in rat tissues. *Journal of Nutrition*, 128, 1172-8.
- POLSON, H. E., DE LARTIGUE, J., RIGDEN, D. J., REEDIJK, M., URBÉ, S., CLAGUE, M. J. & TOOZE, S. A. 2010. Mammalian Atg18 (WIPI2) localizes to omegasome-anchored phagophores and positively regulates LC3 lipidation. *Autophagy*, 6, 506-522.
- PURPERA, M. N., SHEN, L., TAGHAVI, M., MÜNZBERG, H., MARTIN, R. J., HUTSON, S. M. & MORRISON, C. D. 2012. Impaired branched-chain amino acid metabolism alters feeding behavior and increases orexigenic neuropeptide expression in the hypothalamus. *Journal of Endocrinology*, 212, 85-94.
- QU, X., ZOU, Z., SUN, Q., LUBY-PHELPS, K., CHENG, P., HOGAN, R. N., GILPIN, C. & LEVINE, B. 2007. Autophagy Gene-Dependent Clearance of Apoptotic Cells during Embryonic Development. *Cell*, 128, 931-946.
- RAHMAN, I., BISWAS, S. K. & KIRKHAM, P. A. 2006. Regulation of inflammation and redox signaling by dietary polyphenols. *Biochemical Pharmacology*, 72, 1439-1452.
- RALPH A. NIXON, M., PHD, JERZY WEGIEL, PHD, VMD, ASOK KUMAR, PHD, WAI HAUNG YU, PHD, & CORRINNE PETERHOFF, B., ANNE CATALDO, PHD, AND ANA MARIA CUERVO, MD, PHD 2005. Extensive Involvement of Autophagy in Alzheimer Disease: An Immuno-Electron Microscopy Study. *Journal of Neuropathology & Experimental Neurology*, 64, 113-122.
- RAVIKUMAR, B., MOREAU, K., JAHREISS, L., PURI, C. & RUBINSZTEIN, D. C. 2010. Plasma membrane contributes to the formation of pre-autophagosomal structures. *Nature Cell Biology*, 12, 747-757.
- READ, R., SAVELIEVA, K., BAKER, K., HANSEN, G. & VOGEL, P. 2011. Histopathological and Neurological Features of Atg4b Knockout Mice. *Veterinary Pathology Online*, 48, 486-494.
- REAGAN-SHAW S., N. M., AHMAD N. 2007. Dose translation from animal to human studies revisited. *FASEB Journal*, 22, 659-661.
- REAVES, B. J., BRIGHT, N. A., MULLOCK, B. M. & LUZIO, J. P. 1996. The effect of wortmannin on the localisation of lysosomal type I integral membrane glycoproteins suggests a role for phosphoinositide 3-kinase activity in

- regulating membrane traffic late in the endocytic pathway. *Journal of Cell Science*, 109 (Pt 4), 749-762.
- REFOLO, L. M., WITTENBERG, I. S., FRIEDRICH, V. L., JR. & ROBAKIS, N. K. 1991. The Alzheimer amyloid precursor is associated with the detergent-insoluble cytoskeleton. *The Journal of Neuroscience*, 11, 3888-97.
- REIN, D., LOTITO, S., HOLT, R. R., KEEN, C. L., SCHMITZ, H. H. & FRAGA, C. G. 2000. Epicatechin in Human Plasma: In Vivo Determination and Effect of Chocolate Consumption on Plasma Oxidation Status. *The Journal of Nutrition*, 130, 2109S-2114S.
- RICE-EVANS, C. A., MILLER, N. J. & PAGANGA, G. 1996. Structure-antioxidant activity relationships of flavonoids and phenolic acids. *Free Radical Biology and Medicine*, 20, 933-956.
- RILEY, B. E., KAISER, S. E., SHALER, T. A., NG, A. C., HARA, T., HIPPI, M. S., LAGE, K., XAVIER, R. J., RYU, K. Y., TAGUCHI, K., YAMAMOTO, M., TANAKA, K., MIZUSHIMA, N., KOMATSU, M. & KOPITO, R. R. 2010. Ubiquitin accumulation in autophagy-deficient mice is dependent on the Nrf2-mediated stress response pathway: a potential role for protein aggregation in autophagic substrate selection. *The Journal of Cell Biology*, 191, 537-552.
- RIOUX, J. D., XAVIER, R. J., TAYLOR, K. D., SILVERBERG, M. S., GOYETTE, P., HUETT, A., GREEN, T., KUBALLA, P., BARMADA, M. M., DATTA, L. W., SHUGART, Y. Y., GRIFFITHS, A. M., TARGAN, S. R., IPPOLITI, A. F., BERNARD, E.-J., MEI, L., NICOLAE, D. L., REGUEIRO, M., SCHUMM, L. P., STEINHART, A. H., ROTTER, J. I., DUERR, R. H., CHO, J. H., DALY, M. J. & BRANT, S. R. 2007. Genome-wide association study identifies new susceptibility loci for Crohn disease and implicates autophagy in disease pathogenesis. *Nature Genetics*, 39, 596-604.
- ROGINA, B. & HELFAND, S. L. 2004. Sir2 mediates longevity in the fly through a pathway related to calorie restriction. *Proceedings of the National Academy of Sciences USA*, 101, 15998-16003.
- ROMANOV, J., WALCZAK, M., IBIRICU, I., SCHUCHNER, S., OGRIS, E., KRAFT, C. & MARTENS, S. 2012. Mechanism and functions of membrane binding by the Atg5-Atg12/Atg16 complex during autophagosome formation. *The EMBO Journal*, 31, 4304-17.
- RUBINSZTEIN, D. C., DIFIGLIA, M., HEINTZ, N., NIXON, R. A., QIN, Z. H., RAVIKUMAR, B., STEFANIS, L. & TOLKOVSKY, A. 2005. Autophagy and its possible roles in nervous system diseases, damage and repair. *Autophagy*, 1, 11-22.
- SABATINI, D. M., ERDJUMENT-BROMAGE, H., LUI, M., TEMPST, P. & SNYDER, S. H. 1994. RAFT1: A mammalian protein that binds to FKBP12 in a rapamycin-dependent fashion and is homologous to yeast TORs. *Cell*, 78, 35-43.
- SADOWSKI, M., SURYADINATA, R., TAN, A. R., ROESLEY, S. N. & SARCEVIC, B. 2012. Protein monoubiquitination and polyubiquitination generate structural diversity to control distinct biological processes. *IUBMB Life*, 64, 136-42.
- SAITOH, T., FUJITA, N., JANG, M. H., UEMATSU, S., YANG, B. G., SATOH, T., OMORI, H., NODA, T., YAMAMOTO, N., KOMATSU, M., TANAKA, K., KAWAI, T., TSUJIMURA, T., TAKEUCHI, O., YOSHIMORI, T. & AKIRA, S. 2008. Loss of the

- autophagy protein Atg16L1 enhances endotoxin-induced IL-1 β production. *Nature*, 456, 264-268.
- SALBAUM, J. M. & RUDDLE, F. H. 1994. Embryonic expression pattern of amyloid protein precursor suggests a role in differentiation of specific subsets of neurons. *Journal of Experimental Zoology*, 269, 116-127.
- SANCAK, Y., BAR-PELED, L., ZONCU, R., MARKHARD, A. L., NADA, S. & SABATINI, D. M. 2010. Ragulator-Rag Complex Targets mTORC1 to the Lysosomal Surface and Is Necessary for Its Activation by Amino Acids. *Cell*, 141, 290-303.
- SARKAR, S., DAVIES, J. E., HUANG, Z., TUNNAcliffe, A. & RUBINSZTEIN, D. C. 2007. Trehalose, a Novel mTOR-independent Autophagy Enhancer, Accelerates the Clearance of Mutant Huntingtin and α -Synuclein. *Journal of Biological Chemistry*, 282, 5641-5652.
- SARKAR, S., FLOTO, R. A., BERGER, Z., IMARISIO, S., CORDENIER, A., PASCO, M., COOK, L. J. & RUBINSZTEIN, D. C. 2005. Lithium induces autophagy by inhibiting inositol monophosphatase. *The Journal of Cell Biology*, 170, 1101-1111.
- SCAPAGNINI, G., VASTO, S., ABRAHAM, N. G., CARUSO, C., ZELLA, D. & FABIO, G. 2011. Modulation of Nrf2/ARE pathway by food polyphenols: a nutritional neuroprotective strategy for cognitive and neurodegenerative disorders. *Molecular Neurobiology*, 44, 192-201.
- SCHEELE, C. M. & PFEFFERKORN, E. R. 1969. Kinetics of incorporation of structural proteins into Sindbis virions. *Journal of Virology*, 3, 369-75.
- SCHERZ-SHOVAL, R. S. E. F. E. S. H. G. L. E. Z. 2007. Reactive oxygen species are essential for autophagy and specifically regulate the activity of Atg4. *The EMBO Journal*, 26, 1749-1760.
- SCHEWE, T., STEFFEN, Y. & SIES, H. 2008. How do dietary flavanols improve vascular function? A position paper. *Archives of Biochemistry and Biophysics*, 476, 102-106.
- SEGLIN, P. O. & GORDON, P. B. 1982. 3-Methyladenine: Specific inhibitor of autophagic/lysosomal protein degradation in isolated rat hepatocytes. *Proceedings of the National Academy of Sciences USA*, 79, 1889-1892.
- SEPHTON, C. F., GOOD, S. K., ATKIN, S., DEWEY, C. M., MAYER, P., 3RD, HERZ, J. & YU, G. 2010. TDP-43 is a developmentally regulated protein essential for early embryonic development. *Journal of Biological Chemistry*, 285, 6826-34.
- SERRA, A., MACIA, A., ROMERO, M. P., VALLS, J., BLADE, C., AROLA, L. & MOTILVA, M. J. 2010. Bioavailability of procyanidin dimers and trimers and matrix food effects in in vitro and in vivo models. *British Journal of Nutrition*, 103, 944-52.
- SHAID, S., BRANDTS, C. H., SERVE, H. & DIKIC, I. 2012. Ubiquitination and selective autophagy. *Cell Death & Differentiation*, 20, 21-30.
- SHANG, L., CHEN, S., DU, F., LI, S., ZHAO, L. & WANG, X. 2011. Nutrient starvation elicits an acute autophagic response mediated by Ulk1 dephosphorylation and its subsequent dissociation from AMPK. *Proceedings of the National Academy of Sciences USA*, 108, 4788-4793.

- SHAW, R. J., KOSMATKA, M., BARDEESY, N., HURLEY, R. L., WITTERS, L. A., DEPINHO, R. A. & CANTLEY, L. C. 2004. The tumor suppressor LKB1 kinase directly activates AMP-activated kinase and regulates apoptosis in response to energy stress. *Proceedings of the National Academy of Sciences USA*, 101, 3329-3335.
- SHE, P., SHIOTA, M., SHELTON, K. D., CHALKLEY, R., POSTIC, C. & MAGNUSON, M. A. 2000. Phosphoenolpyruvate carboxykinase is necessary for the integration of hepatic energy metabolism. *Molecular and Cellular Biology*, 20, 6508-17.
- SHELLEY, H. J. 1961. Glycogen reserves and their changes at birth and in anoxia.
- SHILATIFARD, A. 2006. Chromatin modifications by methylation and ubiquitination: implications in the regulation of gene expression. *Annual Review of Biochemistry*, 75, 243-69.
- SHINOJIMA, N., YOKOYAMA, T., KONDO, Y. & KONDO, S. 2007. Roles of the Akt/mTOR/p70S6K and ERK1/2 Signaling Pathways in Curcumin-Induced Autophagy. *Autophagy*, 3, 635-637.
- SIEMANN, E. H. & CREASY, L. L. 1992. Concentration of the phytoalexin resveratrol in wine. *American journal of enology and viticulture*, 43, 49-52.
- SIMONSEN, A. & TOOZE, S. A. 2009. Coordination of membrane events during autophagy by multiple class III PI3-kinase complexes. *The Journal of Cell Biology*, 186, 773-782.
- SINGH, I. & HELENIUS, A. 1992. Role of ribosomes in Semliki Forest virus nucleocapsid uncoating. *Journal of Virology*, 66, 7049-7058.
- SINGH, R., KAUSHIK, S., WANG, Y., XIANG, Y., NOVAK, I., KOMATSU, M., TANAKA, K., CUERVO, A. M. & CZAJA, M. J. 2009. Autophagy regulates lipid metabolism. *Nature*, 458, 1131-1135.
- SMIT, J. M., WAARTS, B.-L., KIMATA, K., KLIMSTRA, W. B., BITTMAN, R. & WILSCHUT, J. 2002. Adaptation of Alphaviruses to Heparan Sulfate: Interaction of Sindbis and Semliki Forest Viruses with Liposomes Containing Lipid-Conjugated Heparin. *Journal of Virology*, 76, 10128-10137.
- SMITHBURN, K. C., HADDOW, A. J. & MAHAFFY, A. F. 1946. A neurotropic virus isolated from Aedes mosquitoes caught in the Semliki forest. *The American Journal of Tropical Medicine and Hygiene*, 26, 189-208.
- SOU, Y. S., WAGURI, S., IWATA, J., UENO, T., FUJIMURA, T., HARA, T., SAWADA, N., YAMADA, A., MIZUSHIMA, N., UCHIYAMA, Y., KOMINAMI, E., TANAKA, K. & KOMATSU, M. 2008. The Atg8 conjugation system is indispensable for proper development of autophagic isolation membranes in mice. *Molecular Biology of the Cell*, 19, 4762-75.
- SPENCER, J. P. 2009. Flavonoids and brain health: multiple effects underpinned by common mechanisms. *Genes & Nutrition*, 4, 243-50.
- STAPLES, J. E., BREIMAN, R. F. & POWERS, A. M. 2009. Chikungunya Fever: An Epidemiological Review of a Re-Emerging Infectious Disease. *Clinical Infectious Diseases*, 49, 942-948.
- STEFANI, M. & DOBSON, C. M. 2003. Protein aggregation and aggregate toxicity: new insights into protein folding, misfolding diseases and biological evolution. *Journal of Molecular Medicine*, 81, 678-99.

- STRAUSS, K. A., PUFFENBERGER, E. G. & MORTON, D. H. 1993. Maple Syrup Urine Disease. *In*: PAGON, R. A., ADAM, M. P., ARDINGER, H. H., WALLACE, S. E., AMEMIYA, A., BEAN, L. J. H., BIRD, T. D., FONG, C. T., MEFFORD, H. C., SMITH, R. J. H. & STEPHENS, K. (eds.) *GeneReviews (R)*. University of Washington, Seattle.
- TAN, J. M. M., WONG, E. S. P., KIRKPATRICK, D. S., PLETNIKOVA, O., KO, H. S., TAY, S.-P., HO, M. W. L., TRONCOSO, J., GYGI, S. P., LEE, M. K., DAWSON, V. L., DAWSON, T. M. & LIM, K.-L. 2008. Lysine 63-linked ubiquitination promotes the formation and autophagic clearance of protein inclusions associated with neurodegenerative diseases. *Human Molecular Genetics*, 17, 431-439.
- TEBBENKAMP, A. T. & BORCHELT, D. R. 2009. Protein Aggregate Characterization in Models of Neurodegenerative Disease. *Methods in Molecular Biology*, 566, 85-91.
- THOREEN, C. C., KANG, S. A., CHANG, J. W., LIU, Q., ZHANG, J., GAO, Y., REICHLING, L. J., SIM, T., SABATINI, D. M. & GRAY, N. S. 2009. An ATP-competitive Mammalian Target of Rapamycin Inhibitor Reveals Rapamycin-resistant Functions of mTORC1. *Journal of Biological Chemistry*, 284, 8023-8032.
- TISENBAUM, H. A. & GUARENTE, L. 2001. Increased dosage of a sir-2 gene extends lifespan in *Caenorhabditis elegans*. *Nature*, 410, 227-230.
- TONG, X., SMITH, K. A. & PELLING, J. C. 2011. Apigenin, a chemopreventive bioflavonoid, induces AMP-activated protein kinase activation in human keratinocytes. *Molecular Carcinogenesis*, 51, 268-79.
- TRAVASSOS, L. H., CARNEIRO, L. A., RAMJEET, M., HUSSEY, S., KIM, Y. G., MAGALHÃES, J. G., YUAN, L., SOARES, F., CHEA, E., LE BOURHIS, L., BONECA, I. G., ALLAOUI, A., JONES, N. L., NUÑEZ, G., GIRARDIN, S. E. & PHILPOTT, D. J. 2010. Nod1 and Nod2 direct autophagy by recruiting ATG16L1 to the plasma membrane at the site of bacterial entry. *Nature Immunology*, 11, 55-62.
- TUITTILA, M. & HINKKANEN, A. E. 2003. Amino acid mutations in the replicase protein nsP3 of Semliki Forest virus cumulatively affect neurovirulence. *Journal of General Virology*, 84, 1525-33.
- URBAN, C., RHEME, C., MAERZ, S., BERG, B., PICK, R., NITSCHKE, R. & BORNER, C. 2008. Apoptosis induced by Semliki Forest virus is RNA replication dependent and mediated via Bak. *Cell Death & Differentiation*, 15, 1396-407.
- VINGTDEUX, V., GILIBERTO, L., ZHAO, H., CHANDAKKAR, P., WU, Q., SIMON, J. E., JANLE, E. M., LOBO, J., FERRUZZI, M. G., DAVIES, P. & MARAMBAUD, P. 2010. AMP-activated Protein Kinase Signaling Activation by Resveratrol Modulates Amyloid- β Peptide Metabolism. *Journal of Biological Chemistry*, 285, 9100-9113.
- VITAGLIONE, P., SFORZA, S., GALAVERNA, G., GHIDINI, C., CAPORASO, N., VESCOVI, P. P., FOGLIANO, V. & MARCHELLI, R. 2005. Bioavailability of trans-resveratrol from red wine in humans. *Molecular Nutrition & Food Research*, 49, 495-504.
- VOGIATZI, T., XILOURI, M., VEKRELLIS, K. & STEFANIS, L. 2008. Wild Type α -Synuclein Is Degraded by Chaperone-mediated Autophagy and

- Macroautophagy in Neuronal Cells. *Journal of Biological Chemistry*, 283, 23542-23556.
- WAGURI, S. & KOMATSU, M. 2009. Chapter 9 Biochemical and Morphological Detection of Inclusion Bodies in Autophagy-Deficient Mice. *In*: DANIEL, J. K. (ed.) *Methods in Enzymology*. Academic Press.
- WANG, I.-F., GUO, B.-S., LIU, Y.-C., WU, C.-C., YANG, C.-H., TSAI, K.-J. & SHEN, C.-K. J. 2012. Autophagy activators rescue and alleviate pathogenesis of a mouse model with proteinopathies of the TAR DNA-binding protein 43. *Proceedings of the National Academy of Sciences*, 109, 15024-15029.
- WANG, K., LIU, R., LI, J., MAO, J., LEI, Y., WU, J., ZENG, J., ZHANG, T., WU, H., CHEN, L., HUANG, C. & WEI, Y. 2011. Quercetin induces protective autophagy in gastric cancer cells: involvement of Akt-mTOR- and hypoxia-induced factor 1 α -mediated signaling. *Autophagy*, 7, 966-978.
- WANG, X., FAN, H., YING, Z., LI, B., WANG, H. & WANG, G. 2010. Degradation of TDP-43 and its pathogenic form by autophagy and the ubiquitin-proteasome system. *Neuroscience letters*, 469, 112-116.
- WATERHOUSE, A. L., SHIRLEY, J. R. & DONOVAN, J. L. 1996. Antioxidants in chocolate. *Lancet*, 348, 834.
- WEBB, J. L., RAVIKUMAR, B., ATKINS, J., SKEPPER, J. N. & RUBINSZTEIN, D. C. 2003. α -Synuclein Is Degraded by Both Autophagy and the Proteasome. *Journal of Biological Chemistry*, 278, 25009-25013.
- WILLEMS, W. R., KALUZA, G., BOSCHEK, C. B., BAUER, H., HAGER, H., SCHÜTZ, H. J. & FEISTNER, H. 1979. Semliki forest virus: cause of a fatal case of human encephalitis. *Science (New York, N.Y.)*, 203, 1127-1129.
- WILSCHUT, J., CORVER, J., NIEVA, J. L., BRON, R., MOESBY, L., REDDY, K. C. & BITTMAN, R. 1995. Fusion of Semliki Forest virus with cholesterol-containing liposomes at low pH: a specific requirement for sphingolipids. *Molecular Membrane Biology*, 12, 143-149.
- WOOD, E. J. 1983. Molecular cloning. A laboratory manual by T Maniatis, E F Fritsch and J Sambrook. pp 545. Cold Spring Harbor Laboratory, New York. 1982. \$48 ISBN 0-87969-136-0. *Biochemical Education*, 11, 82-82.
- XIAO, K., JIANG, J., GUAN, C., DONG, C., WANG, G., BAI, L., SUN, J., HU, C. & BAI, C. 2013. Curcumin induces autophagy via activating the AMPK signaling pathway in lung adenocarcinoma cells. *Journal of Pharmacological Sciences*, 123, 102-9.
- YAMAMOTO, A., TAGAWA, Y., YOSHIMORI, T., MORIYAMA, Y., MASAKI, R. & TASHIRO, Y. 1998. Bafilomycin A1 prevents maturation of autophagic vacuoles by inhibiting fusion between autophagosomes and lysosomes in rat hepatoma cell line, H-4-II-E cells. *Cell Structure and Function*, 23, 33-42.
- YAMAMOTO, H., KAKUTA, S., WATANABE, T. M., KITAMURA, A., SEKITO, T., KONDO-KAKUTA, C., ICHIKAWA, R., KINJO, M. & OHSUMI, Y. 2012. Atg9 vesicles are an important membrane source during early steps of autophagosome formation. *The Journal of Cell Biology*, 198, 219-233.

- YAO, H. B., SHAW, P. C., WONG, C. C. & WAN, D. C. 2002. Expression of glycogen synthase kinase-3 isoforms in mouse tissues and their transcription in the brain. *Journal of Chemical Neuroanatomy*, 23, 291-7.
- YLÄ-ANTTILA, P., VIHINEN, H., JOKITALO, E. & E.-L., E. 2009. 3D tomography reveals connections between the phagophore and endoplasmic reticulum. *Autophagy*, 5, 1180 - 1185.
- ZHANG, Z., XU, X., MA, J., WU, J., WANG, Y., ZHOU, R. & HAN, J. 2013. Gene deletion of Gabarap enhances Nlrp3 inflammasome-dependent inflammatory responses. *Journal of Immunology*, 190, 3517-24.
- ZHENG, Y. & KIELIAN, M. 2013. Imaging of the alphavirus capsid protein during virus replication. *Journal of Virology*, 87, 9579-89.
- ZHONG, S. C., LUO, X., CHEN, X. S., CAI, Q. Y., LIU, J., CHEN, X. H. & YAO, Z. X. 2010. Expression and subcellular location of alpha-synuclein during mouse-embryonic development. *Cellular and Molecular Neurobiology*, 30, 469-482.
- ZHOU, J., TAN, S.-H., NICOLAS, V., BAUVY, C., YANG, N.-D., ZHANG, J., XUE, Y., CODOGNO, P. & SHEN, H.-M. 2013. Activation of lysosomal function in the course of autophagy via mTORC1 suppression and autophagosome-lysosome fusion. *Cell Research*, 23, 508-523.
- ZONCU, R., BAR-PELED, L., EFEYAN, A., WANG, S., SANCAK, Y. & SABATINI, D. M. 2011. mTORC1 senses lysosomal amino acids through an inside-out mechanism that requires the vacuolar H(+)-ATPase. *Science*, 334, 678-83.